LBL-22418

Lawrence Berkeley Laboratory
UNIVERSITY OF CALIFORNIA

Materials & Molecular
Research Division

PHOTOIONIZATION OF ATOMS AND SMALL MOLECULES USING SYNCHROTRON RADIATION

T.A. Ferrett
(Ph.D. Thesis)

November 1986

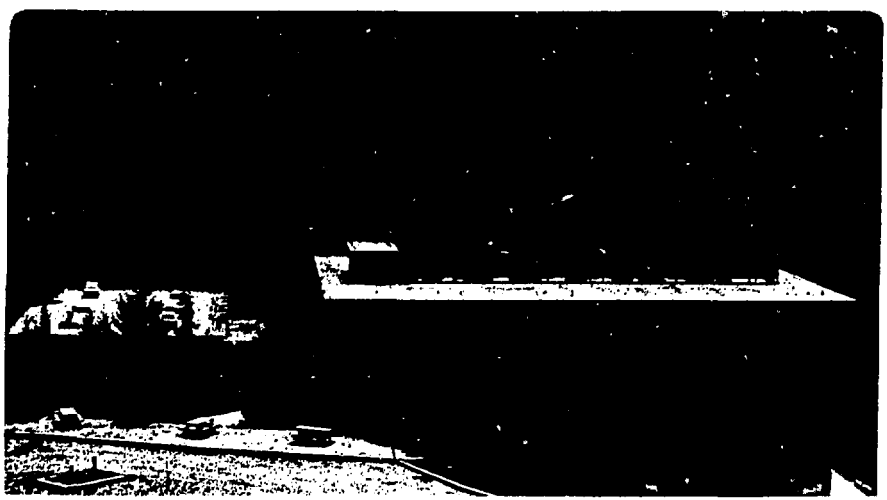

Prepared for the U.S. Department of Energy under Contract DE-AC03-76SF00098

LBL--22418

DE87 0046C0

PHOTOIONIZATION OF ATOMS AND SMALL MOLECULES USING SYNCHROTRON RADIATION

Tricia Anne Ferrett
(Ph.D. Thesis)

Materials and Molecular Research Division
Lawrence Berkeley Laboratory
and
Department of Chemistry
University of California
Berkeley, California 94720

November 1986

This work was supported by the Director, Office of Energy Research, Office of Basic Energy Sciences, Chemical Sciences Division of the U.S. Department of Energy under Contract No. DE-AC03-76SF00098. It was performed at the Stanford Synchrotron Radiation Laboratory, which is supported by the Department of Energy's Office of Basic Energy Sciences.

PHOTOIONIZATION OF ATOMS AND SMALL MOLECULES USING SYNCHROTRON RADIAION

Tricia Anne Ferrett

Abstract

The combination of synchrotron radiation and time-of-flight electron spectroscopy has been used to study the photoionization dynamics of atoms (Li) and small molecules (SF_6, SiF_4, and SO_2). Partial cross sections and angular distribution asymmetry parameters have been measured for Auger electrons and photoelectrons as functions of photon energy. Emphasis is on the basic understanding of electron correlation and resonant effects as manifested in the photoemission spectra for these systems.

Photoemission results for the 1s main line and 1snl satellites (n=2-5) of atomic Li provide a testing ground for the inclusion of many-electron effects in the theoretical treatment of the simplest open shell atom. In addition, decay of the doubly excited state 1s(3s3p) of the neutral has also been studied; cross-section profiles for both the 1s2s main lines and the 1s2p conjugate satellites are reported.

A number of effects have been investigated in the photoionization continua of the molecules SF_6, SiF_4, and SO_2: autoionization, continuum shape resonances, and EXAFS (extended x-ray

absorption fine structure). Experiments on the S 1s, S 2p, and inner-valence ionization of SF_6 present a challenge to the current understanding of these effects. Broad oscillations above the S 1s edge of SF_6 appear to be intermediate between usual shape-resonant and EXAFS behavior. For S 2p ionization, the first observation of shakeup-satellite enhancement at a molecular shape resonance is found for the e_g resonance. The inner-valence study on SF_6 is also the first of its kind in the vicinity of a predicted shape resonance.

Data are presented on the discrete and continuum resonances near the Si 2p and 2s thresholds of SiF_4. The molecular-orbital and Rydberg discrete excitations below these edges decay to spectator satellites of SiF_4^+. The Si 2p shape resonances, in contrast to those in SF_6, do conform qualitatively to one-electron theoretical models. Finally, the S 2p asymmetry parameter for SO_2 is presented and compared with the molecular S 2p asymmetry parameters for SF_6 and SiF_4, and with 2p behavior in analogous atoms.

Table of Contents

Page

Dedication. v

Acknowledgements. vi

I. INTRODUCTION. 1

References. 8

II. EXPERIMENTAL. 9

Tables. 15

References. 16

Figure Captions 18

Figures 19

III. SULFUR 1s CORE-LEVEL PHOTOIONIZATION OF SF_6 22

A. Introduction 23

B. Experimental 27

C. Peak Contributions in the S 1s Photoemission Spectra . 30

D. The Below-Threshold S 1s-->$6t_{1u}$ Resonance. 33

1. Resonant decay channels to SF_6^+ 34

2. Resonant peak shapes and energy shifts 36

3. Sulfur (LVV)/(LLV) Auger intensity ratio 40

4. Resonant asymmetry parameters. 45

E. Above the S 1s Threshold 48

1. The 2507-eV resonances and S 1s satellites 49

2. High-energy features 52

Page

F. Conclusions. 60

Tables. 63

References. 69

Figure captions 76

Figures 80

IV. SHAPE-RESONANT AND MANY-ELECTRON EFFECTS IN THE S 2p PHOTOIONIZATION OF SF_6. 90

A. Introduction 91

B. Experimental 95

C. The S $2p(2t_{2u})$-->$6a_{1g}$ Resonance. 97

D. Above the S 2p Main-line and Satellite Thresholds. . . 100

1. Photoelectron and Auger electron results 102

2. Discussion of the "e_g" resonance 107

E. Conclusions. 115

References. 119

Figure captions 126

Figures 129

V. RESONANCE EFFECTS ON THE INNER-VALENCE LEVELS OF SF_6 IN THE PHOTON-ENERGY RANGE 52-72 eV 139

A. Introduction 140

B. Experimental 143

C. Results and Discussion 144

Page

D. Conclusions. 146

References. 147

Figure captions 149

Figures 150

VI. LITHIUM 1s MAIN-LINE AND SATELLITE PHOTOEMISSION: RESONANT AND NONRESONANT BEHAVIOR 153

A. Introduction 154

B. Experimental 156

C. Nonresonant Results. 159

1. Branching ratios 159

2. Absolute cross sections. 162

D. Resonant Results 168

1. Theoretical background 168

2. Data analysis. 172

3. Discussion of resonant results 173

E. Conclusions. 179

Tables. 181

References. 186

Figure captions 191

Figures 194

VII. SILICON 2p AND 2s RESONANT EXCITATION AND PHOTOIONIZATION OF SiF_4 206

Page

A. Introduction 207

B. Experimental 209

C. The Si 2p continuum. 210

1. Partial cross sections 211

2. Si LVV Auger spectrum. 214

D. Discrete resonances below the Si 2p edge 217

1. The Si 2p$\rightarrow\sigma^*(a_1)$ resonances. 217

2. Higher Resonances: qualitative results 222

E. Si 2s excitations. 225

F. Conclusions. 227

Tables. 230

References. 233

Figure captions 236

Figures 239

VIII. PHOTOELECTRON ASYMMETRY PARAMETER FOR THE S 2p LEVEL of SO_2: A ONE-DIMENSIONAL BARRIER CASE 247

References. 252

Figure captions 255

Figures 256

Dedication

This thesis is dedicated to my grandparents,

Helen and Clyde Neibarger.

Acknowledgements

Many people have contributed scientifically and otherwise to the work presented in this thesis. Dave Shirley has provided me with the freedom to pursue my interests, a privilege I value more than he may realize. His advice, perspective, and encouragement have always been welcome. During my undergraduate days at Grinnell, Luther Erickson and Robert Cadmus taught me to enjoy chemistry and physics, respectively. Their influence has been and continues to be significant.

My two collegues, Dennis Lindle and Phil Heimann, have contributed most to the scientific content in this work by providing excellent experimental help and discussions throughout the last five years. Other visitors and students who assisted with experiments were M. Novella Piancastelli, Hans Kerkhoff, Uwe Becker, Jane Medhurst, ShiHong Liu, Zahid Hussain, and Bill Brewer. Early guidance from Paul Kobrin, Carlton "Trues" Truesdale, and Steve Southworth is appreciated. Finally, a special thanks to Joe Dehmer, whose thoughtful scientific and personal advice I will continue to value.

The scientific and technical staff at SSRL helped in many crisis situations to keep experiments running. Thanks to Brad Pate, Piero Pianetta, Anne Waldhauer, Mike Rowan, and the SSRL operators. And of course, Hobee's breakfasts made life at Stanford much more bearable.

The Shirley group as a whole has been a source of general scientific support- and lots of fun.

A special thanks to my friends at Berkeley (and from Grinnell)- Cindy, Kim and Paul, Lou, Susan, Wini, and of course... Dennis.

I thank my family, and especially my parents, for their encouragement, patience, support, and love.

I. Introduction

Photoelectron spectroscopy is one of the most direct methods for probing the electronic structure of atoms and molecules. The photoionization process can be represented as:

$$h\nu + A \longrightarrow A^+ + e^- (l) \quad , \tag{1}$$

where $h\nu$ is the ionizing photon, A and A^+ are the neutral and ionized atoms or molecules, and l designates the photoelectron angular momentum wave. Energy conservation leads to the formulation:

$$E(h\nu) = E_B + K.E. \quad , \tag{2}$$

where $E(h\nu)$ is the energy of the incident radiation, E_B is the binding energy for ionizing an electron in a bound orbital B, and K.E. is the kinetic energy of the ionized electron. From Koopmans' theorem, the binding energy is equal in magnitude to the one-electron orbital energy.[1] Thus, this one-electron picture provides for a photoelectron spectrum with information about the orbital energy levels in atoms and molecules, with a peak appearing for each quantized level.

Compared with energy information, the dynamics of the photoemission process are much more sensitive to the initial and final state wavefunctions, and to more subtle effects of electron

correlation and resonant processes. Variation of the incident photon energy, $h\nu$, is thus a powerful tool for studying energy-dependent properties of the photoelectric process. Synchrotron radiation has been used as the photon source in this work, where we measure two key properties of the emitted photoelectron:

1) the ionization probability, or cross section (σ), for a given electron.
2) the electron angular distribution asymmetry parameter (β).

Yang's theorem[2] describes the differential cross section, in terms of these properties, assuming linearly polarized light and the dipole approximation:

$$\frac{d\sigma(h\nu,\theta)}{d\Omega} = \frac{\sigma(h\nu)}{4\pi} [1 + \beta(h\nu)P_2(\cos\theta)], \quad (3)$$

where $\sigma(h\nu)$ and $\beta(h\nu)$ are the partial cross section and asymmetry parameter as functions of photon energy $h\nu$, θ is the angle between the photon polarization vector and the electron emission direction, and $P_2(\cos\theta)$ is the second Legendre polynomial equal to $1/2[3\cos^2\theta - 1]$. The photoelectron peak intensites are measured at two angles ($\theta=0^\circ$ and 54.7°), yielding both $\sigma(h\nu)$ and $\beta(h\nu)$. The asymmetry parameter has a dynamic range of -1 to 2, based on the requirement that $\sigma \geq 0$.

The angle-independent cross section is determined at $\theta=54.7^\circ$

[where $P_2(\cos\theta)=0$] and can be expressed as a dipole amplitude connecting the ground and continuum states:

$$\sigma(h\nu) \sim |\langle \psi_i | \vec{r} | \psi_{ion}\, \psi_{\epsilon l} \rangle|^2 \quad , \tag{4}$$

where ψ_i, ψ_{ion}, and $\psi_{\epsilon l}$ are the wavefunctions for the initial, ionic, and continuum electron states, respectively, and $\vec{r}$ is the dipole operator for photoionization. Accurate theoretical modelling of the cross section depends on the details of all the pertinent wavefunctions.

More specifically, each wavefunction ψ can be described as a linear combination of configurations ψ_i, usually with a single dominant component:

$$\psi = \sum_i a_i \psi_i \quad . \tag{5}$$

The transition integral for $\sigma(h\nu)$ shown in Eq. (4) can in some cases be significantly influenced by the smaller configuration admixtures in ψ. In this way experimental determination of σ can indicate the importance of configuration interaction (CI) in the neutral and ionized systems.

The asymmetry parameter provides additional information on the amplitude and phase of the wavefunctions. For simple atomic systems, Cooper and Zare derived the β-expression for ionization of an electron in the l state (s, p, d, etc.):[3]

$$\beta = \frac{l(l-1)R_{l-1}^2 + (l+1)(l+2)R_{l+1}^2 - 6l(l+1)R_{l-1}R_{l+1}\cos(\delta_{l+1} - \delta_{l-1})}{(2l+1)[lR_{l-1}^2 + (l+1)R_{l+1}^2]} \quad (6)$$

Here $R_{l\pm1}$ are transition dipole amplitudes for the l-1 and l+1 photoelectron waves:

$$R_{l\pm1} = \langle \psi_i | \vec{r} | \psi_{ion} \psi_{\epsilon(l\pm1)} \rangle . \quad (7)$$

The δ's are partial wave phase shifts. The expression in Eq. (6) does not apply to molecular photoionization, where a whole range of l waves are produced by scattering off the anisotropic molecular potential. It does illustrate qualitatively that the β is generally dependent on the photoelectron wave phase shifts and transition dipole amplitudes.

Returning to the issue of electron correlation, breakdown of the one-electron picture can be seen most directly by the appearance of "satellite" lines in the photoelectron spectrum.[4] These peaks lie to the high binding-energy side of the expected "parent", or main-line, peak and heuristically result from primary ionization and excitation of a second electron from a bound orbital to a higher level. Though much successful theoretical work has been reported on the σ and β for main-line photoemission, very little is known about how to model the intensities of these correlation satellites. It was recently shown in helium that strong CI in the continuum wavefunctions was necessary for an accurate description of the intensities for the

$He^+(2s)$ and $He^+(2p)$ satellites.[5] The goal of much of this research is to understand the behavior of these valence and core-level satellites in atoms (Li) and molecules (SF_6 and SiF_4).

In general, much of the current interest in gas-phase core-level photoabsorption and photoionization has been directed towards the following processes:

I. Autoionization: resonant excitation to a discrete state (of molecular orbital or Rydberg character) leading up to an ionization threshold.[6]

II. Continuum Shape Resonances (also termed near-edge structure): resonant excitation into quasibound continuum states created by a centrifugal barrier in the effective atomic or molecular potential for the emitted electron.[7]

III. EXAFS (extended x-ray absorption fine structure): a nonresonant interference effect over a broad energy range (several hundred eV) related to single back-scattering off adjacent atoms; only molecules exhibit this phenomenon.[8]

Autoionization (process I) involves excitation to a discrete state embedded in one or more ionization continua. There are two indistinguishable pathways to the same final state: autoionization via the discrete state and direct ionization. Thus, in analogy to the

simple two-slit problem,[9] interference effects (i.e. resonant profiles) appear in the σ and β for the affected continuum levels. Autoionization is inherently a multi-electron process, and is therefore a sensitive probe of the extent of CI in the wavefunctions. Chapters III, IV, VI, and VII involve experiments on autoionizing resonances.

Continuum shape resonances (process II) arise from the sensitive interplay of attractive (Coulombic) and repulsive (centrifugal) forces on the perimeter of the atom or molecule. A barrier probably no greater than 30 eV in height can be present in the effective potential for a photoelectron of a given l, temporarily trapping it in a quasibound state. This is analogous to the simple barrier problem presented in most quantum mechanics texts.[10] To date, most theoretical work has described this effect at a one-electron level. Chapters III, IV, V, VII, and VIII contain data on continuum shape resonances; these resonances have been studied in a variety of molecules including SO_2, SiF_4, and SF_6.

Finally, EXAFS (process III) has been used extensively to determine bond distances in molecules of all sizes. It arises from the interference between the direct photoelectron wave and the back-scattered wave, which occurs at all energies. This nonresonant effect produces relatively small oscillations in the σ (usually less than 25 percent) and β. The back-scattering is primarily off the nucleus and core electrons of the adjacent atom. Chapter III reports on EXAFS oscillations above the S 1s edge of SF_6.

One can think of these three process as probes of different parts of the atomic or molecular potential, with each process sensitive to the portion of the potential important for the interaction. Autoionization involves promotion of an electron into a bound orbital in the potential well of the excited state. Shape resonances arise from interaction with a centrifugal barrier, and EXAFS samples the repulsive wall of the potential (nucleus and core electrons) at very high kinetic energy.

Some of the most notable contributions of this work relate to several experiments which challenge the historical descriptions of autoionization, shape resonances, and EXAFS. In particular, Chapt. III reports on the S 1s photoemission of SF_6, where large oscillations in σ(S 1s) are found to be inconsistent with both shape-resonant (process II) and single-scattering EXAFS behavior (process III). In this respect, sulfur K-edge ionization in SF_6 bridges the gap between these effects, perhaps suggesting that there is an intermediate kinetic-energy regime where interactions with both the core potential and the more diffuse electronic cloud should be considered.

Another interesting example can be found in the S 2p ionization of SF_6 (Chpt. IV) where a continuum shape resonance exhibits strong multi-electron effects in its decay. These results connect the above threshold properties of one-electron shape resonances (process II) to the discrete multi-electron decay of autoionizing states (process I). There has been only one theoretical attempt to include many-electron effects in the description of shape resonances.[11]

References

1. T. Koopmans, Physica 1, 104 (1933).
2. C.N. Yang, Phys. Rev. 74, 764 (1948).
3. J. Cooper and R.N. Zare, J. Chem. Phys. 48, 942 (1968).
4. For examples see U. Gelius, J. Electron Spectrosc. 5, 985 (1974).
5. See D.W. Lindle, T.A. Ferrett, U. Becker, P.H. Kobrin, C.M. Truesdale, H.G. Kerkhoff, and D.A. Shirley, Phys. Rev. A 31, 714 (1985) and experimental and theoretical references therein.
6. First described by U. Fano, Phys. Rev. 124, 1866 (1961).
7. J.L. Dehmer in Resonances in Electron-Molecule Scattering, van der Waals Complexes, and Reactive Chemical Dynamics, edited by D.G. Truhlar (American Chemical Society, Washington, D.C., 1984); J.L. Dehmer, D. Dill, and A.C. Parr in Photophysics and Photochemistry in the Vacuum Ultraviolet, edited by S.P. McGlynn, G. Findley, and R. Huebner (Reidel, Dordrecht, Holland, 1985); J.L. Dehmer, A.C. Parr, and S.H. Southworth in Handbook on Synchrotron Radiation, Vol. II, edited by G.V. Marr (North Holland, Amsterdam, 1986).
8. P.A. Lee, P.H. Citrin, P. Eisenberger, and B.M. Kincaid, Rev. Mod. Phys. 53, 769 (1981).
9. C. Cohen-Tannoudji, B. Diu, and F. Laloë, Quantum Mechanics (Hermann, Paris, France, 1977), p. 11.
10. For example G. Baym, Lectures on Quantum Mechanics (Benjamin/Cummings, Reading, MA, 1966), pp. 208-211.
11. J.A. Stephens and D. Dill, Phys. Rev. A 31, 1968 (1985).

II. Experimental

All of the measurements presented in this thesis utilized synchrotron radiation at the Stanford Synchrotron Radiation Laboratory (SSRL) for photoionization of effusive jets of gas or metal vapors. Two angle-resolved time-of-flight (TOF) electron detectors were placed at 0° and 54.7° with respect to the photon polarization. Relative cross sections (σ) and asymmetry parameters (β) were obtained using Yang's theorem [see Chpt. I, Eq. (3)]. Figure 1 shows schematically the experimental scheme. The photon source, the electron detectors, and some other miscellaneous aspects of the experiment are discussed below. Many of the experimental details have been addressed elsewhere.[1-3]

Synchrotron radiation has a number of properties[4] which make it ideal for photoemission studies: a continuous energy spectrum, high photon polarization, and (at SSRL) good time structure (300 psec pulses every 200-780 nsec). First, the linear polarization of the light makes the determination of electron angular distributions (β) more sensitive than measurements with unpolarized or partially polarized radiation. This sensitivity results from modification of Yang's theorem [Chpt. I, Eq. (3)] where the constant multiplier for β is most favorable for linearly polarized light.

Many experimental systems for photoionization include a device for measuring the beam polarization.[5] Perhaps one of the shortcomings of our apparatus is the lack of a polarization

measurement. However, our calibration procedure with rare gases is to a large extent self-correcting for small deviations from complete linear polarization. For example, with 85 percent polarized light and for $\beta=1$, the absolute error induced in β is only 0.03.

Of course the most attractive property of synchrotron radiation is the continuum of photon energies emitted by electrons accelerating at relativistic speeds. Photons in the range of 50-2600 eV were used for the core-level ionization work presented here. Specifically, two monochromators were utilized at SSRL. Most of the experiments (Chpts. 4-8) were performed on a grazing incidence "grasshopper" monochromator on Beamline III-1 which operates with holographically ruled gratings (300, 600, and 1200 l/mm), interchangeable in vacuum.[6] This monochromator covers the photon energy range from 50-1000 eV. However, resolution at the higher energies is poor; for example, at the carbon K edge (290 eV) and with open entrance and exit slits (200μ), the bandpass is at best 9 eV. As a result, all of the work reported here was done below 300 eV. Between 50 and 100 eV, the resolution varies between 0.3 and 1.0 eV for open slits. Reduction of the slit size (and the photon flux) to as little as 10μ is possible for high resolution work. The monochromator bandpass for experiments described here can be found in the appropriate chapter. A refocussing mirror located after the grating reduces the beam spot size in our interaction region to ~1 mm high and ~2mm wide, with a depth of focus of about 6 inches.

A second double-crystal monochromator (termed "JUMBO") on

Beamline III-3 operates in the soft x-ray regime of 800-4500 eV.[7] For one of the SF_6 experiments (Chpt. III), Ge(111) crystals were used with a bandpass of ~2.4 eV FWHM.

It is necessary to monitor the photon-beam intensity for normalization of partial cross sections. This was accomplished on JUMBO by detecting the total electron yield of graphite using a channeltron placed at the back of the sample chamber. On the "grasshopper", sodium salicylate (Nasal) was used as a scintillator[8] by measuring the fluorescent photons with a photomultiplier tube (RCA 8850). Recent measurements[9] show that the salicylate response increases at higher photon energy; this correction has been applied to the cross sections reported in Chpts. IV and VII. Other groups[10] have measured the Nasal quantum yield versus photon energy, observing the same qualitative increase with energy. However, the relative increase seems to vary significantly from one system to another. Thus, we believe our calibration for the Nasal response[9] (which has been confirmed by repeated measurements) is suitable for our system, but may not apply to the apparatus of other workers.

The gas samples were introduced into the sample chamber with an efffusive source mounted on an XYZ manipulator. A microchannel plate with either 5 or 10μ pores of 1mm in length served to collimate the gas jet and enhance the forward intensity relative to a simple effusive source. Backing pressures of 1-100 torr were monitored with a capacitance manometer at the exit of a separate gas manifold. A leak valve regulated the gas pressure at a constant value typically to

within 2 percent. For the Li experiment (Chpt. VI), a metal vapor oven[11,12] constructed of molybdenum was used to produce an effusive beam. A liquid nitrogen cold finger was situated directly opposite the metal vapor beam. The metal vapor relative pressure could not be monitored directly, so a reference spectrum at a given photon energy was repeated frequently (every 3rd spectrum). Some oven details are found in Chpt. VI. In addition, Fig. 2 shows a schematic drawing of the oven.

The unique time structure of the electron storage ring (SPEAR), with 780 nsec between pulses for parasitic running, makes time-of-flight (TOF) for electrons extremely efficient compared with traditional electrostatic detectors. Because electrons of all energies ($\geq$ 3 eV) are detected at once, the TOF analyzers are at least 100 times more efficient than electrostatic detectors, which collect only a narrow band or energies. Furthermore, the noise is distributed evenly in time, producing an excellent signal/noise ratio. Determination of the relative amounts of higher-order light ($2h\nu$, $3h\nu$, etc.) is obtained directly from the photoemission peaks, found in the TOF spectrum at high kinetic energy, created by these photons. The efficiency of TOF detection increases with the complexity of the spectrum and is best suited for studies on low kinetic-energy electrons, where the analyzer resolution is optimized. The time resolution is limited mostly by the dimensions of the interaction region (defined by the photon beam and analyzer aperatures). Electrons originating at opposite sides of the beam contribute to this

time difference, which is constant in time but increases with kinetic energy (K.E.) since

$$T = CL/(K.E.)^{1/2} \quad , \tag{1}$$

where T is the flight time, L is the length of the flight path (~28 cm), and C is a constant.

The electron TOF detectors have a fairly simple design in vacuum and contain a Chevron channel plate assembly for multichannel detection.[13] Figure 3 displays the detector timing scheme with electronics. The electron serves as the "start" and the photon pulse as the "stop". There is capability for retarding and acceleration over a portion (~20 cm) of the flight path. Each detector collects a solid angle of $\pm 3^{\circ}$. For the metal vapor experiment on Li (Chpt. III), an additional retarding grid was mounted at the front of each detector. In this way, a constant 2 volts was applied to cut off the low-energy thermally produced electrons.

Very thin windows (1000-1500 Å) of Al, Si, and C were obtained from Luxel Corporation and used to isolate the UHV monochromators (10^{-10} torr) from the typical running pressures in our gas chamber (10^{-5} torr).

During the course of my graduate work, many students, postdocs, and visitors helped on the various experimental runs. Table I lists the TOF runs, gas samples, and participants. In particular, some of the experiments on runs TOF-19 and later (not reported here) utilized

a threshold electron detector (TEA) constructed by Phil Heimann. SSRL runs typically lasted for 2-3 weeks, with 24 hour running covered by 2 or 3 shifts with 2 experimenters per shift. Dedicated running was in the 4x1 timing mode (four equally spaced electron bunches giving 195 nsec spacing between pulses), with ring currents averaging 40 mA. Parasitic running consisted of 1 bunch of electrons in the ring (for 780 nsec pulse spacing) and typical currents of 10 mA or less.

Table I: Record of SSRL runs.

TOF run	Beamline	Dates	Samples	Participants[a]
14, D [b]	4°	Dec. '82-Jan. '83	Ne, Li, SF_6, Sm, Tm	TAF, PAH, DWL, PHK, HBK, UB, WB
15, P	4°, JUMBO	March-April '83	SO_2, Ar, SF_6, Ne	TAF, PAH, HGK, UB
16, D	JUMBO	June '83	Ar, SF_6, Hg, Ne, Eu	TAF, PAH, HGK, UB, DWL, ZH
17, D	4°	April '84	Xe, Kr, SF_6, He, Li	TAF, PAH, DWL
18, P	4°	Nov.-Dec. '85	TEA (diagnostics)[c]	PAH, TAF, MNP, DWL
19, D	4°	Feb. '85	He, Ne, Xe, H_2O, Kr, CO, SiF_4	TAF, PAH, DWL, MNP, CEB
20, D	4°	May-June '85	Kr, Ne, He, SF_6	PAH, TAF, DWL,
21, P	4°	Nov. '85-Jan. '86	Ar, Kr, Ne, SF_6, He	PAH, SHL, LJM, DWL, TAF
22, D	4°	June '86	C_6H_6, CO, Ar, C_2H_4, N_2, SF_6	LJM, SHL, PAH, TAF, DWL

a TAF=Trish Ferrett, PAH=Phil Heimann, DWL=Dennis Lindle, HGK=Hans Kerkhoff, UB=Uwe Becker, WB=Bill Brewer, ZH= Zahid Hussain, LJM=Jane Medhurst, SHL=Shi Hong Liu, CEB=Chris Brion.

b P and D stand for parasitic and dedicated running, respectively.

c Threshold electron anlayzer (TEA) constructed by PAH used for experiments on TOF-19 and later.

References

1. M.G. White, R.A. Rosenberg, G. Gabor, E.D. Poliakoff, G. Thornton, S. Southworth, and D.A. Shirley, Rev. Sci. Instrum. 50, 1288 (1979).
2. S. Southworth, C.M. Truesdale, P.H. Kobrin, D.W. Lindle, W.D. Brewer, and D.A. Shirley, J. Chem. Phys. 76, 143 (1982).
3. S.H. Southworth, U. Becker, C.M. Truesdale, P.H. Kobrin, D.W. Lindle, S. Owaki, and D.A. Shirley, Phys. Rev. A 28, 261 (1983).
4. H. Winick and S. Doniach, Synchrotron Radiation Research (Plenum Press, New York, 1980), Chpts. 2 and 3.
5. See for example A.C. Parr, R. Stockbauer, B.E. Cole, D.L. Ederer, J.L. Dehmer, and J.B. West, Nucl. Instrum. Meth. 172, 357 (1980).
6. B.B. Pate, Ph.D. Thesis, Stanford University, 1984.
7. Z. Hussain, E. Umbach, D.A. Shirley, J. Stöhr, and J. Feldhaus, Nucl. Instrum. Meth. 195, 115 (1982).
8. J.A.R. Samson and G.N. Haddad, J. Opt. Soc. Am. 64, 1346 (1974).
9. D.W. Lindle, T.A. Ferrett, P.A. Heimann, and D.A. Shirley, Phys. Rev. A 34, 1131 (1986).
10. J. Nordgren and R. Nyholm (private communication); J.A.R. Samson (private communication).
11. P.H. Kobrin, Ph.D. Thesis, University of California, Berkeley, 1983.
12. P.H. Kobrin, U. Becker, S. Southworth, C.M. Truesdale, D.W. Lindle, and D.A. Shirley, Phys. Rev. A 26, 842 (1982).

13. J.L. Wiza, Nucl. Instrum. Meth. 162, 587 (1979).

Figure Captions

Fig. 1 A schematic of the experimental apparatus, including the synchrotron radiation photon source, monochromator (MONO), and TOF electron detectors. The time structure of the photons during parasitic time is also displayed.

Fig. 2 The metal vapor oven. The labelled parts are: 1) molybdenum sample cup which holds about 3.5 ml and has an inner diameter of 10 mm, 2) the molybdenum oven body, 3) resistive heating coils, 4) alumina heat shields, and 5) nozzle and part of the skimmer arrangement.

Fig. 3 Timing diagram and electronics for TOF electron detection. A=1M Ω. B=422k Ω. C=1M Ω. D=619 k Ω. E=750 k Ω. CS=ceramic spacer. MCP=40 mm nonimaging quality microchannel plate. DC=decoupling capacitor. CA=coaxial anode. DT=decoupling transformer. CFD=constant fraction discriminator. ATTN=attenuator. DD=differential discriminator. TAC=time-to-amplitude converter. PHA/MCA=pulse height analyzer and multichannel analyzer.

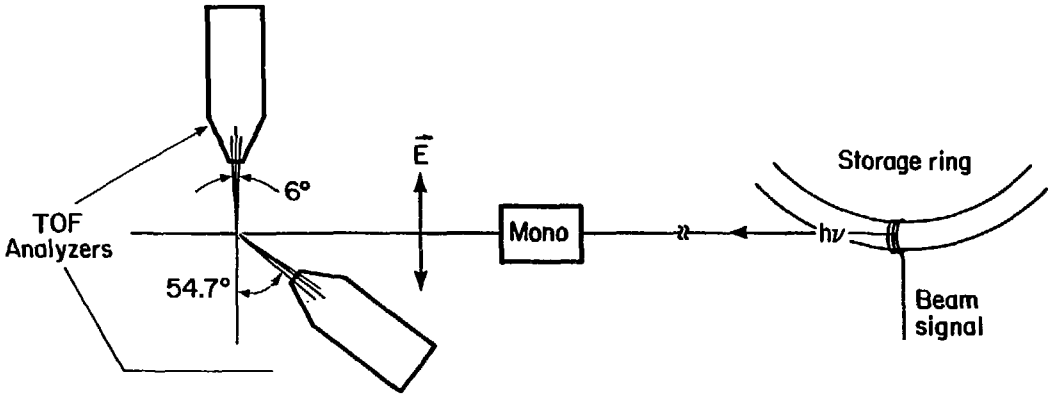

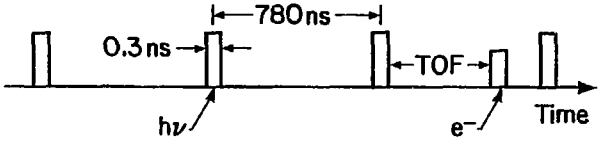

XBL 7910-4225

Figure 1

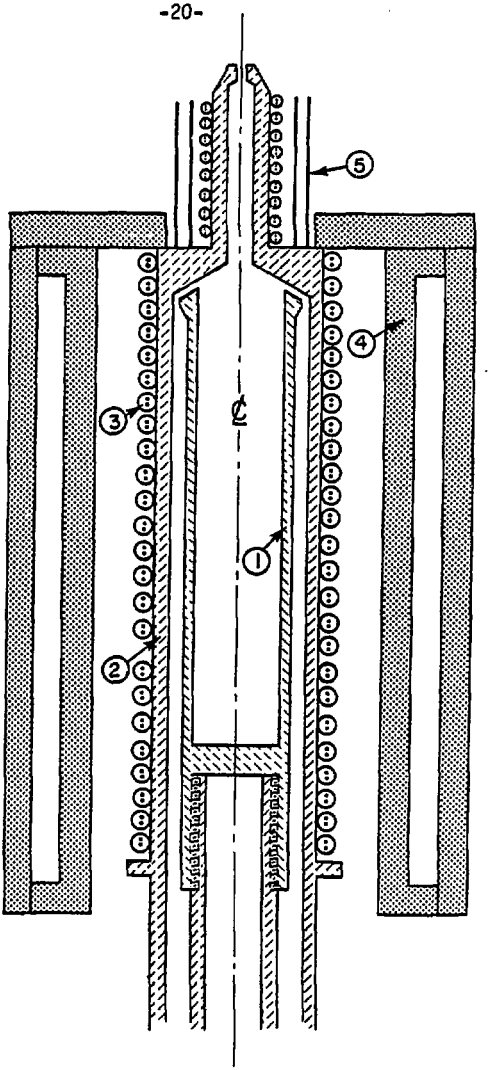

XBL 819-2499

Figure 2

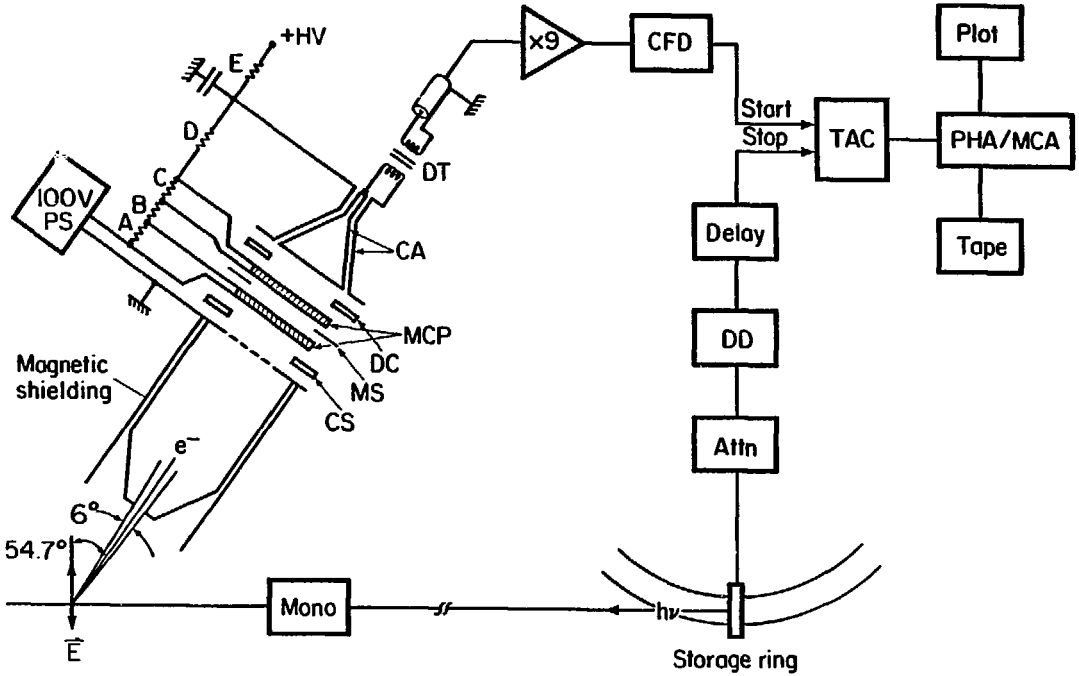

Figure 3

XBL 792-619

III. Sulfur 1s Core-level Photoionization of SF_6^*

Abstract

Photoelectron spectra have been taken between 2460 and 2600 eV photon energy across the discrete and continuum resonances in the vicinity of the sulfur K edge in gaseous SF_6. Results at the below-threshold S 1s-->$6t_{1u}$ resonance indicate that "highly excited" S 2p and S 2s satellites (with two core holes) are the primary autoionization final states of SF_6^+. An observed asymmetric profile in the S(LVV) Auger angular distribution suggests interference effects in the alignment of these resonantly produced SF_6^+ ions. Decay of the low-energy S 1s continuum resonances near 2507 eV photon energy into S 2p, S 2s, and/or valence photoemission channels indicates autoionizing character. These features are assigned as doubly excited states, leading to S 1s satellite thresholds observed here for the first time. At higher photon energies, between 2520 and 2570 eV, large oscillations in the S 1s cross section are reproduced well by MSM-$X\alpha$ calculations, but are not explained adequately by single-scattering plane-wave extended X-ray absorption fine structure (EXAFS) effects. We speculate that improvements in the description of both the electron-scattering process and the molecular potential are necessary to model the diffractive and nondiffractive (barrier interaction) effects in this energy region.

A. Introduction

When the first gas-phase photoabsorption measurement near the sulfur K edge in SF_6 (reproduced in Fig. 1) was published in 1966, the appearance of the spectrum was described as being "unusually rugged" from the S 1s threshold (2490 eV) up to about 2570 eV photon energy.[1] Several years later, a line-up of the S 1s, S 2p, and F 1s core-level photoabsorption spectra of SF_6 referenced to their respective ionization thresholds revealed an interesting correlation of the resonant features in kinetic energy to within a few eV.[2,3] This correlation led to the assignment of continuum features in these spectra as e_g and t_{2g} shape resonances,[3,4] and in particular suggested that some of the "rugged" continuum features in the S 1s spectrum were related to potential-barrier effects.

Theoretically, there have been major advances in the basic understanding of potential-barrier effects in atoms[5-8] and, initially with the application of the multiple-scattering method (MSM-Xα), in molecules.[9-15] In a simple one-electron model, a shape resonance is a pure final-state effect. It should thus occur at approximately the same kinetic energy for different core levels of a given molecule. The continuum electron can be pictured as being trapped temporarily by a centrifugal barrier, producing a resonance at a kinetic energy roughly comparable to the barrier height. The large observed photoabsorption intensities of discrete states also fit into this scheme; the unusual potential can enhance the discrete molecular

orbital transitions at the expense of Rydberg excitations and nonresonant continuum intensity. Because the core-level spectra of SF_6 exhibit strong resonances that have been associated with an unusually high potential barrier,[3,4] SF_6 has become a prototypical example of potential-barrier effects and shape resonances.[16]

The present assignments for the S 1s absorption spectrum of SF_6 shown in Fig. 1 are as follows. We use the letter assignments in Fig. 1 throughout the paper to refer to features "a" through "g". The interpretation of the only intense below-threshold resonance (b) as a discrete excitation of a S 1s electron to the unoccupied $6t_{1u}$ level is straightforward.[3] The SF_6 energy-level diagram in Fig. 2 illustrates this transition. For the S 1s continuum, the shape-resonance model was used to assign two features at ~2493 (c) and 2506 eV (d) photon energy.[3] However, this interpretation is not so straightforward because these transitions [S $1s(1a_{1g})$-->t_{2g}, e_g] are symmetry-forbidden in the simple shape-resonance picture.[3] Furthermore, we note that assignment of resonance features based solely on photoabsorption data can be uncertain; effects due to satellite continua and doubly excited resonances may not be distinguishable from those caused by continuum shape resonances.[17,18] Finally, the nature of the higher-energy features (f and g) remains unexplained.

To examine in more detail the core-level excitation of the "classic" potential-barrier molecule, we undertook a gas-phase photoemission study of the features near the sulfur K edge of SF_6

using synchrotron radiation and time-of-flight electron analysis. By investigating the behavior of the individual photoemission channels, we hoped to ascertain the nature of the "rugged" continuum structure and the autoionization decay characteristics of the S 1s-->$6t_{1u}$ discrete resonance. No other photoemission measurements have been reported on the S and F core levels in SF_6, but related gas-phase[19,20] and condensed-phase[21] photoemission experiments on the outer-valence orbitals in the photon-energy range 10-54 eV have been reported. These low-photon-energy results show that the assigned t_{2g} shape resonance exhibits unusual behavior by coupling to neighboring symmetry-forbidden valence channels.[19-21] In addition, the lack of evidence for the e_g shape resonance in the valence subshells remains puzzling.

Related core-level photoemission results in other molecules include recent studies of autoionization below the carbon and nitrogen K edges of CO and N_2. These studies have revealed interesting decay channels leading to singly-charged ions, identified by peaks termed "spectator" satellites.[22-25] The dominance of these channels is rationalized as follows. A core-level electron is promoted to an unoccupied molecular orbital and remains as a spectator while the remaining electrons decay, with one electron filling the core hole and a second electron being ionized.[24,26] The singly-charged ion configurations thus produced contain an excited electron and <u>two</u> valence holes; these final states are therefore valence satellites. This autoionization decay of the excited neutral in some cases may

parallel the Auger decay of the corresponding ion with the excited electron removed.

We observe similar "spectator" satellite decay channels at the S 1s($1a_{1g}$)-->$6t_{1u}$ excitation (b) below the S 1s threshold of SF_6. The satellites produced contain S 2p and/or S 2s vacancies. In addition, the subsequent relaxation of the resonantly produced SF_6^+ ions via Auger decay of the L holes permits the measurement of the Auger electron cross sections and, of more interest, the angular distribution asymmetry parameter β. We report the first measurement of the angular distribution of Auger electrons from an ion produced by an autoionization process. Autoionization can produce aligned +1 ions, and the subsequent Auger decay can retain some memory of this alignment, which may affect the Auger β.[27] No previous angular-distribution measurements have been performed at photon energies high enough such that the single ions produced by autoionization are energetically able to Auger decay.

Turning to the S 1s continuum in SF_6, we have examined the resonant features in the vicinity of 2507 eV (d and e) and at higher energies (f and g). The results near 2507 eV demonstrate that these resonant states decay into channels other than the S 1s continuum (e.g. S 2p, S 2s, valence). This decay pattern, combined with the observation of S 1s correlation-satellite thresholds slightly higher in energy, suggests assignment of these features as arising from doubly excited states.

In order to explain the higher-energy effects and the large

oscillations in the cross section between 30 and 70 eV kinetic energy (f and g), the application of recent advances in extended x-ray absorption fine structure (EXAFS) theory, including spherical-wave[28-31] and multiple-scattering corrections,[28,31-35] would probably be required. In addition, we propose that the details of the molecular potential also are important for intermediate-energy electrons which can interact significantly both with the diffuse electron cloud (large r) and with the localized atomic centers (small r). Our interpretation of the S 1s continuum generally indicates that the kinetic energy region 30-100 eV is especially complicated and probably displays neither simple shape-resonance nor EXAFS behavior.

The experimental details of this work are presented in Sec. B. In Sec. C, we lay the groundwork for interpretation of the results by describing our photoemission spectra. We discuss the results for the S 1s-->$6t_{1u}$ below-threshold resonance in Sec. D, and for the S 1s continuum in Sec. E. Our conclusions appear in Sec. F.

B. Experimental

The experiment was performed at the Stanford Synchrotron Radiation Laboratory (SSRL) using photons from "JUMBO", a double-crystal monochromator operating with Ge(III) crystals on Beam Line III-3. The polarization of the photons from "JUMBO" is unknown, but probably somewhat greater than 90 percent. This uncertainty leads to an absolute error in the β values reported here of less than ± 0.05

because of our calibration procedure. Finally, though the dipole approximation is assumed valid for this experiment, deviations may occur with very high-energy photons in the keV range. However, such effects should be small for these particular measurements, where the dipole processes are strong.

Peak intensities obtained at 54.7° must be corrected for fluctuations in sample pressure and photon intensity in order to determine relative partial cross sections. The photon intensity was monitored by measuring the total electron yield of graphite with a channeltron placed at the back of the sample chamber. A 1500 Å thick Al window separated the monochromator vacuum (10^{-10} torr) from the sample-chamber pressure (10^{-4} torr), which was recorded with a capacitance manometer. We estimate that systematic errors in our relative cross section (not represented by the statistical error bars in our plots) are 10 percent or less.

Time-of-flight spectra were taken from $h\nu$=2460 to 2600 eV with a monochromator bandpass of about 2.4 eV. Energy calibration of the monochromator was accomplished by scanning over the below-threshold resonance (S 1s-->$6t_{1u}$) in SF_6 at 2486 eV.[1] The 54.7° analyzer transmission as a function of electron kinetic energy was determined using atomic argon, by comparing Ar 1s photoemission intensity to Ar LMM Auger intensity. Variations in this ratio were attributed to changes in the analyzer transmission at the kinetic energy of the Ar 1s peak. The asymmetry-parameter measurements were calibrated in the kinetic-energy range of about 7-100 eV by measuring the Ar 1s peak

at varying kinetic energies, and assuming the β(Ar 1s)=2.0. At intermediate kinetic energies (110-200 eV), the S(LVV) Auger peak was used as a calibrant by assuming arbitrarily a nonresonant β value of zero. For very high kinetic energy electrons (>1800 eV), the F 1s photoemission peak in SF_6 was used for calibration with an assumed β of 2.0.

During the experiment there were significant fluctuations in the position of the photon beam which changed the relative analyzer efficiency by as much as 20 percent and the 54.7° analyzer transmission by a factor of two. Within a set of spectra unaffected by beam movement, we observed that the intensity and asymmetry parameter for the F(KVV) Auger peak were relatively constant in the photon-energy range 2460-2600 eV. Thus, corrections were made in each spectrum for beam fluctuations using the F Auger peak as a standard. These experimental complications involving the movement of the photon beam also made calibration for the β measurements at low kinetic energies especially difficult, leading to possible systematic errors not represented by the statistical error bars shown in our asymmetry-parameter plots. We estimate that the uncertainty in the S 1s β between 2530 and 2550 eV is ±0.15. Likewise, at the lower kinetic energies (below 12 eV), the analyzer efficiency changes dramatically, also increasing the β uncertainty to ±0.15.

A representative S 1s time-of-flight spectrum is shown in Fig. 3. Count rates for the S 1s peak were 4-30 counts/sec with 1000 sec collection times. There are F 1s, S 2p, S 2s, and valence

photoemission contributions to the high energy peak A, as well as S(KLL, KLV, and KVV) Auger intensity. The relative importance of these components will be discussed in more detail in Sec. C.

C. Peak Contributions in the S 1s Photoemission Spectra

Interpretation of experimental results in Sec. D and E requires knowledge of the processes that contribute to the peaks in the S 1s photoelectron spectra. These contributions must be considered together because some of them are not resolved in our spectra. The kinetic-energy resolution in the TOF spectra is limited by time dispersion due to the finite dimensions of the photon beam, and to a lesser extent by the time resolution inherent in the time-of-flight technique. For the measurements on the JUMBO monochromator, this corresponds to ~9 percent of the kinetic energy, or as much as 180 eV at 2000 eV kinetic energy.

The TOF spectrum in Fig. 3, taken 91 eV above the S 1s threshold at 2490 eV, includes the S 1s main-line and satellite peaks, the S(LVV) Auger peak, the F(KVV) Auger peak, and peak A. Figure 4 illustrates a second spectrum taken below the S 1s threshold, showing the very weak $S(L_1L_{2,3}V)$ Auger peak. Several of the peaks in Fig. 3 arise from only one process at all photon energies used in this study. Specifically, the S 1s main-line and satellite peaks and the peak comprised of the F(KVV) Auger transitions remain well-resolved from all other peaks.

There are, on the other hand, several dissimilar components in peak A and in the S(LVV) and S($L_1L_{2,3}V$) Auger peaks. The processes that contribute to each of these observed peaks in three energy regions are listed in Table I. We define the energy ranges as follows: below the sulfur K edge, between the S 1s main-line and the first satellite threshold, and above the first S 1s satellite threshold.

Peak A has the most complicated structure because it includes all photoemission main lines and satellites with binding energies less than 700 eV. Below the sulfur K edge, the photoemission contributions to peak A are from F 1s, S 2s, S 2p, and valence main lines and satellites. Some "highly excited" S 2p and S 2s satellite configurations ($2p^{-2}v^*$, $2s^{-2}v^*$, and $2s^{-1}2p^{-1}v^*$, where the valence state v^* is probably either the $6t_{1u}$ or $6a_{1g}$ molecular orbital) also contribute to peak A in the vicinity of the S 1s-->$6t_{1u}$ resonance at 2486 eV. There is a slight double peak structure to peak A, as shown in the spectrum in Fig. 4, because the F 1s peak is at a lower kinetic energy, while the remaining resonant satellite contributions are unresolved at higher energy. Finally, as the photon energy is increased to above the S 1s main-line and S 1s satellite thresholds, the primary Auger decay from S 1s hole states produces high-kinetic-energy S(KLL, KLV, and KVV) Auger electrons which also contribute to the peak A intensity.

Below the sulfur K edge, the S($L_{1,2,3}VV$) and S($L_1L_{2,3}V$) peaks result from Auger decay of resonantly and nonresonantly

produced SF_6^+ ions ($2s^{-1}$, $2p^{-1}$, $2p^{-2}v^*$, etc...) with S 2p and/or S 2s holes, e.g.,

$$SF_6 + h\nu\ (<2490\ eV) \longrightarrow SF_6^+(2p^{-1}) + e^- \qquad (1)$$

$$SF_6^+(2p^{-1}) \longrightarrow SF_6^{2+}(2p^6 val^{-2}) + L_{2,3}VV\ \text{Auger}\ e^-.$$

The especially complicated Auger decay cascades occurring at the discrete S 1s-->$6t_{1u}$ resonance will be presented in the next section. In particular, the characteristics of the Auger decay of aligned SF_6^+ ions produced by autoionization will be discussed.

Moving above the S 1s main-line and satellite thresholds, the S(LVV) and S($L_1L_{2,3}V$) Auger peaks include the subsequent decay of S 1s hole states, e.g.,

$$SF_6 + h\nu\ (\geq 2490\ eV) \longrightarrow SF_6^+(1s^{-1}) + e^- \qquad (2)$$

$$SF_6^+(1s^{-1}) \longrightarrow SF_6^{2+}(1s^2 2p^{-2}) + KL_{2,3}L_{2,3}\ \text{Auger}\ e^-$$

$$SF_6^{2+}(1s^2 2p^{-2}) \longrightarrow SF_6^{3+}(1s^2 2p^{-1} val^{-2}) + L_{2,3}VV\ \text{Auger}\ e^-$$

$$SF_6^{3+}(1s^2 2p^{-1} val^{-2}) \longrightarrow SF_6^{4+}(1s^2 2p^6 val^{-4}) + L_{2,3}VV\ \text{Auger}\ e^-.$$

Note that in the particular example given above, it is also possible to produce a tertiary S($L_{2,3}VV$) Auger electron in the decay of

SF_6^{3+} to SF_6^{4+}. Because tertiary and occasionally quaternary Auger decay processes can occur in filling the S 2p and S 2s core holes, the observed $S(L_1L_{2,3}V)$ and S(LVV) Auger peaks will include all of these emitted Auger electrons. By writing these simple illustrative processes, we do not wish to imply that the complex Auger decay necessarily occurs stepwise. Dissociation has also been ignored in the above scheme, but will be considered later.

The reader is referred to Table I for specific peak contributions in each energy range appropriate to the discussion of results in Secs. D and E.

D. The Below-Threshold S 1s-->$6t_{1u}$ Resonance

For the S 1s-->$6t_{1u}$ resonance, the possible decay channels to SF_6^+ are described in Sec. 1. We examine in Sec. 2 the energies and shapes of peak A and the $S(L_1L_{2,3}V)$ and S(LVV) Auger peaks to deduce qualitatively the important decay channels leading to SF_6^+. We show in Sec. 3 that an analysis of the sulfur Auger cross-section ratio LVV/LLV implies a dominance of a particular single-ion resonant configuration, the $2p^{-2}v^*$ "spectator" satellite. In Sec. 4, we present asymmetry-parameter results for peak A and the LVV Auger peak in the S 1s-->$6t_{1u}$ resonance region. The observed asymmetric profile for the S(LVV) Auger β is discussed with respect to ion alignment[27] and its implications for the Auger-electron angular distribution.

1. Resonant Decay Channels to SF_6^+

At this resonance, the excited neutral state $1s^{-1}6t_{1u}$ will decay to any continua that are energetically accessible: F 1s, S 2p, S 2s, and valence main-line and satellite final states of SF_6^+.[36] The intensity in peak A below the S 1s threshold includes contributions from all of these channels. The below-threshold S $1s(1a_{1g})$-->$6t_{1u}$ resonance appears in the cross section for both peak A and S(LVV) Auger (Fig. 5). The energy-level diagram in Fig. 2 illustrates these decay channels (solid lines).

The many SF_6^+ states to which the excited $1s^{-1}6t_{1u}$ state can autoionize are listed generically in Table II. Our photoemission spectra indicate no resonant enhancement in the F 1s channel [as mirrored in the F(KVV) Auger peak], and qualitatively there is very little enhancement of peaks with binding energies below 150 eV. Therefore, we have considered only the SF_6^+ decay channels which have S 2p and/or S 2s holes. Columns 1-4 of Table II describe these available continuum channels in terms of the configurations, decay types, and approximate binding energies of the states. We use Auger notation in column 3 only to denote the <u>type</u> of autoionization decay to each SF_6^+ photoemission channel.[37]

Each available channel can be described as a S 2s or S 2p main line or satellite. The satellites can be split further into two groups. First, the S 2p and S 2s satellite configurations with binding energies about 10-40 eV above the respective main-line

thresholds have a valence electron promoted to an unoccupied molecular orbital. Decay to the main lines and to these low-excitation photoemission satellites can be viewed as KLV Auger-type transitions. Furthermore, the transition can either leave the initially excited $6t_{1u}$ electron as a spectator (KLV) or involve it as a participant (KLV^*) in the decay. In this context, decay to the main-line and some satellite channels must involve the excited $6t_{1u}$ electron, while the satellite configurations with a $6t_{1u}$ electron are "spectator" satellites. The nonresonant intensity for low-excitation-energy satellites may vary from a few percent to as much as 25 percent relative to the main-line intensity.[38]

The second class of satellites, which we shall call "highly excited" satellites, possess two core holes (S 2p and/or S 2s) and an excited electron, and have binding energies in the 350-500 eV range. The excited electron is likely to be in the $6t_{1u}$ orbital, although our limited resolution does not permit confirmation of this. These states are S 2p and S 2s satellites in the sense that they could be formed from SF_6 by core-hole ionization plus excitation from a core orbital to a $6t_{1u}$ or other valence molecular orbital. These "highly excited" satellites are produced from KLL-type decay and can also be termed "spectator" satellites if the excited electron is in the $6t_{1u}$ level. In general, we expect that "highly excited" satellites with excitation energies greater than 100 eV will have negligible nonresonant intensity.

2. Resonant Peak Shapes and Energy Shifts

Conclusions about the important decay channels of SF_6^+ in the vicinity of the S 1s-->$6t_{1u}$ resonance can be drawn by examining the structure of peak A with reference to Table II. Off resonance (2460 - 2470 eV), we find that peak A consists of a F 1s peak with a binding energy of ~700 eV and a second much less intense peak with a binding energy of approximately 200 eV. This lower binding-energy peak is composed primarily of S 2p and S 2s main lines, with probable small contributions from low-excitation-energy satellites and valence peaks. At 2486 eV (on resonance), peak A appears as a single intense peak with a binding energy of 400(50) eV. The shape of the peak indicates very little intensity at binding energies less than 200 eV. The F 1s peak in Fig. 4 can be seen, partly resolved from the more intense contributions at binding energy ~400 eV. We conclude directly from the above qualitative observations that "highly excited" satellites produced by KLL-type transitions are the most important autoionization decay channels for the S 1s-->$6t_{1u}$ resonance.

Another indication that the photoemission channels of SF_6^+ change at the S 1s-->$6t_{1u}$ resonance energy can be found in the kinetic-energy shift of the S(LVV) and S(LLV) Auger peaks. The kinetic energies of these broad peaks are higher on resonance than off resonance. Some additional structure on the high kinetic-energy side of the S(LVV) Auger peak also is observed on resonance. The size of the overall energy shift strongly suggests the accessibility of some

new SF_6^+ states other than the S 2p and S 2s main lines. The fact that the shift is to higher kinetic energy is qualitatively rationalized below to be consistent with production of "highly excited" ions.

As an example, we consider the $S(L_{2,3}VV)$ Auger decay of SF_6^+ to SF_6^{2+} for the single-ion configurations with 2p holes postulated to be important off and on resonance, e.g.,

$$\text{off: } SF_6^+(2p^{-1}) \longrightarrow SF_6^{2+}(2p^6 val^{-2}) + \text{LVV Auger } e^-, \tag{3}$$

$$\text{on: } SF_6^+(2p^{-2}6t_{1u}) \longrightarrow SF_6^{2+}(2p^{-1}val^{-2}6t_{1u}) + \text{LVV Auger } e^-. \tag{4}$$

The kinetic energies (ε) of the S(LVV) Auger electrons in processes (3) and (4) are just the differences in energy between the ions:

$$(\varepsilon_{LVV})_{off} = E(2p^{-1}) - E(2p^6 val^{-2}), \tag{5}$$

$$(\varepsilon_{LVV})_{on} = E(2p^{-2}6t_{1u}) - E(2p^{-1}val^{-2}6t_{1u}). \tag{6}$$

The observable kinetic-energy shift ($\delta\varepsilon$) can be defined as:

$$\begin{aligned}\delta\varepsilon &= (\varepsilon_{LVV})_{on} - (\varepsilon_{LVV})_{off} \\ &= [E(2p^{-2}6t_{1u}) - E(2p^{-1})] - \\ &\qquad [E(2p^{-1}val^{-2}6t_{1u}) - E(2p^6 val^{-2})] \\ &= [E_1] - [E_2].\end{aligned} \tag{7}$$

The energies E_1 and E_2 both correspond superficially to the energy for promotion of a S 2p electron to a $6t_{1u}$ orbital, but E_1 is expected to be greater than E_2 because it requires more energy to remove a molecular core electron (i.e. 2p) from its orbital in the presence of another core hole than in the presence of one or two diffuse holes in the valence shell, due to differences in screening. This clearly would suggest that E_1 is greater than E_2. However, the difference in the energy of the $6t_{1u}$ level in the two configurations $2p^{-2}6t_{1u}$ and $2p^{-1}val^{-2}6t_{1u}$ also must be considered.[39] Because the $6t_{1u}$ orbital is least tightly bound, the dominant effect on its binding energy should be the Coulomb interaction, which is proportional to the ionic charge. Thus, the $6t_{1u}$ orbital in the $SF_6^{2+}(2p^{-1}val^{-2}6t_{1u})$ configuration will experience a larger contraction than in the $SF_6^{+}(2p^{-2}6t_{1u})$ configuration, with the result that E_2 would be smaller than E_1. We conclude that $\delta\epsilon$ is positive for the initial Auger decay of 2p hole states [processes (3) and (4)].

This positive shift for $\delta\epsilon$ is in contrast to a shift to lower kinetic energy for Auger satellite transitions from 2-hole initial states to 3-hole final states.[40] However, the initial state for many Auger satellites has the second hole "exterior" to the deepest hole (e.g. KL-LLL in Ne).[41] The major effect in this case is an increased binding energy for the outer electrons which fill the core, resulting in a lower Auger kinetic energy relative to the "parent" KLL line. For Auger decay of SF_6^{+} $(2p^{-2}6t_{1u})$, the second 2p hole

is in the same shell as the deepest hole, significantly affecting the screening in the core shell as well as in the valence shells.

The presence of Auger electrons from subsequent cascades to higher SF_6^{n+} ions (n=3-5) significantly complicates the above discussion. Autoionization to "highly excited" satellites results in ions with two L-shell core holes, thus allowing for several Auger cascades. The secondary and higher Auger decay steps produce electrons with kinetic energies different from the primary Auger electron due to core and valence screening differences and the degree of involvement of the excited $6t_{1u}$ electron. The additional structure in the S(LVV) Auger peak may arise from such effects. Further explanation of these issues will be warranted when higher resolution spectra become available.

As further support for the importance of the resonant SF_6^+ "highly excited" satellite channels and subsequent Auger cascades, we can compare the S(LVV) Auger peak observed at the S 1s-->$6t_{1u}$ resonance with the S(LVV) peak observed above the S 1s threshold. We find that the S(LVV) peak shapes are very similar in these two cases. The primary contributions to the S(LVV) peak above the S 1s threshold (see Table I) must be from secondary and higher-order Auger decay following S 1s ionization, because sulfur K-shell ionization is stronger at these energies than the sulfur L-shell ionization processes. Furthermore, the initial Auger decay of the S 1s hole will be mostly KLL because the S 2p and S 2s orbitals (more than F 1s and valence) reside on the sulfur atom, providing good overlap with the

S 1s orbital. This result for the initial decay step also can be deduced by comparison with Ar,[42] and shows that higher-order Auger decay from SF_6^{2+} starts primarily from configurations with two holes in the sulfur L shell ($2p^{-2}$, $2s^{-1}2p^{-1}$, and $2s^{-2}$). Still another way to reach the same conclusion is to note that KLL decay is the principle de-excitation process in light elements. The similarity of the S(LVV) peaks above and below threshold indicates that configurations with two L-shell holes (e.g. $2p^{-2}6t_{1u}$) probably provide important decay channels for the S 1s-->$6t_{1u}$ resonance.

3. Sulfur LVV/LLV Auger Intensity Ratio

The qualitative assertion that "highly excited" satellites dominate the decay of the $1s^{-1}6t_{1u}$ state can be documented further using the observable sulfur Auger intensity ratio LVV/LLV.[43] Experimentally, the LVV/LLV intensiy ratio changes from 3.0(3) off resonance to 25(5) at 2486 eV (Fig. 6). The enhancement in the Auger intensity ratio depends directly on the relative resonant cross sections for the "highly excited" satellite states. In fact, careful examination of the contributions to the observable Auger ratio leads to the identification of the most important "highly excited" satellite channel.

We shall now show that it is possible to express the LVV/LLV Auger ratio in terms of the dominant SF_6^+ cross sections provided that all subsequent Auger decay steps are accounted for. Columns 5-7

of Table II outline the primary through quaternary decay steps to form SF_6^{n+} (n=2-5) for each photoemission channel. For this estimate, we first assume that the ions Auger decay quickly enough to fill all core holes (S 2p and S 2s) before dissociation can occur. A comparison of SF_6 ground-state vibrational lifetimes ($\sim 5\times10^{-14}$ sec)[44] with S 2p and S 2s core-hole lifetimes (5×10^{-15} and 1.4×10^{-15} sec, respectively)[45] indicates that Auger decay of these holes is probably at least ten times faster than the dissociation rate. If infrequent dissociation does occur, leaving an ion fragment SF_n^+ (n<6) with a sulfur L hole, the fragment itself will Auger decay to fill the core hole. Thus, the issue of dissociation does not significantly affect the following analysis of the S(LLV) and S(LVV) Auger peaks.

An additional factor necessary for deriving the LVV/LLV ratio is the fraction of S 2s holes which decays via the Coster-Kronig $S(L_1L_{2,3}V)$ Auger pathway,

$$SF_6^+(2s^{-1}) \longrightarrow SF_6^{2+}(2s^2 2p^{-1} val^{-1}) + L_1L_{2,3}V \text{ Auger } e^- \qquad (8)$$

rather than the $S(L_1VV)$ pathway,

$$SF_6^+(2s^{-1}) \longrightarrow SF_6^{2+}(2s^2 val^{-2}) + L_1VV \text{ Auger } e^-. \qquad (9)$$

In our analysis, we have assumed that this partitioning into the $S(L_1L_{2,3}V)$ and $S(L_1VV)$ Auger decay pathways is <u>independent</u> of

the configuration containing the S 2s hole. For example, the fraction f of S 2s holes decaying via the Coster-Kronig $S(L_1L_{2,3}V)$ channel is assumed to be the same for the configurations $SF_6^+(2s^{-1})$ and $SF_6^+(2s^{-2}6t_{1u})$. The presence of these two possible Auger-decay channels is evident in column 5 of Table II for each SF_6^+ state containing a S 2s hole.

The intensity ratio LVV/LLV in general (on and off resonance) can be derived in terms of f by adding up all the singly-charged ion cross sections which can subsequently Auger decay via LVV and LLV pathways as:

$$\left[\frac{LVV}{LLV}\right] = \frac{1}{f}\left\{\frac{\sigma(2p) + \sigma(2p\ sat) + \sigma(2s) + \sigma(2s\ sat) + 2[\sigma(2p^{-2}v^*) + \sigma(2s^{-2}v^*) + \sigma(2p^{-1}2s^{-1}v^*)]}{\sigma(2s) + \sigma(2s\ sat) + \sigma(2p^{-1}2s^{-1}v^*) + 2\sigma(2s^{-2}v^*)}\right\} \quad (10)$$

where $\sigma(x)$ represents the cross section for the SF_6^+ photoemission channel x.

The fraction f can be determined from the nonresonant LVV/LLV Auger ratio and the $\sigma(2p)/\sigma(2s)$ cross-section ratio. Away from the S $1s\rightarrow 6t_{1u}$ resonance ($h\nu<2480$ eV), the expression for the LVV/LLV ratio can be simplified with the assumption that the S 2s and S 2p main lines are the only SF_6^+ channels which contribute to the S(LVV) and S(LLV) Auger peaks. With all satellite cross sections assumed negligible, the nonresonant ratio becomes:

$$\left[\frac{LVV}{LLV}\right]_{off} = \frac{1}{f}\left[\frac{\sigma(2s) + \sigma(2p)}{\sigma(2s)}\right] = \frac{1}{f}\left[1 + \frac{\sigma(2p)}{\sigma(2s)}\right]. \quad (11)$$

The $\sigma(2p)/\sigma(2s)$ cross-section ratio in Eq. (11) can best be estimated from measurements of this ratio in atoms excited with high-energy x-ray sources. From these trends in low-Z elements, we expect that for sulfur, the $\sigma(2s)/\sigma(2p)$ ratio should be between 1.0 and 3.0.[45] This assumption leads ultimately to a value of f greater than 0.4. This crude result can be compared to the Ar $L_1L_{2,3}M$ and L_1MM Auger intensities which show that the Coster-Kronig channel in Eq. (8) is the overwhelmingly favored decay pathway for an Ar 2s hole.[46] The fraction f for Ar has been determined from experiment and theory to be greater than 0.35.[46]

Considering Eq. (10) for the resonant LVV/LLV ratio, we use the assertion from Sec. B that the "highly excited" satellite channels dominate the decay of the S 1s-->$6t_{1u}$ resonance to simplify the expression for the LVV/LLV Auger ratio:

$$\left[\frac{LVV}{LLV}\right]_{on} = \frac{2}{f}\left[\frac{\sigma(2p^{-2}v^{*}) + \sigma(2s^{-2}v^{*}) + \sigma(2p^{-1}2s^{-1}v^{*})}{\sigma(2p^{-1}2s^{-1}v^{*}) + 2\sigma(2s^{-2}v^{*})}\right]$$

$$= \frac{2}{f}\left[\frac{\sigma_{Total}}{\sigma(2p^{-1}2s^{-1}v^{*}) + 2\sigma(2s^{-2}v^{*})}\right] . \qquad (12)$$

It is clear upon inspection of Eq. (12) that in order for $[LVV/LLV]_{on}$ to be as large as the observed ratio on resonance (25±5), the cross sections $\sigma(2s^{-2}v^{*})$ and $\sigma(2p^{-1}2s^{-1}v^{*})$ must be relatively small. In fact, the expression in brackets on the right-hand side of Eq. (12) must lie in the range 4-15 (using $0.4 \leq f \leq 1.0$). Even with this large uncertainty, these values indicate

that at least 75 percent of the S 1s-->$6t_{1u}$ resonant cross section appears in the $2p^{-2}v^*$ channel.

The dominance of the resonant $SF_6^+(2p^{-2}v^*)$ channel is not surprising if one examines the expected partitioning of the cross sections within an Auger-like decay scheme. In other words, if the $6t_{1u}$ electron is left always as a "spectator", we can consider the core decay to be much like normal K-hole Auger decay. The KLL-type decay channels ("highly excited" satellites) should then dominate over the KLV(V^*) decay pathways (main lines and low-excitation-energy satellites), which is observed qualitatively in our analysis of peak A on resonance. Furthermore, the partitioning into the three important KLL-type channels can be compared with three schemes: 1) statistical, 2) Ar KLL Auger decay,[42,47] and 3) SF_6 S(KLL) Auger decay.[48] The partitioning in these scenarios is shown in Table III. It is clear that an Auger-like decay mechanism (similar to Ar and SF_6 KLL Auger rates) with dominant decay to the $2p^{-2}6t_{1u}$ state is consistent with our interpretation of the LVV/LLV ratio on resonance, within the assumptions made.

In summary, the $1s^{-1}6t_{1u}$ resonant state decays predominantly to the "highly excited" satellite configurations of SF_6^+ ($2p^{-2}v^*$, $2p^{-1}2s^{-1}v^*$, and $2s^{-2}v^*$). The decay of the excited state is such that the $6t_{1u}$ electron (v^*) probably remains as a "spectator", and the S 1s hole decays in a manner similar to Ar and SF_6 KLL Auger decay. Consistent with this, we find that at least 75 percent of the resonant cross section appears in the

SF_6^+ ($2p^{-2}v^*$) channel.

4. Resonant Asymmetry Parameters

The asymmetry parameters for the S(LVV) peak and peak A provide additional information on the photoemission and subsequent Auger-decay channels at the S 1s-->$6t_{1u}$ resonance. Figure 7 shows β values for the S(LVV) Auger peak and peak A, both demonstrating marked changes on resonance. We note that the behavior of the β(peak A) mostly is due to the photon-energy-dependent changes in the cross sections of the unresolved components of peak A. Below the S 1s-->$6t_{1u}$ resonance, about 85 percent of the peak A intensity is F 1s photoemission, yielding β near 2.0. On resonance, the F 1s cross section remains unaltered while the other components of peak A exhibit a large increase in cross section, as seen in Fig. 4. The dominance of the S 2p and S 2s "highly excited" spectator-satellite cross sections causes the β(peak A) to mimic the β value for these resonant levels, which appears to be near zero or slightly negative on resonance. The presence of unresolved contributions (spectator satellites) in peak A prohibits the measurement of the individual-channel asymmetry parameters.

Unlike the oscillations in β(peak A), the asymmetric profile for the β(LVV) at the S 1s-->$6t_{1u}$ resonance cannot be dismissed as arising from variations in peak-component cross sections. Although the oscillation is small (±0.12) and more data on the wings of the

resonance are needed to confirm the exact shape, the β(LVV) clearly is affected. In addition, the maximum in σ(peak A) in Fig. 5, σ(LVV) and σ(LLV) in Fig. 6, and the minimum in β(peak A) in Fig. 7 all lie at 2486.0(5) eV, the energy at which the β(LVV) crosses its background value, further confirming the asymmetric shape. This result for an Auger angular distribution is particularly intriguing because no previous studies have reported angle-resolved Auger decay emanating from ions resonantly produced by autoionization below a deep core-level threshold. Even though this unusual resonant profile for an Auger β should be considered tentative, some implications of an asymmetric shape are worthy of discussion.

An asymmetric profile in β ordinarily signals an interference effect. However, the interference in the autoionization process occurs one step previous to the observed Auger decay. That is, the direct-ionization and excited-state autoionization pathways leading to SF_6^+ interfere, causing oscillations in the σ and β values for the single-ion channels. Subsequent Auger decay cannot experience this interference phenomenon directly, but may retain "memory" of the process due to ion alignment.

Following up the idea of ion alignment, the Auger electron β is, in a sense, a "snapshot" of the molecular orientation of the SF_6^+ ion prior to Auger decay. According to Dehmer and Dill's formalism, β_{Auger} can be expressed as:[27]

$$\beta_{Auger} = c\,\beta_m \qquad (13)$$

where c is a constant characteristic of each individual Auger-decay channel, and β_m is the asymmetry of the molecular ion orientation following photionization. Because autoionization to $2p^{-2}v^*$ dominates the S 1s-->$6t_{1u}$ resonance, the oscillation in β(LVV) should reflect primarily the orientation of this particular SF_6^+ ion configuration in the resonance region. A varying energy dependence of single-ion alignment due to autoionization has been observed previously in atomic Cd for the double excitations above the 4d threshold $[4d^9(5s5p^3P)6s^1P]$[49] and over the 4d-->np ($n\geq 8$) and nf ($n\geq 5$) Rydberg series.[50]

A remaining point to consider is the relationship between the molecular-ion asymmetry, β_m, and the resonant photoelectron asymmetry parameter for the major channel $2p^{-2}v^*$. The asymmetry in the alignment of the $2p^{-2}v^*$ ion suggested by the S(LVV) β results also should appear in the β of the $2p^{-2}v^*$ photoelectron, which is convoluted in the total β(peak A). However, the individual profile cannot be determined from the β(peak A) because of the unresolved components and the rapidly changing cross sections.

To summarize, the asymmetric profile for the S(LVV) Auger β over the S 1s-->$6t_{1u}$ resonance, though tentative, is highly unusual. Though the conceptual link between the Auger electron β and single-ion alignment is provided by Dehmer and Dill's theory,[27] there are no available calculations for the specific shape of the molecular orientation asymmetry, β_m, over a discrete resonance.

E. Above the S 1s Threshold

For the data taken above tne sulfur K edge, both σ(peak A) and σ(LVV) cross sections (Fig. 5) show characteristic undulations in the S 1s continuum. In particular, the peak near 2507 eV is evident in our data (the unresolved d and e features in Fig. 1), as are broader features at ~2525 and 2555 eV (f and g in Fig. 1). Oscillations also appear in σ(S 1s) and β(S 1s) shown in Fig. 8. For the sake of illustration, the σ(S 1s) data for SF_6 have been normalized to the absorption curve.[1] The MSM-Xα σ(S 1s) and β(S 1s) are also shown.[13]

The S 1s continuum results will be discussed in two parts. In Sec. 1 we examine our data near the 2507 eV resonances and interpret sharp changes in the cross-section ratios (peak A)/1s and LVV/1s as indications of resonant enhancement in the S 2p, S 2s, and valence main-line and satellite channels. This behavior and the observation of S 1s satellites lead to an assignment of the two resonances visible in the photoabsorption cross section at 2506 and 2511 eV (d and e) as doubly excited states.

Section 2 will address the nature of the features at 2525 and 2555 eV photon energy. We compare the experimental data with a single-scattering plane-wave EXAFS calculation and with MSM-Xα results. This is followed by a discussion in terms of approximations to the electron-scattering process and the description of the molecular potential in EXAFS and MSM-Xα calculations which attempt to

model the effects in this energy region.

1. The 2507 eV Resonances and S 1s Satellites

The σ(S 1s) data in Fig. 8, in contrast to σ(LVV) and σ(peak A) cross sections in Fig. 5, do not show a sharp feature at 2507 eV. To illustrate the differing behavior at this resonance, the cross-section ratios (peak A)/(S 1s) and (LVV)/(S 1s) are plotted in Fig. 9. In the ratio plots, the behavior at 2507 eV is much more pronounced. This peak appears as one resonance in Fig. 9 and is 4-5 eV full width at half maximum. Both the 2506 and 2511 eV resonances discernable in the photoabsorption measurement[1] (see Fig. 1, d and e) probably are present in our lower-resolution results. Because of the contributions included in the measured peaks (see Table I), we stress that any sharp changes in the ratios below the S 1s satellite thresholds are due to resonant contributions of the S 2p, S 2s, and valence main lines and satellites (low-excitation and "highly excited" satellites). Furthermore, the peak at 2506 eV and its shoulder at 2511 eV in the photoabsorption curve do not appear in the MSM-Xα theory curve, indicating that they probably are caused by a multi-electron resonance or a symmetry-forbidden process.

The β(S 1s) in Fig. 8 also shows a dramatic effect in this low-energy region. The β falls from 2 at high photon energy to a minimum at 2507 eV of 1.1. The MSM calculation shows a decrease in β_{1s} in this region, even though it does not predict the

photoabsorption features at 2506 and 2511 eV. Thus, it is not clear from comparison with theory whether the β(S 1s) effect is associated with the 2507 eV feature. The departure of β(S 1s) from the atomic value of 2.0 for an s orbital is a direct indication of the anisotropy of the molecular potential.

Pertinent to this resonance region, two S 1s correlation satellite peaks were observed directly at higher photon energies. Figure 3 shows the satellites at a representative photon energy of 2581 eV. We report an average branching ratio for the total satellite intensity relative to the S 1s main line of 15(3) percent in the photon-energy range between 2570 and 2590 eV. The satellite thresholds were measured from a series of spectra to be 2510(1) and 2514(1) eV, 20 and 24 eV above the S 1s threshold, respectively. Note that the satellite binding energies are located 3-4 eV above the 2506 and 2511 eV photoabsorption features (d and e).

The observed satellite binding energies, combined with the sharp changes in the cross-section ratios discussed above, present a strong case for assignment of the resonant features as doubly excited autoionizing states preceding the satellite thresholds. The general assignment of features d and e as multiple excitations has been suggested previously.[4] The possible decay channels of the postulated doubly excited resonances are depicted in Fig. 2 (dotted lines). The two resonances somewhat resolved in the absorption measurement may be leading to the two observed satellite thresholds. In analogy to the S 1s-->$6t_{1u}$ resonance, the configurations for the

neutral doubly excited states could be $1s^{-1}(val)^{-1}v^{*}6t_{1u}$, leading to the satellite ionic states $1s^{-1}(val)^{-1}v^{*}$ of SF_6^+. The $6t_{1u}$ electron is included in the excited-neutral configuration because the energy spacing of the resonance below the satellite thresholds (3-4 eV) is similar to the spacing of the S 1s-->$6t_{1u}$ transition below the S 1s edge. However, multiplet splitting of the resonant states can be significant and will complicate the details of this simple assignment.

The intensity of these doubly excited resonances seems reasonable by comparison to the S 1s-->$6t_{1u}$ resonant intensity. The increase in the total cross section at one of the doubly-excited resonances is about 3(1) percent of the increase at the S 1s-->$6t_{1u}$ resonance, while the total photoemission intensity of the S 1s satellites relative to the S 1s main-line photoemission is approximately 15 percent.

There have been no calculations to help identify the possible S 1s satellite configurations. Therefore, using the current valence ordering of Dehmer et al.[20] and the $4t_{1u}$-->$6a_{1g}$ transition energy of ~17 eV in the neutral molecule,[20] we crudely approximated the possible shake-up and conjugate shake-up satellites in the energy region of interest.[51] We have considered only promotion of an outer-valence electron to the $6a_{1g}$ and $6t_{1u}$ unoccupied orbitals. Based on energetics alone, this approach indicates that the observed S 1s satellites have the possible SF_6^+ configurations:

$1s^{-1}(5a_{1g})^{-1}6a_{1g}$,
$1s^{-1}(4t_{1u})^{-1}6t_{1u}$,
$1s^{-1}(5a_{1g})^{-1}6t_{1u}$, (conjugate shake-up)

though the conjugate shake-up state seems less likely. These configurations correspond to excitation from the deepest outer-valence orbitals.

The general identification of these resonances as doubly excited states is reasonably clear, but in disagreement with the earlier assignment of one of them (2506 eV, feature d) as a symmetry-forbidden shape resonance.[3] Detailed theoretical calculations are needed to determine the energy positions of both the autoionizing states and satellite thresholds, and the intensity effects at the resonances.

2. High-energy Features

For the two higher-energy maxima at about 2525 and 2555 eV in σ(S 1s), there is good agreement with the MSM calculation (Fig. 8). The S 1s kinetic energies at these maxima are about 35 and 65 eV, respectively. The magnitude of the increase in the experimental S 1s cross section near 2555 eV is quite large, about a factor of two over an energy range of 15 eV. The cross-section effect is probably accentuated by the suppression of the continuum intensity related to the huge enhancement of the S 1s-->$6t_{1u}$ discrete resonance.

The significant scatter and uncertainty in the β(S 1s)

measurements above 2530 eV preclude any strong statements about an effect in the angular distribution associated with the rise in the cross section around 2545 eV. The MSM curve shows a minimum in β(S 1s) which coincides with the S 1s cross-section minimum.

Because of the agreement between the MSM and experimental cross sections, we further consider the general MSM results for SF_6. The nature of these high kinetic-energy oscillations was mentioned briefly by Wallace as originating from EXAFS behavior.[13] The MSM theory to some extent includes all single- and multiple-scattering events in the calculation of partial cross sections, so the particular physical effect(s) producing the oscillations is not clear when only cross section results are available. Wallace noted that there are no calculated symmetry-allowed shape-resonant states in this energy region; the presence of such quasi-bound states would be unusual considering the required barrier height (>35, 65 eV) needed for trapping the photoelectron. However, the eigenphase sum for S $1s(1a_{1g})$-->εt_{1u} photoionization rises by ~$\pi/3$ over an energy range of 15 eV centered at ~2549 eV photon energy,[52] which is the center of the rise in the S 1s cross section. There is also a marked similarity among the calculated MSM cross sections for the various core levels of SF_6 in this kinetic-energy range. We will not elaborate on this similarity except to note that the intensity changes around 60 eV kinetic energy may be caused by a single phenomenon.

Because Wallace[13] interpreted the high-energy features as EXAFS, we have performed a single-scattering plane-wave EXAFS

calculation for comparison with experiment to help determine the physical origin of these features by identifying the EXAFS portion of the continuum oscillations. The factors of short bond distance (r = 1.58 Å) and strong back-scattering amplitude which make single-scattering EXAFS pronounced are indeed present in SF_6. The calculated EXAFS oscillatory amplitudes using a Debye-Waller factor of σ=0 (best case for large amplitude) and two different central-atom phase shifts (sulfur and "adjusted" phase shifts) are shown in Fig. 10, plotted with the absorption curve (where the below-threshold nonresonant intensity has been subtracted) and the MSM-Xα S 1s partial cross section. For the F backscattering atoms, the published Clementi-Roetti phase shifts and amplitudes were used.[53,54] Various central-atom phase shifts other than those for sulfur were tried until the calculated high kinetic-energy oscillations coincided with the experimental energies of approximately 140, 215, and 295 eV (see Fig. 10, vertical lines). The resulting "adjusted" central-atom phase shift corresponds to a curve between that for Na and Mg (the Clementi-Roetti l=1 phase shifts with the Z+1 approximation); quantitatively, this equals the Si phase shift minus a value of 1.25 radians.[53] Though the variation of the central-atom phase shift did serve to line up the high kinetic-energy EXAFS features, it also reduced the effect in the cross section by a factor of two. For this reason, we also show in Fig. 10 the calculated EXAFS curve using the unadjusted sulfur phase shifts (dashed curve, bottom).

A comparison between the calculated EXAFS curve (with "adjusted"

phase shifts) and experiment shows good agreement above ~120 eV kinetic energy in the amplitude of the EXAFS oscillations when an estimated background cross section is used (see top of Fig. 10, dotted line). The features below 100 eV, however, are not as well reproduced. It is difficult to assess the relative intensity effect for SF_6 in this region because of the uncertainty in the nondiffractive experimental "background", though we can set a lower limit on the effect in the S 1s cross section at about 50 percent. The EXAFS calculation with the "adjusted" phase shift shows a 25 percent effect in this energy region, while the EXAFS curve using the sulfur-atom phase shift shows a 50 percent effect. We believe that the uncertainties in both the experimental and calculated amplitudes below 100 eV kinetic energy do not permit any conclusions based on intensity arguments.

Using the "adjusted" phase shifts to reproduce the energies of the high-kinetic-energy wiggles, the maximum of the large peak at 65 eV kinetic energy is off by ~20 eV in energy. This particularly poor energy agreement is reinforced when similar calculations on Br_2 and $GeCl_4$ are examined. The calculations for these molecules reproduce the corresponding experimental energies at both high energies and between 4 and 5 $Å^{-1}$ (60-100 eV).[54] It is known that atoms less electronegative than flourine are not as effective in creating a barrier in the molecular potential which can modify the atomic effects.[3] These facts point to the possible importance of molecular effects in SF_6. Considering all of these factors, we

conclude that the cross-section features at 35 and 65 eV kinetic energy in SF_6 (f and g in Fig. 1) do not arise exclusively from a simple single-scattering plane-wave EXAFS phenomenon.

Summarizing the results to this point, our conclusions are that the MSM-Xα calculation[13] reproduces the experimental S 1s cross section well below 100 eV kinetic energy (Fig. 10, top, dot-dashed curve), whereas our single-scattering plane-wave EXAFS calculation does not. The next question is how to improve the general theoretical treatment of this problem. Two types of "fine-tuning" of the theory involve first, a better description of the electron-scattering process, and second, improvement in the treatment of the molecular potential. These two improvements are not necessarily separate developments.

EXAFS theorists recently have been interested in improving the description of the scattering process by introducing spherical waves into the single-scattering calculations.[28-31] One can make an intuitive argument that the curvature of the wave front will be more important at low kinetic energies and for molecules with short bond distances.[31] From a more quantitative point of view, Lee and Pendry have done plane- and spherical-wave calculations on crystalline Cu.[28] The spherical-wave corrections to the Cu EXAFS curve shift the oscillations by an energy on the order of 20 eV and reduce the amplitude by a factor of two below 100 eV. Based on these crude estimates, we think that curved-wavefront corrections (which we have neglected in our calculation) should be important for SF_6 in the

kinetic-energy range below 100 eV, affecting both the amplitude and phase of the EXAFS features.

The complication of multiple-scattering events should also be considered in this energy range (MSM theory of course includes these events). Multiple-scattering contributions to EXAFS have been calculated on a variety of systems with the following trends having been exhibited. First, the most important effect occurs with an arrangement of collinear atoms where the intervening atom serves to "focus" amplitude back onto the central atom.[33-35] This focussing effect usually involves only one backscattering event and can result in a significantly enhanced amplitude and a phase shift at all energies.[33] A similar multiple-scattering path for SF_6 can be denoted S-F_1-S-F_2-S, where F_1 and F_2 are flourine atoms collinear with the sulfur atom. Secondly, large-angle scattering can be significant, especially at low kinetic energy where electron scattering becomes more isotropic. Bunker and Stern[35] estimated that below 30 eV kinetic energy for Mn 1s ionization of $KMnO_4$, the large-angle multiple-scattering amplitude relative to single scattering is about 25-50 percent (and about 10-20 percent at higher energy).

However, even with spherical-wave and multiple-scattering corrections included which improve the treatment of the electron-scattering process, there may still be significant interaction with the more diffuse molecular potential below 100 eV kinetic energy. A recent experimental study on the oxygen K-edge

EXAFS spectra of O_2, CO, and CO_2 concludes that the observed disagreement between these experiments and single-scattering EXAFS theory is probably caused by inappropriate atomic parameters in the EXAFS calculation.[55] The atomic parameters and potential were thought to be inaccurate for modeling the electron scattering in the molecular orbitals.[55] The current degree of modification of EXAFS theory fails to include the complicated electronic structure and interaction due to the molecular nature of the problem. For example, in the atomic phase-shift EXAFS calculations of Lee and Beni,[56] two atomic muffin-tin potentials are calculated separately and overlapped. Of course, the details of the potential between the atoms are not muffin-tin-like, as the authors note. The inaccuracies in this region should not affect the EXAFS calculations at high energy because any complexity will not be experienced by a high-energy electron. It is exactly in this region, however, where low-energy electrons may interact more with the details of the molecular potential.

MSM-Xα calculations use as a starting point atomic potentials similar to those used in EXAFS theory.[13,15] The molecular detail between the atoms is picked up, albeit indirectly, by a self-consistent treatment of the molecular potential. The possible nature of the interaction with the molecular field above approximately 30 eV kinetic energy has not been considered previously. The same interaction at lower kinetic energy can result in shape resonances, which are reasonably well understood. However, even in this respect

SF_6 seems to be an especially complicated case.[19,20,57]

In order to imagine qualitatively how a high-energy (30-60 eV kinetic energy) interaction might occur, it is useful to think of the simple square-barrier potential problem where:[58]

$$\begin{aligned} V &= V_0 && 0 \leq r \leq r_0, \\ V &= 0 && r < 0 \quad \text{and} \quad r > r_0. \end{aligned} \tag{14}$$

When the energy of a wave is greater than the barrier height V_0, the wave is quantum-mechanically transmitted and reflected, giving oscillations in the continuum cross section, frequently called transmission resonances. The largest effect occurs with a large barrier width and/or height. Certainly, the realistic addition of a potential well and a repulsive wall may perturb even the qualitative aspects of this effect, but we use this simple example to illustrate the possible nature of an interaction between the photoelectron and a possibly large barrier induced by the electronegative flourines in SF_6.

We believe that the future understanding of this phenomenon will come primarily from detailed theoretical work which examines the origins of the dipole matrix-element changes in this energy range. The results of a step-by-step EXAFS calculation for SF_6, where spherical-wave and multiple-scattering corrections are added sequentially, would certainly help to estimate the importance of interaction with the atomic cores (EXAFS) relative to that with the

more diffuse aspects of the molecular potential. Improvements in the potential itself are necessary also to pick up the possible nondiffractive (barrier) interactions that occur in this intermediate-energy range. Combined with this, a careful examination of the results of the MSM-Xα calculation, which quantitatively reproduces the cross section between 25 and 100 eV kinetic energy, could yield some insight into the physical origin(s) of these high-energy features.

F. Conclusions

To summarize, the specific conclusions which can be drawn from our data near the sulfur K edge in SF_6 are as follows:

1. For the S 1s ($1a_{1g}$)-->$6t_{1u}$ resonance, "highly excited" satellites with <u>two</u> core holes (S 2p, S 2s) are the important SF_6^+ decay channels. These configurations ($2p^{-2}v^*$, $2s^{-2}v^*$, and $2p^{-1}2s^{-1}v^*$), if regarded as S 2s and S 2p satellites, have exceptionally high excitation energies (>150 eV) and, according to the spectator model, probably contain a $6t_{1u}$ electron in the excited v^* orbital. In general, our data suggest that the decay of the neutral excited state proceeds much like Ar KLL and SF_6 S(KLL) Auger decay, with the $2p^{-2}v^*$ channel as the dominant one. Furthermore, an asymmetric resonant profile for the S(LVV) Auger β is

observed, probably caused by ion alignment in the previous photoemission step.

2. The resonances around 2507 eV are probably doubly excited autoionizing states (leading to observed satellite thresholds), because decay into S 2p, S 2s, and/or valence photoemission channels is observed. The interpretation emphasizes the general requirement for results on individual photoemission channels in order to distinguish satellite continua and autoionization effects from shape resonances in the assignment of absorption features.

3. The data further above the S 1s threshold (30-100 eV kinetic energy) are difficult to interpret. The experimental results show a factor of two increase in the S 1s cross section near 2550 eV, but no conclusive effect in the S 1s β. MSM-Xα calculations successfully reproduce the effects in the S 1s cross section, indicating their one-electron nature.[13] We conjecture that the large effects are caused by a combination of spherical-wave and multiple-scattering effects in EXAFS and an interaction of the photoelectron with the details of the molecular potential.

There is an obvious need for further experimental work in several areas. High kinetic-energy resolution would help to assign the

SF_6^+ resonant states (i.e., the location of the excited electron) and possibly the structure of the broad sulfur LLV and LVV Auger peaks on and off resonance. The decay of core-level discrete states in molecules has been examined in just a few systems to date.[22-26,57,59-61] We predict that future resonant work below deep core-level thresholds will confirm the predominance of "highly excited" satellites and the importance of spectator decay. The study of core levels of other octahedral molecules with electronegative ligands and of substituted hexaflourides (like SF_5X) with respect to the continuum effects above 30 eV kinetic energy may help to determine the origin of the cross-section effects in this energy region.

On the theory side, resonance calculations are needed for individual cross sections and angular distributions. More general work on the theory for Auger-electron angular distributions is called for to elucidate how autoionization produces an aligned molecular ion prior to Auger decay. Finally, advances in EXAFS theory as applied to molecules, especially concerning the treatment of the electron-scattering process and of the molecular potential, are needed to investigate the nature of interactions with low-energy (<100 eV) electrons.

TABLE I: Peak Contributions for the SF_6 S 1s Photoelectron Spectra.

Photon-Energy [a] Range	Peak A	Peak S(LVV) Auger	Peak $S(L_1L_{2,3}V)$ Auger
<2490 eV	F 1s, S 2p, S 2s, valence (main lines and satellites)	$L_{1,2,3}VV$ Auger decay of S 2p, S 2s holes (main lines and satellites)	Auger decay of S 2s holes (main line and satellites)
2490 - 2510 eV	all of above plus KLL, KLV, KVV Auger decay of S 1s hole (main line)	all of above plus $L_{1,2,3}VV$ secondary Auger decay of S 1s hole (main line)	all of above plus secondary Auger decay of S 1s hole (main line)
>2510 eV	all of above plus KLL, KLV, KVV Auger decay of S 1s hole (satellites)	all of above plus $L_{1,2,3}VV$ secondary Auger decay of S 1s hole (satellites)	all of above plus secondary Auger decay of S 1s hole (satellites)

[a] The energy ranges above designate the regions: below the S 1s threshold (<2490 eV), between the S 1s main-line and first satellite threshold (2490-2510 eV), above the first S 1s satellite threshold (>2510 eV).

TABLE II: Complete Description of Autoionization of the SF_6 ($1s^{-1}6t_{1u}$) State to SF_6^+ Photoemission Channels, and Subsequent S(LVV and LLV) Auger Cascades to Form SF_6^{n+} (n=2-5)

Autoionization to SF_6^+ via $1s^{-1}6t_{1u}$				Auger decay of SF_6^+ to SF_6^{n+} (n=2-5)		
SF_6^+ photoemission channel	configuration[a]	autoionization decay "type"[b]	Binding energy(eV)	Auger transitions to fill all S $2p_c$ and S 2s holes	Total number of Auger electrons[d] LLV	LVV
main lines:						
2p	$2p^{-1}$	$KL_{2,3}V^*$	181.0[e]	$L_{2,3}VV$	0	1
2s	$2s^{-1}$	KL_1V^*	244.7[f]	1. L_1VV	0	1
				2. $L_1L_{2,3}V$ + $L_{2,3}VV$	1	1
satellites:						
2p	$2p^{-1}val^{-1}6t_{1u}$ $2p^{-1}val^{-1}v^{*}{}_{1u}$	$KL_{2,3}V$ and $KL_{2,3}V^*$	~190-220[g]	$L_{2,3}VV$	0	1

TABLE II: (cont.)

Autoionization to SF_6^+ via $1s^{-1}6t_{1u}$				Auger decay of SF_6^+ to SF_6^{n+} (n=2-5)		
SF_6^+ photoemission channel	configuration[a]	autoionization decay "type"[b]	Binding energy(eV)	Auger transitions to fill all S 2p[c] and S 2s holes	Total number of Auger electrons[d] LLV	LVV
2s	$2s^{-1}val^{-1}6t_{1u}$ $2s^{-1}val^{-1}v^{*}{}_{1u}$	KL_1V and KL_1V^*	~255-285[g]	1. L_1VV 2. $L_1L_{2,3}V$ + $L_{2,3}VV$	0 1	1 1
"highly excited" satellites:						
2p	$2p^{-2}6t_{1u}$ $2p^{-2}v^{*}{}_{1u}$	$K_{2,3}LL_{2,3}$	~360[h]	2 $L_{2,3}VV$	0	2

TABLE II: (cont.)

Autoionization to SF_6^+ via $1s^{-1}6t_{1u}$				Auger decay of SF_6^+ to SF_6^{n+} (n=2-5)		
SF_6^+ photoemission channel	configuration[a]	autoionization decay "type"[b]	Binding energy(eV)	Auger transitions to fill all S $2p_c$ and S 2s holes	Total number of Auger electrons[d] LLV	LVV
2s	$2s^{-2}6t_{1u}$ $2s^{-2}v^*$	KL_1L_1	~490[h]	1. $L_1VV + L_1VV$	0	2
				2. L_1VV $+ L_1L_{2,3}V$ $+ L_{2,3}VV$	1	2
				3. $L_1L_{2,3}V$ $+ L_1L_{2,3}V$ $+ 2\,L_{2,3}VV$	2	2
"mixed"	$2p^{-1}2s^{-1}6t_{1u}$ $2p^{-1}2s^{-1}v^*$	$KL_1L_{2,3}$	~430[h]	1. $L_1VV + L_{2,3}VV$	0	2
				2. $L_1L_{2,3}V$ $+ 2\,L_{2,3}VV$	1	2

TABLE II: (cont.)

[a] Inner- and outer-valence orbitals (Binding energies 16 to 44 eV) are denoted by "val". Excitation to an unoccupied molecular orbital other than $6t_{1u}$ (probably $6a_{1g}$) is denoted by "v*".

[b] The Auger notation is used here to describe the decay type to the SF_6^+ photoemission final state. V designates that the $6t_{1u}$ electron has remained as a "spectator"; V* denotes that the excited $6t_{1u}$ electron has participated in the decay to SF_6^+.

[c] All 2s holes can decay via $S(L_1L_{2,3}V)$ or $S(L_1VV)$ Auger channels with some partitioning assumed independent of the configuration containing the 2s hole state.

[d] Auger electrons are divided into sulfur LLV and LVV categories corresponding to the two observable Auger peaks in our photoemission spectra. The totals here include all primary through quaternary decay to give Auger electrons within the kinetic-energy region of the two observable peaks.

[e] The S 2p binding energy is an average of the $2p_{3/2}$ and $2p_{1/2}$ spin-orbit binding energies which are 180.4 and 181.7 eV, respectively.[45]

[f] Ref. 45.

[g] This energy range is based on observed S 2p satellite excitation energies.[57]

[h] Binding energy is estimated crudely by summing the binding energies (in the neutral) of the two core holes. Relaxation has not been included.

TABLE III: Relative Intensities for the "Highly Excited" Satellite Channels for the S 1s-->$6t_{1u}$ Resonance in SF_6 Compared to KLL Auger Decay.

Scheme	Relative Intensity		
	$2p^{-2}$	$2s^{-1}2p^{-1}$	$2s^{-2}$
1. statistical decay:	0.54	0.43	0.04
2. Ar KLL-like decay:[42,47]	0.74(5)	0.22(5)	0.04(1)
3. SF_6 S(KLL)-like decay:[48]	0.72(1)	0.21(2)	0.07(3)
4. observed decay:	> 0.75	-	-

References

* Published in Phys. Rev. A 34, 1916 (1986). Work done in collaboration with D.W. Lindle, P.A. Heimann, H.G. Kerkhoff, U.E. Becker, and D.A. Shirley. We would like to acknowledge Z. Hussain for assistance with the experimental preparations and discussions with J.L. Dehmer, J.A. Stephens, J.J. Barton, and M.N. Piancastelli.

1. R.E. LaVilla and R.D. Deslattes, J. Chem. Phys. 44, 4399 (1966).
2. T.M. Zimkina and A.S. Vinogradov, J. Phys. (Paris) 32, C4-3 (1971) and references therein.
3. J.L. Dehmer, J. Chem. Phys. 56, 4496 (1972) and references therein.
4. F.A. Gianturco, C. Guidotti, and U. Lamanna, J. Chem. Phys. 57, 840 (1972).
5. S.T. Manson and J.W. Cooper, Phys. Rev. 165, 126 (1968).
6. J.P. Connerade, Contemp. Phys. 19, 415 (1978).
7. K.T. Cheng and C. Froese-Fischer, Phys. Rev. A 28, 2811 (1983).
8. K.T. Cheng and W.R Johnson, Phys. Rev. A 28, 2820 (1983).
9. V.P. Sachenko, E.V. Polozhentsev, A.P. Kovtun, Yu.F. Migal, R.V. Vedrinski, and V.V. Kolesnikov, Phys. Lett. 48A, 169 (1974).
10. D. Dill and J.L. Dehmer, J. Chem Phys. 61, 692 (1974).
11. J.L. Dehmer and D. Dill, Phys. Rev. Lett. 35, 213 (1975).
12. J.L. Dehmer and D. Dill, J. Chem. Phys. 65, 5327 (1977).
13. R.S. Wallace, Ph.D. thesis, Boston University, 1980.
14. D. Loomba, S. Wallace, D. Dill, and J.L. Dehmer, J. Chem. Phys.

75, 4546 (1981).

15. J.L. Dehmer, D. Dill, and A.C. Parr in Photophysics and Photochemistry in the Vacuum Ultraviolet, edited by S.P. McGlynn, G. Findley, and R. Huebner (D. Reidel Publishing Co., Dordrecht, Holland, 1985), p. 341.
16. J. Berkowitz, Photoabsorption, Photoionization, and Photoelectron Spectroscopy (Academic Press, New York, 1979).
17. A.P. Hitchcock and C.E. Brion, Chem. Phys. 37, 319 (1979).
18. R.C.C. Perera, J. Barth, R.E. LaVilla, R.D. Deslattes, and A. Henins, Phys. Rev. A 32, 1489 (1985).
19. T. Gustafsson, Phys. Rev. A 18, 1481 (1978).
20. J.L. Dehmer, A.C. Parr, S. Wallace, and D. Dill, Phys. Rev. A 26, 3283 (1982).
21. J.-H. Fock and E.E. Koch, Chem. Phys. 96, 125 (1985).
22. L. Ungier and T.D. Thomas, Chem. Phys. Lett., 96, 247 (1983).
23. H.W. Haak, G.A. Sawatzky, L. Ungier, J.K. Gimzewski, and T.D. Thomas, Rev. Sci. Instrum. 55, 696 (1984).
24. L. Ungier and T.D. Thomas, J. Chem. Phys. 82, 3146 (1985).
25. U. Becker, R. Hölzel, H.G. Kerkhoff, B. Langer, D. Szostak, and R. Wehlitz, Phys. Rev. Lett. 56, 1455 (1986).
26. C.M. Truesdale, S.H. Southworth, P.H. Kobrin, U. Becker, D.W. Lindle, H.G. Kerkhoff, and D.A. Shirley, Phys. Rev. Lett. 50, 1265 (1983).
27. D. Dill, J.R. Swanson, S. Wallace, and J.L. Dehmer, Phys. Rev. Lett. 45, 1393 (1980).

28. P.A. Lee and J.B. Pendry, Phys. Rev. B 11, 2795 (1975).

29. J.E. Muller and W.L. Schaich, Phys. Rev. B 27, 6489 (1983).

30. W.L. Schaich, Phys. Rev. B 29, 6513 (1984).

31. J.J. Barton, Ph.D. thesis, University of California, Berkeley, 1985.

32. C.A. Ashley and S. Doniach, Phys. Rev. B 11, 1279 (1975).

33. B.K. Teo, J. Am. Chem. Soc. 103, 3990 (1981).

34. J.J. Boland, S.E. Crane, and J.D. Baldeschwieler, J. Chem. Phys. 77, 142 (1982).

35. G. Bunker and E.A. Stern, Phys. Rev. Lett. 52, 1990 (1984).

36. We note that direct decay to double-ionization (shake-off) channels also is possible, resulting in SF_6^{2+} configurations such as $2p^{-2}$, $2s^{-2}$, $2s^{-1}2p^{-1}$, $2s^{-1}val^{-1}$, $2p^{-1}val^{-1}$, and val^{-2}. The energy distribution of the emitted electrons would be very broad and somewhat peaked near 0 eV and the threshold energy for the shake-off process, with the high-energy part of the distribution unresolved from the other components in peak A in our TOF spectra. Thus, we cannot assess what percentage of excited neutrals decay directly to shake-off channels at the S 1s-->$6t_{1u}$ resonance, although we speculate that this fraction probably is less than 20 percent.

37. It is important to recall that the peaks enhanced at the S 1s-->$6t_{1u}$ resonance are not KLL Auger peaks, but rather autoionization to photoemission channels. The autoionizing decay of the neutral $SF_6(1s^{-1}6t_{1u})$ state can, however, be

described in terms (using Auger notation) similar to those used to describe the Auger decay of the single-ion $SF_6^+(1s^{-1})$.

38. Some representative examples for relative intensities of atomic and molecular satellites are given in U. Gelius, J. Electron Spectrosc. 5, 985 (1974).

39. For the Auger decay of the resonantly produced state, we assume that the $6t_{1u}$ electron is not involved in the decay because other t_{1u} orbitals have more overlap with the S $2p(2t_{1u})$ hole. If the $6t_{1u}$ electron is involved, the S(LVV) Auger kinetic energy will shift to even higher energy.

40. D.A. Shirley, Phys. Rev. A 9, 1549 (1974).

41. H. Korber and W. Melhorn, Z. Phys. 191, 217 (1966); M.O. Krause, T.A. Carlson, and W.E. Moddeman, J. Phys. (Paris) Colloq. 32, C4-139 (1971).

42. L. Asplund, P. Kelfve, B. Blomster, H. Siegbahn, and K. Siegbahn, Phys. Scr. 16, 268 (1977).

43. In the following analysis, we neglect the previously mentioned direct shake-off decay on resonance,[36] which would leave L-hole ions which subsequently Auger decay with intensity appearing in the observable S(LVV) and S(LLV) Auger peaks. As long as the relative abundance of two-core-hole configurations within the shake-off manifold ($2p^{-2}$:$2s^{-2}$:$2p^{-1}2s^{-1}$) is similar to that for the single-ion manifold reached by autoionization ($2p^{-2}v^*$:$2s^{-2}v^*$:$2p^{-1}2s^{-1}v^*$), the qualitative conclusions about the SF_6^+ decay channels are unaffected. Furthermore,

double-Auger processes such as $SF_6^+(2p^{-1}) \rightarrow SF_6^{3+}(val^{-3}) + 2e^-$ are not included in the observed S(LVV) and S(LLV) Auger peaks. We estimate that off resonance these Auger shake-off processes account for only ~10 percent of the total L-hole Auger decay, based on the measured double-Auger processes for L holes in Ar.[62] On resonance, double-Auger decay may occur somewhat more frequently (though single-Auger decay probably will still dominate) because "highly excited" ions like $2p^{-2}6t_{1u}$ undergoing Auger decay may have a greater probability for shaking off the $6t_{1u}$ electron relative to shake-off of a valence electron in the Auger decay of a $2p^{-1}$ ion.

44. G. Herzberg, Electronic Spectra and Electronic Structure of Polyatomic Molecules (D. Van Nostrand Co., Princeton, New Jersey, 1966).

45. K. Siegbahn, C. Nordling, G. Johansson, J. Hedman, P.F. Hedén, K. Hamrin, U. Gelius, T. Bergmark, L.O. Werme, R. Manne, and Y. Baer, ESCA Applied to Free Molecules (North-Holland, Amsterdam, London, 1969).

46. W. Mehlhorn, Z. Phys. 208, 1 (1968).

47. J. Vayrynen, R.N. Sodhi, and R.G. Cavell, J. Chem. Phys. 79, 5329 (1983); M.O. Krause, Phys. Rev. Lett. 34, 633 (1975).

48. L. Asplund, P. Kelfve, B. Blomster, H. Siegbahn, K. Siegbahn, R.L. Lozes, and U.I. Wahlgren, Phys. Scr. 16, 273 (1977); K. Faegri, Jr. and O. Keski-Rahkonen, J. Electron Spectrosc. 11, 275 (1977).

49. W. Kronast, R. Huster, and W. Mehlhorn, J. Phys. B 17, L51 (1984).

50. Z.M. Goodman, C.D. Caldwell, and M.G. White, Phys. Rev. Lett. 54, 1156 (1985); 54, 2381 (1985).

51. The latest valence ordering, though supported by many-body calculations,[63] is not completely certain due to the presence of a possible shape resonance affecting several valence cross sections at about 23 eV photon energy.[19-21]

52. J.A. Stephens and P. Dittman (private communication of calculations by R.S. Wallace).

53. B.K. Teo and P.A. Lee, J. Am. Chem. Soc. 101, 2815 (1979).

54. B.K. Teo, P.A. Lee, A.L. Simons, P. Eisenberger, and B.M. Kincaid, J. Am. Chem. Soc. 99, 3854 (1977); P.A. Lee, B.K. Teo, and A.L. Simons, 99, 3856 (1977).

55. B.X. Yang, J. Kirz, and T.K. Sham, Phys. Lett. 110A, 301 (1985).

56. P.A. Lee and G. Beni, Phys. Rev. B 15, 2862 (1977).

57. T.A. Ferrett, D.W. Lindle, P.A. Heimann, M.N. Piancastelli, P.H. Kobrin, H.G. Kerkhoff, U.E. Becker, W.D. Brewer, and D.A. Shirley (unpublished results- see Chpt. IV).

58. G. Baym, Lectures on Quantum Mechanics (Benjamin Cummings, Reading, Massachusetts, 1969); A. Messiah, Quantum Mechanics Vol. 1 (North-Holland, Amsterdam, and John Wiley and Sons, Inc., New York, 1961).

59. G.G.B. de Souza, P. Morin, and I. Nenner, J. Chem. Phys. 83, 492 (1985).

60. P. Morin, G.G.B. de Souza, I. Nenner, and P. Lablanquie, Phys.

Rev. Lett. 56, 131 (1986).

61. S. Aksela, K.H. Tan, H. Aksela, and G.M. Bancroft, Phys. Rev. A 33, 258 (1986).

62. T.A. Carlson and M.O. Krause, Bull. Am. Phys. Soc. 10, 455 (1965); T.A. Carlson and M.O. Krause, Phys. Rev. Lett. 17, 1079 (1966).

63. W. von Niessen, L.S. Cederbaum, G.H.F. Diercksen, and G. Hohlneicher, Chem. Phys. 11, 399 (1975); P.J. Hay, J. Am. Chem. Soc. 99, 1013 (1977); W. von Niessen, W.P. Kraemer, and G.H.F. Diercksen, Chem. Phys. Lett. 63, 65 (1979).

Figure Captions

Fig. 1 Photoabsorption spectrum of SF_6 near the S 1s threshold (2490 eV) from Ref. 1. The features discussed in the text are: the S 1s-->$6t_{1u}$ resonance (b), the resonances near 2507 eV (d and e), and the higher-energy feat..es (f and g). Features a and c are not discussed in this work, but have been interpreted as the symmetry-forbidden transitions S 1s($1a_{1g}$)-->$6a_{1g}$ (a) and ct_{2g} (c).[3]

Fig. 2 Sulfur 1s resonance energy-level diagram for SF_6. The $1s^{-1}6t_{1u}$ neutral excited state and its available photoemission decay channels to SF_6^+ are shown with solid lines. Note the presence of "highly excited" S 2p and S 2s satellites produced by decay of the $1s^{-1}6t_{1u}$ state. Two postulated doubly excited states (see text for details) of the neutral are shown also, with some of the corresponding decay channels illustrated by dotted lines. Some excitation and decay pathways have been omitted for clarity. The designations "val" and "v^*" represent outer-valence orbitals, and either $6a_{1g}$ or $6t_{1u}$ orbitals, respectively.

Fig. 3 TOF spectrum of SF_6 taken at $\theta=0^\circ$ and 2581 eV photon energy above the S 1s threshold at 2490 eV. The components for peak A are listed in Table I.

Fig. 4 A TOF spectrum of SF_6 taken at θ=54.7° and 2484 eV near the S $1s(1a_{1g})$-->$6t_{1u}$ resonance.

Fig. 5 Peak A (top) and S(LVV) Auger (bottom) relative cross sections and the photoabsorption measurement (Ref. 1, solid curve). The below-threshold nonresonant intensity has been subtracted from the data and the absorption curve. The data have been scaled to the absorption curve at 2497 eV for comparison. The cross-section scale (in Mb) thus refers strictly only to the photoabsorption data, and not to the photoemission and Auger cross sections.

Fig. 6 Relative cross sections for the $S(L_{1,2,3}VV)$ and $S(L_1L_{2,3}V)$ Auger electrons over the S 1s-->$6t_{1u}$ resonance. The scale for the two lowest-energy points has been expanded times 100.

Fig. 7 Angular-distribution parameters for peak A (top) and S(LVV) Auger (bottom) over the S 1s-->$6t_{1u}$ resonance. The oscillations in β(peak A) above the S 1s threshold mainly are caused by added contributions from S(KLL, KLV, and KVV) Auger electrons.

Fig. 8 S 1s partial cross section (top) and asymmetry parameter (bottom) plotted with MSM results (dashed curve).[13] The

solid curve is the photoabsorption measurement[1] with the below-threshold nonresonant contributions subtracted. The cross-section data have been scaled to this "adjusted" absorption curve at 2535 eV.

Fig. 9 Cross-section ratios (peak A)/(S 1s) (top) and (LVV)/(S 1s) (bottom) in the vicinity of the 2507 eV resonances. For the ratio (peak A)/(S 1s), the F 1s cross section has been subtracted from the peak A intensity using the F(KVV) Auger intensity in each spectrum. Observed S 1s satellite and main-line thresholds also are shown.

Fig. 10 S 1s single-scattering plane-wave EXAFS oscillatory amplitudes χ (percent) for SF_6 as a function of kinetic energy (bottom). The solid and dashed curves represent the χ (percent) calculated with the "adjusted" and sulfur central-atom phase shifts, respectively. The photoabsorption curve[1] is plotted on an absolute scale for comparison (solid curve, top), along with the MSM-Xα S 1s partial cross section[13] (dot-dashed curve, top). The "non-EXAFS" background cross section has not been subtracted from the experimental absorption data. Above 100 eV kinetic energy, an estimation of the sloping background can be made (dashed curve, top) for comparison of the amplitude effects for that energy range. The vertical lines are drawn to emphasize the

energy agreement between the "adjusted" phase shift EXAFS calculation and the experimental absorption data.

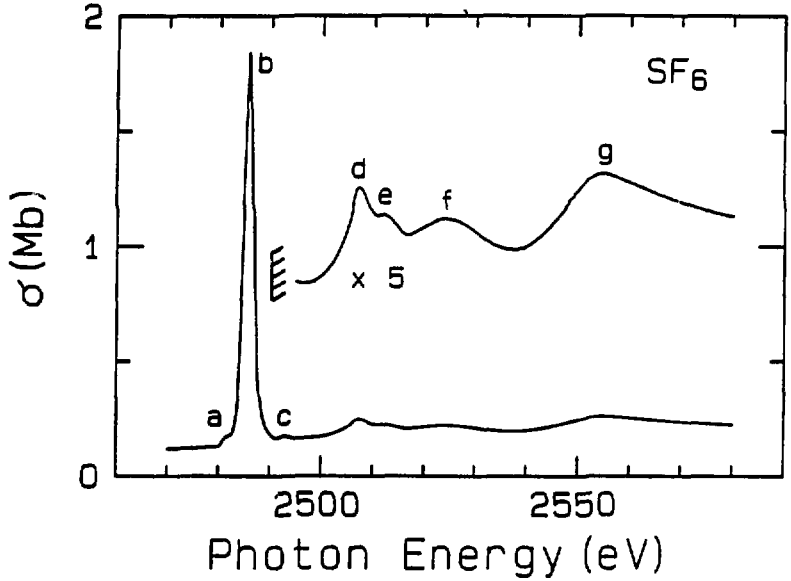

XBL 862-360

Figure 1

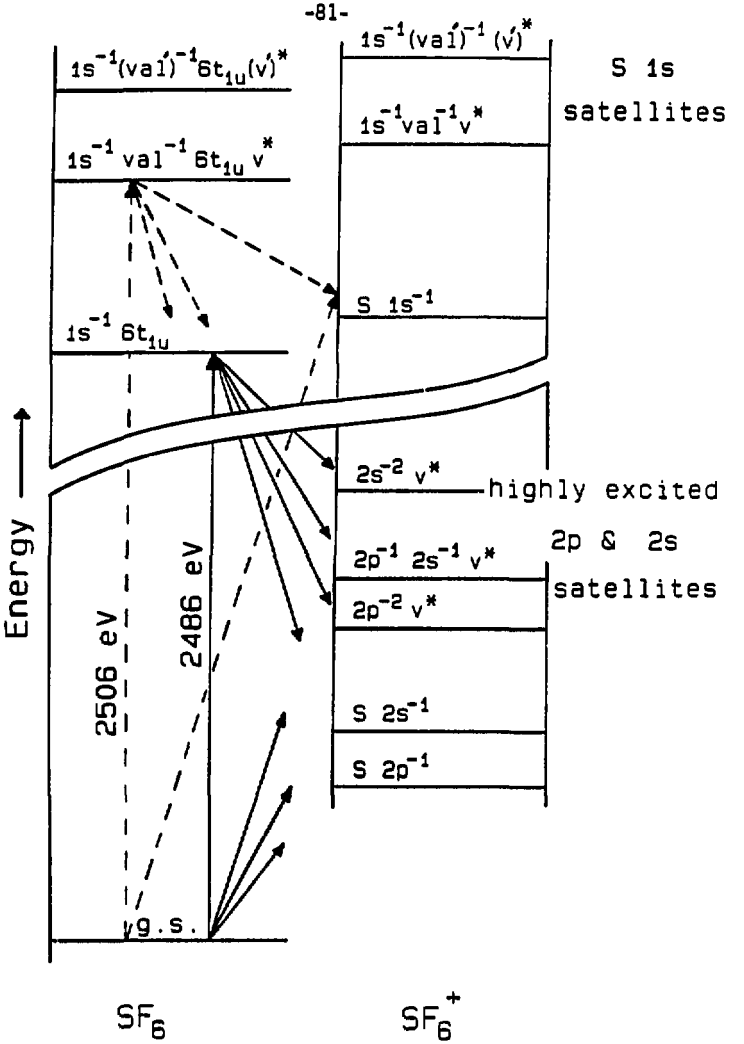

XBL 862-365

Figure 2

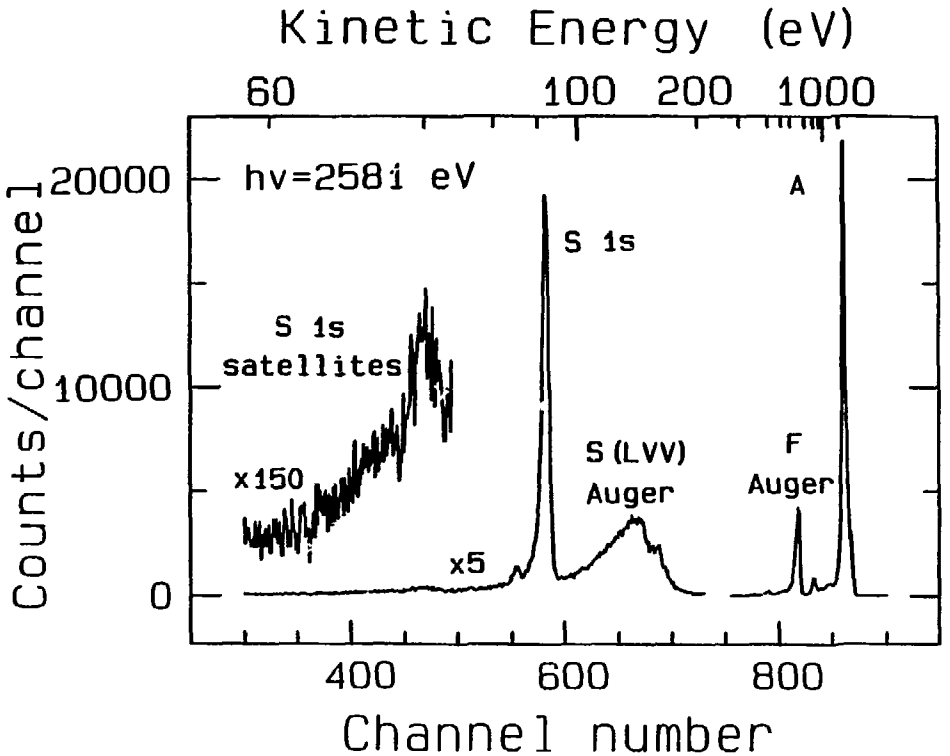

xBL 862-361

Figure 3

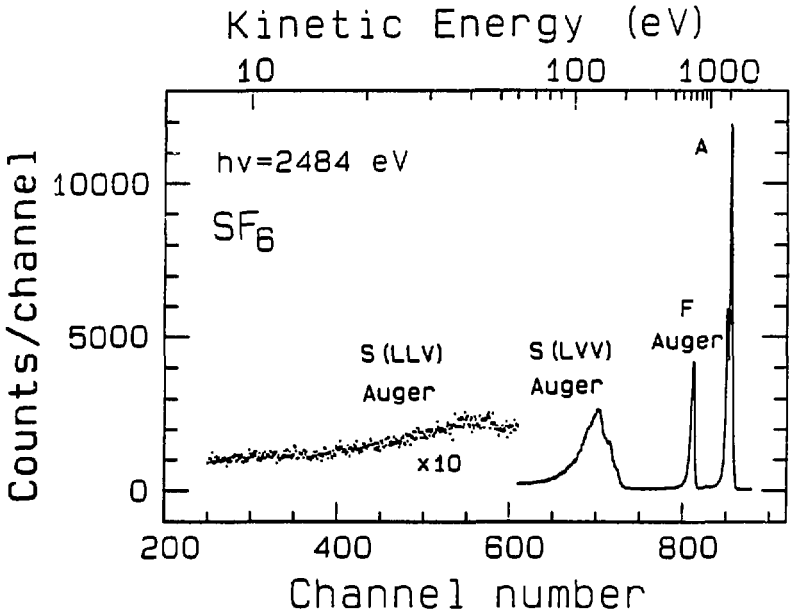

XBL 862-369

Figure 4

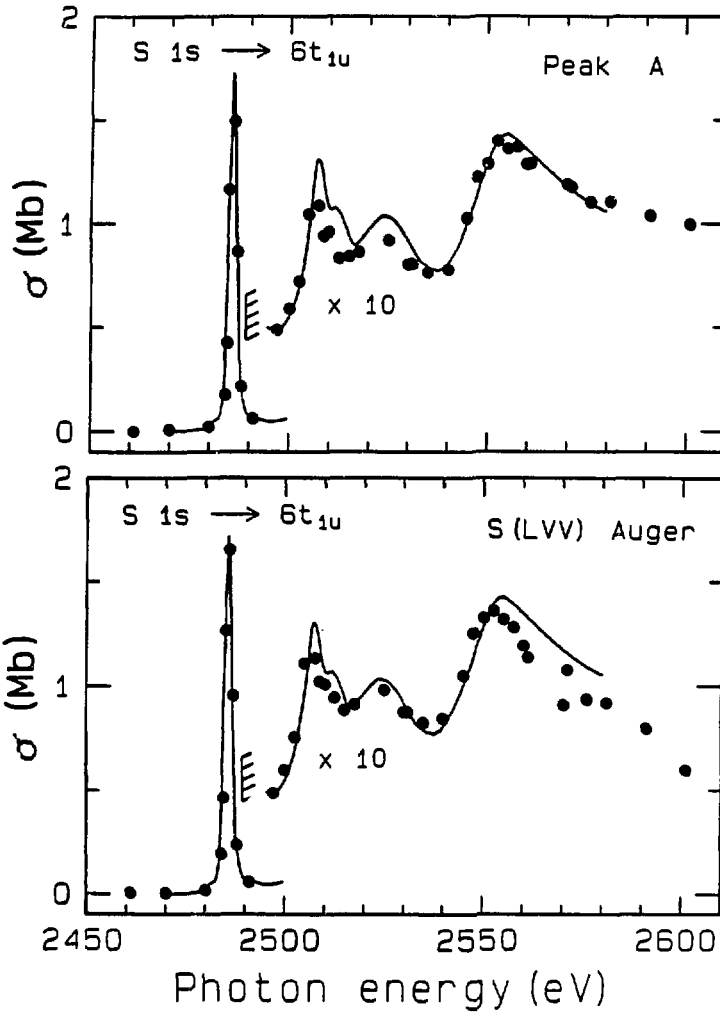

XBL 862-362

Figure 5

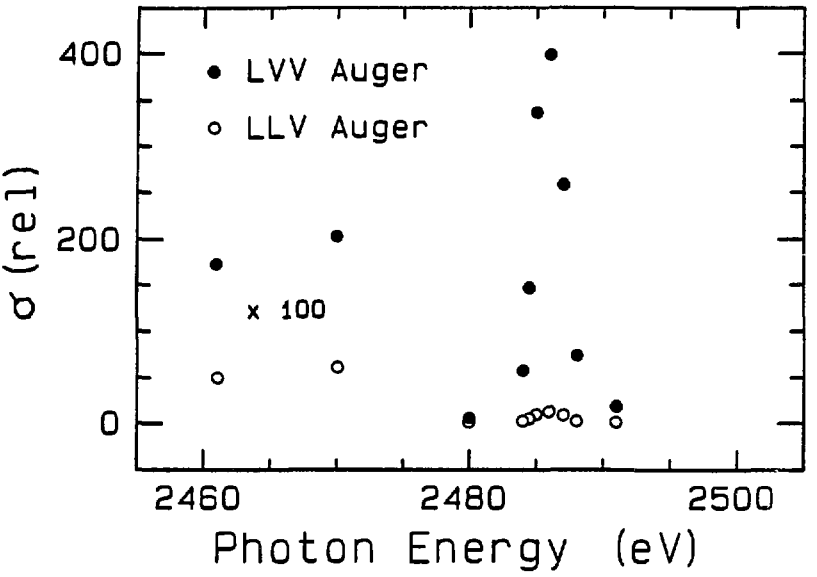

XBL 862-368

Figure 6

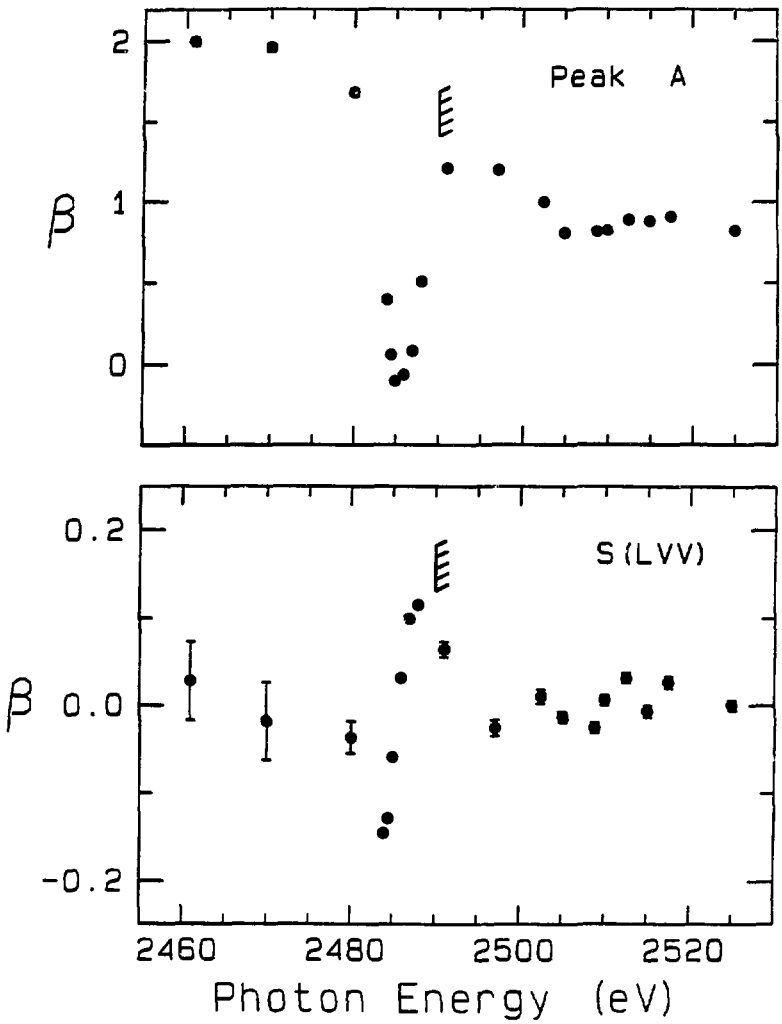

XBL 862-367

Figure 7

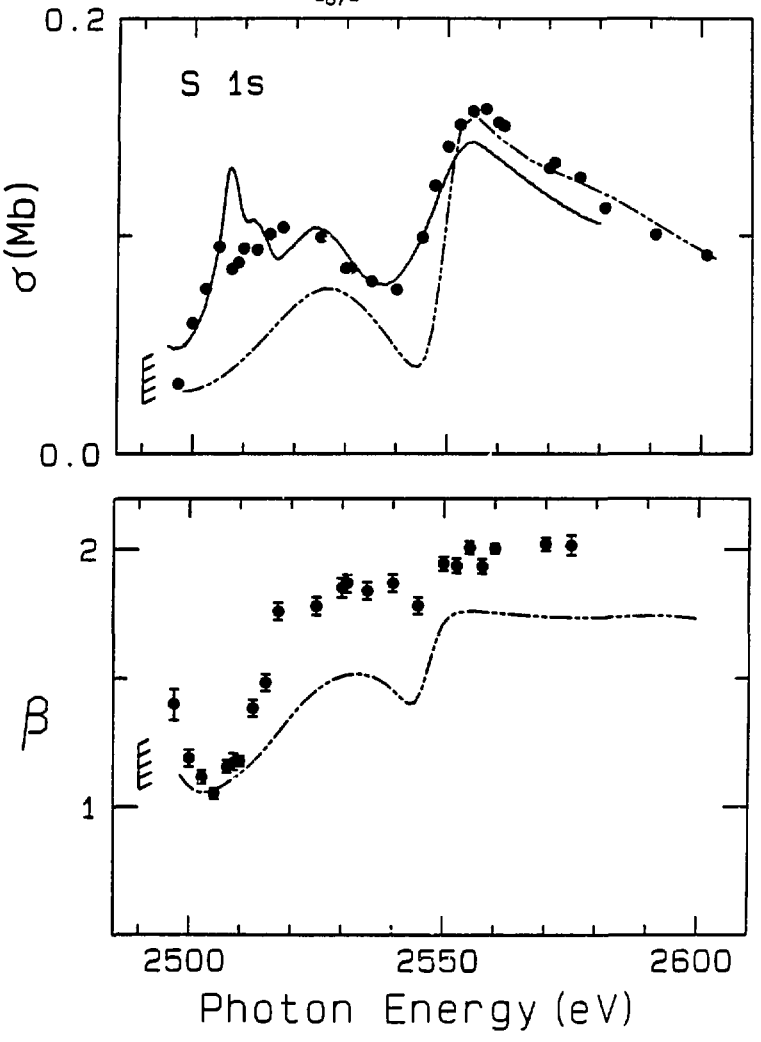

Figure 8

XBL 862-363

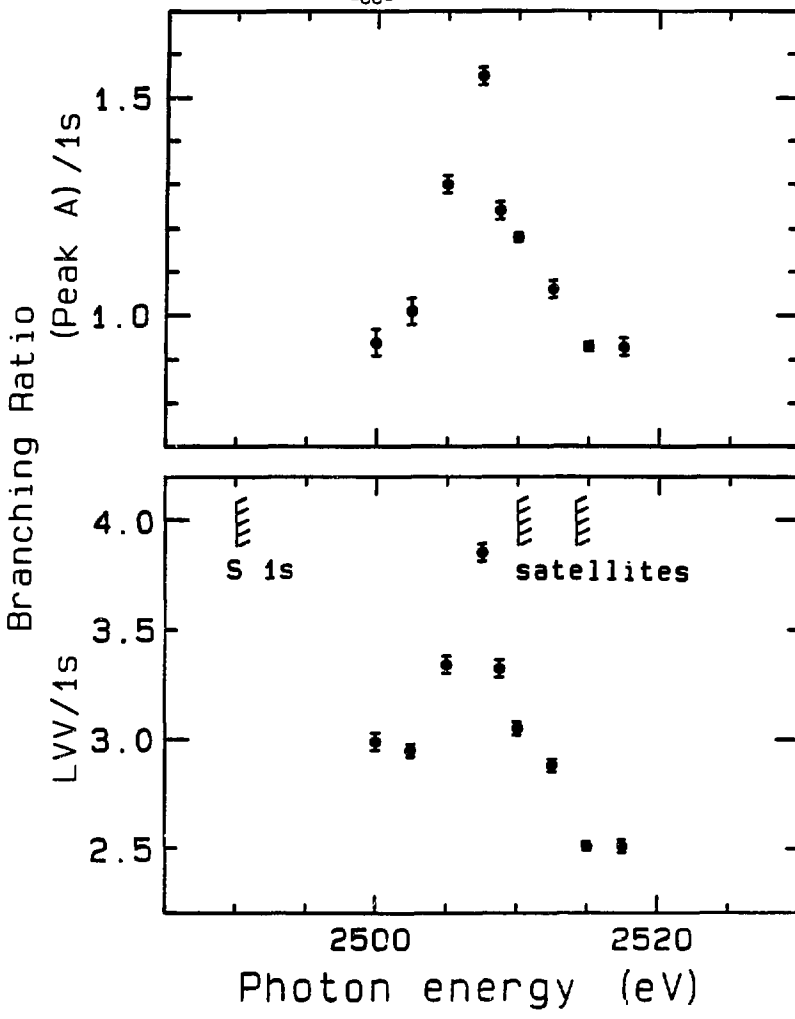

Figure 9

XBL 862-366

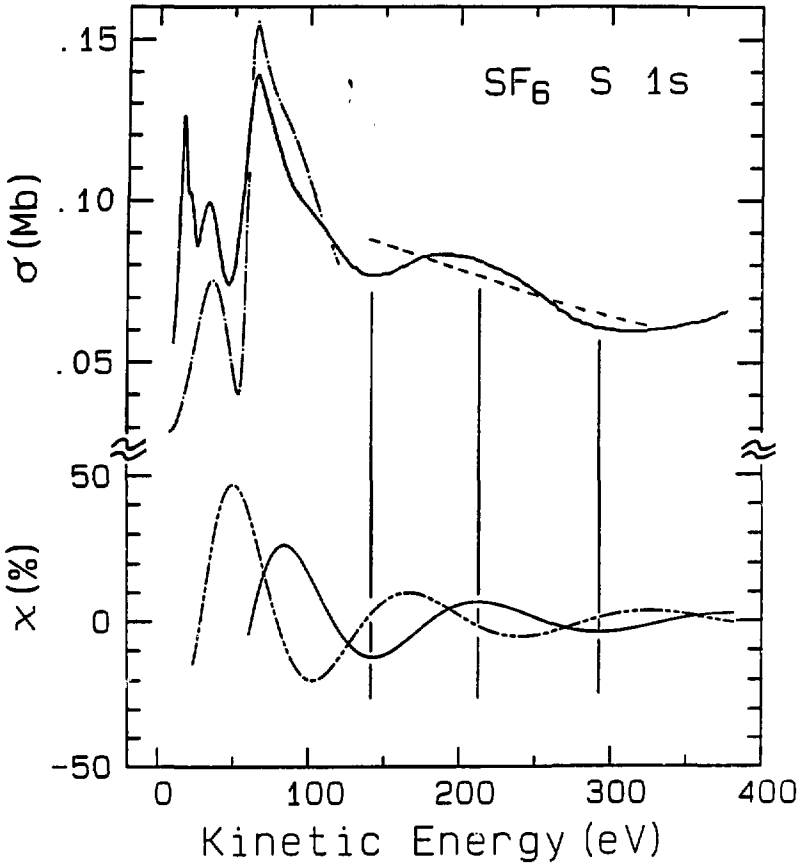

XBL 862-364

Figure 10

IV. Shape-resonant and Many-electron Effects in the S 2p Photoionization of SF_6 *

Abstract

The core-level photoexcitation and photoionization of SF_6 has been studied in the vicinity of the resonances below and above the S 2p threshold. Qualitative results for the decay channels of the S 2p-->$6a_{1g}$ discrete excitation were obtained, with dominant decay to valence satellites. The S 2p continuum results on the e_g shape resonance indicate strong multi-electron properties for this state, because a resonant S 2p shakeup satellite is observed. We propose a model which includes configuration interaction in the quasibound state and in the ionic and continuum state manifolds to explain this unusual behavior. Finally, the S(LVV) Auger electron asymmetry parameter shows no significant deviation from zero near the t_{2g} and e_g shape resonances.

A. Introduction

The distinctive structures in the photoabsorption spectra around the K and L thresholds of highly symmetric molecules have received much attention in recent years.[1-10] For example, spectra near the sulfur and silicon 2p edges in SF_6, SiF_4, and SO_2 are each characterized by two resonances in the L continua, as shown in Fig. 1.[3] The S 2p absorption spectrum for SF_6 exhibits the narrowest (2-4 eV) and most intense continuum resonances, relative to the discrete resonant intensity, in this series.[3] The resonances in these absorption spectra have been interpreted within a potential-barrier model, with the strongest effects being present in high-symmetry molecules containing the most electronegative ligands.[3,5,8,10] Both of these factors tend to enhance the spatial extent and height of the barrier.

The potential-barrier or shape-resonance model that has been widely used in the literature to interpret the molecular absorption spectra is described within a one-electron framework. In this picture, an emerging photoelectron experiences a centrifugal barrier in the molecular potential, through which it can tunnel and propagate in the continuum, with an enhanced photoionization cross section and a perturbed angular distribution, at a particular kinetic energy. Within this description, a shape resonance is strictly a single-channel final-state effect. Shape resonances have been treated as such[10-13] in all but one theoretical calculation[14] to date.

Because of its final-state nature, the shape resonance is usually interpreted as decaying into only one continuum channel (e.g., only the 2p main-line photoemission intensity is enhanced at a shape resonance above the $L_{2,3}$ edge). Because the trapped photoelectron often has a particular angular momentum, it can also be thought of as forming a quasi-bound state associated with an unoccupied molecular orbital in the continuum.[2,4-5] The relation of this model to the potential-barrier approach has been discussed.[7]

Though numerous photoabsorption measurements have been made near the K and L edges in small molecules,[1-3,15] only a handful of photoemission experiments have been performed to study the decay properties of core-level shape resonances.[16-20] Photoionization experiments on the C and N 1s levels in CO, CO_2,[16] N_2, and NO[17] indicate that the one-electron potential barrier model is adequate to explain the observed decay to single-ion final states with a core hole (photoemission main lines). However, the continuum resonances in these molecules are not very intense, and they have widths on the order of 10 eV,[16,17] in contrast to the especially narrow and intense continuum resonances of the S 2p photoabsorption spectrum in SF_6.[3]

To understand the unusual aspects of the resonances in SF_6, we have investigated the resonance behavior of the S 2p main line and its correlation satellites using angle-resolved time-of-flight (TOF) photoelectron spectroscopy. We have measured the photoionization partial cross sections and angular distribution asymmetry parameters

for the S 2p and valence photoelectrons and the S(LVV) Auger electrons in the photon-energy range hν=150-260 eV. Figure 2 illustrates a molecular orbital diagram for SF_6, including the transitions studied in this work. Below the S 2p ($2t_{1u}$) core-level threshold, we have attempted to characterize qualitatively the decay of the $2t_{1u}$-->$6a_{1g}$ discrete resonance by measuring the cross sections and asymmetry parameters for the important photoemission decay channels to SF_6^+. Above the S 2p threshold, we have observed several correlation satellites of the S 2p main line, one of which participates in the continuum e_g resonance at 196.5 eV photon energy. The cross section and asymmetry parameter for this S 2p satellite over the resonance region are also reported.

In the vicinity of the S 2p edge, our observation of a S 2p satellite enhanced at the same photon energy as the S 2p main-line at the so-called e_g shape resonance (196.5 eV) forces us to consider the many-electron nature of this continuum resonance. Because of these unusual decay properties, we will refer to the resonance at 196.5 eV as the "e_g" resonance to indicate uncertainty in its historical assignment. The naive shape resonance picture of a "pure" one-electron final-state effect is clearly inadequate because the S 2p main-line and satellite photoelectrons are at different kinetic energies at the "e_g" resonance. Recent photoemission studies of the valence shells of SF_6 also indicated that something beyond a one-electron description is needed to explain the valence t_{2g} resonance, which exhibits coupling to neighboring channels at 23 eV

photon energy.[21,22] In that case, continuum-continuum coupling was proposed to explain the participation of the final states of even g symmetry in the t_{2g} shape resonance.[21] However, the absence of the e_g shape resonance in the valence shells of SF_6 is especially surprising since in our present understanding it seems to play an important and unusual role above the S 2p edge.

On the theoretical side, K-matrix calculations have established a precedent for continuum-continuum coupling to neighboring channels for a valence shape resonance in N_2,[14] where the angular distribution of the $2\sigma_u$ photoelectrons is affected at the σ_u shape resonance.[23-24] *Continuum-continuum interchannel coupling* as proposed in N_2 (Ref. 14) may cause the S 2p main-line and satellite continuum states to share in the "e_g" resonance intensity. Interchannel coupling effects of this sort are typically small;[25] however, the production of a quasibound shape-resonant continuum state provides a situation where the coupling may be enhanced because of the larger continuum-state amplitude within the molecule.[14]

We propose a more general approach to explain the "e_g" resonance decay, which includes continuum-continuum coupling as well as congifurational mixing in the quasibound state. Electron correlation in this model allows for continuum coupling and the possible energy degeneracy of discrete doubly excited states with the "e_g" resonance; it adequately describes the observed decay to both main-line and satellite channels.

The experimental procedures are described in Sec. B. The discrete

S 2p ($2t_{1u}$)-->$6a_{1g}$ resonance data near ~173 eV photon energy are discussed in Sec. C. The extended-energy-range (185-260 eV) results for the S 2p main line, satellites, and S($L_{2,3}VV$) Auger electrons appear in Sec. D, with emphasis on the behavior at the "e_g" shape resonance (196.5 eV). Section E concludes the interpretation of the SF_6 data.

B. Experimental

Synchrotron radiation from Beam line III-1, equipped with a "grasshopper" monochromator, at the Stanford Synchrotron Radiation Laboratory (SSRL) was used to photoionize an effusive jet of gas. Photoelectrons and Auger electrons were detected simultaneously at 0° and 54.7° relative tc the photon polarization direction using the double-angle time-of-flight (TOF) technique[26-28] and Yang's theorem.[29] Calibration of the TOF analyzers was accomplished using the 2s and 2p levels of Ne^+(Ref. 30) and the 3d level of Kr^+(Ref. 31), for which the partial cross sections and angular distribution asymmetry parameters are known. We estimate that systematic errors (not represented by the statistical error bars in our plots) are less than 10 percent for the relative cross section (σ) and ±0.10 for the asymmmetry parameter (β).

A 1000Å thick vitreous carbon window separated the sample-chamber pressure (10^{-4} torr) from the monochromator vacuum (10^{-10} torr). Photoelectron spectra were taken in the photon-energy range

160<hν<250 eV using a 1200 l/mm holographically ruled grating. The monochromator resolution varied from 1.3 to 3.3 eV over this range. Energy calibration of the monochromator to within 0.5 eV was based on the positions of the resonances in the SF_6 total cross section at 173 eV ($2t_{1u}$-->$6a_{1g}$), 184 eV ($2t_{1u}$-->t_{2g}), and 196.5 eV ($2t_{1u}$-->e_g).[5]

The SF_6 relative sample pressure was monitored with a capacitance manometer and the photon intensity was monitored by a sodium salicylate scintillator with an optical photomultiplier tube (RCA 8850). Corrections have been made in the measured cross sections for the varying response of sodium salicylate in our system over the photon-energy range of this study.[32]

A S 2p time-of-flight spectrum taken for 300 sec at θ=54.7° and at hν=196.5 eV is plotted in Fig. 3, showing the S 2p main-line (binding energy=181 eV)[33] and satellite peaks, the S(LVV) Auger peaks, and the inner- and outer-valence peaks at high kinetic energy. Typical off-resonance count rates were 50 counts/sec for the S 2p level, 5-10 counts/sec for the S 2p satellites, and 300 counts/sec for the total valence intensity.

The major discrete and continuum resonance effects near the S 2p edge can be seen in Fig. 4. The experimental data below the S 2p threshold represent the total inner- and outer-valence intensity, and above threshold, the sum of the valence and $S(L_{2,3}VV)$ Auger intensity. For comparison, the photoabsorption curve[1] is plotted, along with our total measured valence main-line cross section.

C. The S 2p ($2t_{1u}$)-->$6a_{1g}$ Resonance

Recent work on the decay properties of discrete core-level excitations in atoms and small molecules has provided a framework in which to describe decay to singly-charged ionic final states.[34-39] These final ionic states are often "spectator" satellites in the photoelectron spectrum; they are correlation satellites of the ion with two holes and an additional electron in the orbital initially reached by the excitation process in the neutral. For decay to these final states, the excited electron is pictured as a "spectator" to the relaxation of the core hole.

However, not all decay proceeds with the initially excited electron as a noninteracting spectator. The involvement of this electron in the decay usually produces photoemission "main lines", final states corresponding to singly-charged ions with one hole. Nonspectator satellites can be produced in this participatory decay when the excited electron is left in an orbital other than the one to which it is initially excited. The overall extent to which the excited electron participates is generally not negligible, accounting for 5-25 percent of the resonance intensity in the few systems studied to date.[37]

The relative amounts of spectator and participatory decay have been found to vary at the intense 1s-->π^* resonances below the C, O, and N K edges in CO and N_2.[37] The variations are related to the coupling of the initially excited electron to the rest of the ion in

the decay process. To a first approximation, participatory decay is expected to be more favored when the excited π^* electron is localized on the atom containing the core hole.[37]

Below the S 2p edge in SF_6, the $(2t_{1u})^{-1}6a_{1g}$ neutral excited state can autoionize to outer- and inner-valence main-line photoemission channels and valence shake-up satellites (participatory decay), and to "spectator" satellites. These states are illustrated in the binding-energy spectra taken on (172.9 eV) and off (176.1 eV) resonance, shown in Fig. 5. Qualitatively, the unresolved outer-valence peaks with binding energies between 15 and 27 eV show little enhancement, in contrast to the large intensity increase in the binding-energy range 35-60 eV. Included in the region labelled "inner" valence are the unresolved outer- and inner-valence satellites, plus the inner-valence main-line peaks ($2e_g$, $3t_{1u}$, and $4a_{1g}$).[40] The total valence intensity (main lines and satellites) over the $6a_{1g}$ resonance is plotted in Fig. 4.

Though it is not possible in the TOF photoelectron spectrum to resolve the outer-valence satellites from the inner-valence main lines, there is a difference in the peak shapes on and off resonance in the binding-energy region of 35-45 eV. On resonance, there are greater contributions at binding energy ~35 eV, indicating some enhancement of outer-valence satellites. This result has been confirmed qualitatively by electron energy-loss measurements at the S 2p-->$6a_{1g}$ resonance.[42] In addition, there is a resonantly-enhanced peak at 55 eV binding energy, corresponding

energetically to an inner-valence satellite(s). Thus, we have direct spectroscopic evidence for autoionization decay to satellite channels, although we can not assess quantitatively the importance of these channels relative to inner-valence main-line decay. However, we observe that decay to outer-valence main lines is not large, accounting for less than 7 percent of the total resonant enhancement.

To further document the dominant decay into SF_6^+ final states with binding energies $\geq$35 eV, the partial cross-section data for the observed outer- and "inner" valence peaks are shown in Fig. 6, along with the "inner" valence asymmetry parameter. The "inner" valence peak integration included the binding energy range 30 to 100 eV.[42] This energy region carries most of the resonant intensity, in contrast to the small effect on the outer-valence levels. Consistent with this, the outer-valence β is relatively constant over the resonance at a value of 1.36(7), while the "inner" valence β decreases from an off-resonant value above 1.0 to 0.3 on resonance.

We conclude that valence satellites are important decay channels for the S 2p-->$6a_{1g}$ resonance, with the prospect that most of the satellites are probably spectator in nature (containing a $6a_{1g}$ electron), though higher kinetic-energy resolution studies are needed to confirm this. The amount of enhancement of the inner-valence main lines ($2e_g$, $3t_{1u}$, and $4a_{1g}$) is not clear because these photoemission peaks are unresolved from the outer-valence satellites. In terms of the $2p^{-1}6a_{1g}$ excited-state localization, the 2p hole is well-localized on the sulfur atom where the $6a_{1g}$ orbital has

significant intensity. Thus, some participation of the $6a_{1g}$ electron in the decay to SF_6^+ seems possible, explaining the small effect seen in the outer-valence cross section (Fig. 6).

Finally, the added complication of many-electron correlations in the inner-valence region should be considered, because this produces many overlapping peaks in the photoelectron spectrum, each representing possibly more than one ionic configuration. In the molecules H_2O (Ref. 33, 43) and especially H_2S (Ref. 44), the nonresonant inner-valence spectrum is more complex than the one-electron molecular orbital picture would dictate. Thus, progress in understanding the extent of the many-electron interactions in the inner-valence orbitals are necessary before a more complete picture of the resonant decay to these states can be acquired.

D. Above the S 2p Main-Line and Satellite Thresholds

The extended energy-range behavior of the S 2p main line (binding energy 181 eV)[33] is depicted in Fig. 7. The assigned "e_g" shape resonance is evident in the S 2p cross section at 196.5 eV, and the S 2p β undergoes an oscillation in the vicinity of this resonance. The broader weak feature at ~205 eV in the absorption data (Fig. 4) may also be present in the S 2p partial-cross-section data. The MSM-Xα S 2p (Ref. 8) and the experimental SiF_4 Si 2p (Ref. 45) asymmetry parameters are plotted for comparison, along with the atomic β(2p) for Al.[46] Although we were not able to extend our S 2p

measurements to the t_{2g} shape resonance at 184 eV photon energy (except for one point at 185.7 eV), we do note that no enhancement of the valence main lines was observed at the t_{2g} resonance (see dashed curve, Fig. 4). Thus, the following discussion will center on the observation of S 2p shake-up satellites, and the S 2p main-line and satellite behavior near the e_g resonance.

Several S 2p correlation satellites were visible in the photoemission spectra with binding energies of 189(1), 194(1), and 205(2) eV. The corresponding excitation energies above the S(2p) threshold are 8(1), 13(1), and 24(2) eV. The satellites were easily distinguished only at low kinetic energies for each satellite; thus, we show only the resonant satellite [binding energy 189(1) eV] in Fig. 3. We have used the recently proposed valence ordering[21] confirmed by many-body theoretical calculations[47] to estimate the energies of the configurations responsible for the observed satellites. Also utilizing the $4t_{1u} \rightarrow 6a_{1g}$ transition energy of 17 eV in the neutral, we find that the most likely configuration for the lowest binding-energy satellite is $2p^{-1}1t_{1g}^{-1}6a_{1g}$, which corresponds to an excitation from the highest occupied ($1t_{1g}$) to the lowest unoccupied ($6a_{1g}$) molecular orbital. We cannot assign with certainty the remaining satellite peaks (with excitation energies of ~13 and 24 eV), but there are several possible configurations in these energy ranges assuming that the 189 eV satellite configuration is correct. The likely possibilities are:

$2p^{-1}1t_{2g}^{-1}6a_{1g}$
$2p^{-1}3e_{g}^{-1}6a_{1g}$
$2p^{-1}(5t_{1u}$ or $2t_{1u})^{-1}6t_{1u}$ } B.E. 194(1) eV

$2p^{-1}4t_{1u}^{-1}6t_{1u}$
$2p^{-1}5a_{1g}^{-1}6a_{1g}$ } B.E. 204(2) eV

The rest of this section will address the results obtained at the t_{2g} and "e_g" continuum resonances, with emphasis on the "e_g" resonance (196.5 eV). Section 1 includes presentation of the cross-section and asymmetry-parameter data for the S 2p main-line and the 189 eV satellite peaks and for the $S(L_{2,3}VV)$ Auger peak. In Sec. 2, we interpret the unusual observation of coupling to other channels at the "e_g" shape resonance, and discuss the possible explanations for this behavior.

1. Photoelectron and Auger Electron Results

The overall shape of the S 2p cross section and β over the "e_g" resonance appears in Fig. 7, and over a smaller energy range in Fig. 8. The S 2p satellite (binding energy=189 eV) cross section and β are plotted in Fig. 8, with the main-line results for direct comparison. We observe a large cross-section enhancement of both the S 2p main line and the 189 eV satellite at the same photon energy. The main-line and satellite asymmetry parameters (Fig. 8) also

correlate well as a function of photon energy over the resonance region. This is the first observation of a molecular shake-up satellite with enhanced intensity at a feature assigned as a shape resonance.

The time-of-flight (TOF) spectrum in Fig. 3 taken on the "e_g" resonance shows the large satellite intensity. Off resonance, the satellite intensity is about 15 percent relative to the main line, and it increases to ~30 percent on resonance. The intensity of the 189(1) eV satellite could only be monitored up to about 200 eV photon energy, above which it became unresolved from the satellite of binding energy 194(1) eV.

Having observed decay into a channel other than the S 2p main line at the "e_g" resonance, we also checked the total valence intensity over the "e_g" resonance region. No measurable enhancement was observed, as seen in the valence cross section shown in Fig. 4 (dashed curve).

The effect in the S 2p β near the "e_g" resonance is dramatic, and is reproduced qualitatively by the MSM-Xα calculation[8] when the theory curve is shifted to the experimental resonance energy (i.e., theory shifted to lower energy by 1.8 eV). The width of the resonance is too narrow in the calculation, which is expected because vibrational,[48] orbital relaxation,[8,49] and intrachannel coupling effects[50] (all of which tend to broaden the theoretical resonant profiles) have not been included.

We next consider to what extent the observed effect in β(S 2p) is

correlated with the "e_g" resonance rather than with the natural energy dependence of the angular distribution. Previously, it has been observed experimentally[16,45] and theoretically[8,51] that an increase in the cross section at a core-level molecular shape resonance is generally accompanied by a minimum in the β (sometimes offset in energy from the cross-section maximum) for the affected continuum channel.

To assess whether the β effect in SF_6 is induced primarily by the resonance, we first examine the atomic behavior for a 2p orbital. No calculations of β are available for the 2p level of atomic sulfur, but the shape should be similar to the atomic Al curve calculated by Manson,[46] also shown in Fig. 7. The shape of the atomic β(2p) within ~30 eV of threshold is the result of the changing Coulomb phase shift differences between the l+1 and l-1 transitions.[46] The atomic curve has the same overall shape as the experimental β results for SF_6, with a minimum in β within 15 eV of threshold, followed by a climb to an asymptotic value of $\beta \geq 1$. The atomic curve is also at higher values of β at all energies relative to the S 2p asymmetry parameter curve for SF_6. We do note that the minimum in β(S 2p) for SF_6 is more pronounced and occurs over a narrower energy range compared to the atomic β(2p), suggesting a molecular resonance effect.

Secondly, we compare our β(S 2p) curve to β(Si 2p) of SiF_4,[46] shown in Fig. 7 (open circles). Within experimental error, the two curves are identical as a function of kinetic energy with possible small differences in the asymptotic β value. This result is

surprising if one believes that the pronounced minima in β are indicative of the shape resonances in the two molecules (see Fig. 1), which occur at different kinetic energies (3 and 15.5 eV for SF_6; 5.5 and 21.5 eV for SiF_4).[1,52] Furthermore, the decay characteristics of the second resonance for each molecule are markedly different. The SF_6 continuum "e_g" resonance decays to the S 2p main line and to a S 2p shake-up satellite; in contrast, the broad (~10-15 eV) SiF_4 t_2 shape resonance (21.5 eV kinetic energy) seen in Fig. 1 decays only to the Si 2p main line,[19] thus fitting the one-electron shape-resonance model.

In addition, the Si 2p β curve for $Si(CH_3)_4$,[45] which has been compared previously with SiF_4, has a similar shape but a higher value of β between about 5 and 15 eV kinetic energy relative to SiF_4. This difference has been attributed in part to the different electron densities in the two Si-containing molecules.[45] We also note that the Si 2p cross section in $Si(CH_3)_4$ is different as a function of kinetic energy from both SiF_4 and SF_6, with a series of resonances very near threshold and one broad (~10 eV FWHM) continuum resonance at about 18 eV kinetic energy.[15,20]

The variation in the energies and nature of the continuum resonances in these molecules, coupled with the observation of different decay patterns for the resonances in SiF_4 and SF_6 and the known atomic behavior, strongly suggest that the overall shape of β(S 2p) may have origins in atomic effects as well as shape resonance effects in these S- and Si-containing molecules. In fact, MSM-Xα

asymmetry-parameter results on the Si 2p level in SiF_4 are qualitatively very similar to the atomic Si 2p Hartree-Slater results.[45] Photoemission measurements and calculations on the Si and S 2p levels in molecules which do not exhibit pronounced continuum resonances would help to identify the nonresonant "molecular" behavior of the β at low kinetic energy.

In addition to the effect on the photoelectron asymmetry parameter, the angular distribution of Auger electrons may become anisotropic in the vicinity of a shape resonance. Theoretically, the Auger electron angular distribution (β_{Auger}) has been related to the asymmetry in the molecular orientation of the ion (β_m) as:[53]

$$\beta_{Auger} = c\,\beta_m, \qquad (1)$$

where c is a constant characteristic of a single Auger decay channel. The possibility for ion orientation at a shape resonance may induce an anisotropy in the Auger electron emission, weighted by the factor c. However, there are no known examples of detectable changes in β_{Auger} at a continuum molecular shape resonance, although KVV Auger electron measurements have been reported above the C, O, and N K edges in a number of molecules.[16-17] The lack of anisotropy has been explained by the low-resolution experimental measurements which effectively sum over many individual Auger transitions, and by the possibly small values of c which would serve to reduce any substantial oscillation in a given ion orientation β_m.[16]

For the t_{2g} and "e_g" resonances in SF_6, the β for the $S(L_{2,3}VV)$ Auger peak was determined by deconvolution from the valence peaks using the measured total valence cross section (Fig. 4) and assuming an unchanging total valence β over the resonances. The estimated error is 10 percent in the total valence cross section and ± 0.10 for the total valence asymmetry parameter. The resulting S(LVV) Auger β, shown in Fig. 9, is not strongly affected by the resonances, within the experimental errors stated above. This result may be rationalized with the previous arguments that low resolution measurements sum over individual Auger lines weighted by small values for c, smearing out effects in any one channel. Higher resolution measurements will be valuable in testing this hypothesis. Meanwhile, the lack of a definite resonance effect on β_{Auger} is perplexing. If this observation is sustained by more careful meausurements, the lack of any significant anisotropy for β_{Auger} at the intense continuum resonances in SF_6 and other molecules would call for a reexamination of the predictions that a shape resonance should produce anisotropic emission of Auger electrons.

2. Discussion of the "e_g" Resonance

The most significant result at the "e_g" resonance is the satellite and main-line intensity enhancement at the same photon energy (Fig. 8). This behavior suggests that an excited state (quasibound or discrete) is decaying to several final states. In this

section, we discuss and evaluate interpretations for this behavior.

If the 196.5 eV resonance is truly the e_g shape resonance, its decay into several channels is in conflict with the one-electron picture of shape-resonance phenomena, which predicts decay into one channel. Because shape resonances have been described as final-state effects, where a continuum electron is trapped by a potential barrier at a particular kinetic energy, we would expect, in a strict one-electron picture, to see satellite enhancement at the same kinetic energy as main-line enhancement,[54] rather than at the same photon energy. In other words, each satellite might show a shape resonance. The resonance kinetic energies would ordinarily be quite similar because the potential-field barriers would differ little from one satellite to another. In this simplest picture, each shape resonant event would proceed via a unique channel, through a particular barrier state to the corresponding final state in SF_6^+. Each channel would be resonant at its own characteristic kinetic energy.

Contrary to this simple model, correlations of shape-resonant effects in several channels as a function of photon energy have been observed previously. In fact, a similar coupling to nearby channels at $h\nu$=23 eV has been seen in SF_6 for a feature interpreted as the valence t_{2g} shape resonance.[21-22] In N_2, some experimental[23-24] and theoretical[14] evidence indicates that continuum-continuum coupling could lead to an effect on β in the neighboring $2\sigma_u$ channel at about the photon energy of the $3\sigma_g \rightarrow \varepsilon\sigma_u$ shape resonance. However, these valence resonances in SF_6 and

N_2 are not yet completely understood. For example, there may be possible complications in the SF_6 valence region due to autoionizing states.[21] Also, the K-matrix calculations for N_2 (Ref. 14) are preliminary at this point; there is a minimum in the $2\sigma_u$ experimental cross section,[55] but it is not clearly attributable to coupling with the $3\sigma_g \rightarrow \varepsilon\sigma_u$ shape resonance.

In atoms, the results are more definite. A similar coupling of shape resonances to other channels has been observed in Xe and Ba.[56-60] For Xe, the 5p and 5s main-line photoemission cross sections are affected at the $4d \rightarrow \varepsilon f$ shape resonance.[56-57] However, Xe 4d photoemission still dominates the other channels by an order of magnitude.[56] In addition, measurements up to 75 eV photon energy suggest that some 5p and 5s correlation satellites are enhanced at the Xe 4d shape resonance.[58] For the $4d \rightarrow 4,\varepsilon f$ giant resonance in Ba just above the 4d threshold, preliminary reports indicate that 4d satellite intensities are influenced by the shape resonance, though the intensity maximum in the satellite cross sections may be offset in photon energy from the 4d main-line maximum.[60]

These examples illustrate the many-electron nature of the broad "collective" shape resonances in atoms. Similar interchannel interactions may also occur at molecular shape resonances; the SF_6 resonance behavior (t_{2g} in the valence shell[21-22] and e_g in the S 2p level) may in fact be the first examples where multi-electron effects are exhibited in molecular shape resonances. Furthermore, the correlation of the S 2p main-line and satellite β's versus photon

energy (Fig. 8) may also argue for this interpretation, which retains the qualitative aspects of the nature of a shape resonance while allowing for continuum state coupling.

More generally, we postulate configuration interaction not only in the continuum as discussed above, but also in the quasibound state itself. Figure 10 illustrates the general aspects of our interpretation. Configurations will mix, to form eigenstates, both in the SF_6^+ ion and continuum manifolds and in the manifold of quasibound states, each consisting of an electron trapped in a barrier. This coupling also includes possible admixtures of doubly excited states with the quasibound state.

Significant admixtures of discrete doubly excited states would complicate the dynamics of the "e_g" shape resonance. If a doubly excited state were an important component in the "e_g" quasibound eigenstate, then there should be a corresponding satellite threshold at higher photon energy. As mentioned earlier, we do observe a satellite with a binding energy of 205(2) eV, which is 7-11 eV above the "e_g" resonant feature. The energy separation of the S 2p-->$6a_{1g}$ discrete resonance and the S 2p threshold is also in this energy range (8 eV). This implies that the neutral doubly excited state and satellite configurations may be $SF_6(2p^{-1}val^{-1}6a_{1g}v^*)$ and $SF_6^+(2p^{-2}val^{-1}v^*)$ respectively, where val and v^* are generalized valence orbitals initially occupied (val) or unoccupied (v^*) in the neutral. The presence of an excited $6a_{1g}$ electron in the resonant state configuration would help to explain the strong observed coupling

to the 189(1) eV satellite which we have proposed in Sec. D to have the configuration $SF_6^+[2p^{-1}(1t_{1g})^{-1}6a_{1g}]$.

We also might expect to see doubly excited resonances leading to the other satellite thresholds observed by us [189(1) and 194(1) eV]. For the 189(1) eV satellite, we believe that the most intense resonant states below this threshold would involve excitations into $6a_{1g}$ and $6t_{1u}$ molecular orbitals. One symmetry-allowed transition would be to the configuration $2p^{-1}(1t_{1g})^{-1}6a_{1g}^2$, which would fall at about 186 eV (that is, 3 eV below the satellite threshold). The assigned t_{2g} shape resonance at 184 eV might include interaction with this state.

For the 194(1) eV satellite and parallel to the above arguments, we would expect to see doubly excited resonances 3 and 8 eV below this satellite threshold. The neutral resonant configurations would be $2p^{-1}val^{-1}v^*6t_{1u}$ (191 eV) and $2p^{-1}val^{-1}v^*6a_{1g}$ (186 eV), leading to the satellite configurations $2p^{-1}val^{-1}v^*$. Again, 186 eV photon energy is a little higher than the resonance at 184 eV, and there is no resonance evident at ~191 eV photon energy.

We encourage caution in presenting the above arguments for assessing the importance of doubly excited states in the sulfur L continuum. First, our total knowledge of molecular autoionizaton is very limited, especially with respect to doubly excited states. Secondly, the energies of the doubly excited states postulated above have been estimated using the energy spacing of the single excitations relative to the sulfur K and L shells of SF_6. This relative spacing

will be different for a doubly excited state referenced to its corresponding satellite threshold. For example, in atomic Ne, the energy difference between the 1s-->3p resonance and the Ne K edge is 3 eV.[61] Above the K edge, there are several doubly excited states (with configurations $1s2s^22p^53p^2$) which lead to satellite thresholds of Ne^+ ($1s2s^22p^53p$), with a relative spacing of 5-6 eV.[61] The change in the energy spacing from 3 to 5-6 eV is a reflection of screening differences in the neutral and ionic configurations.

Finally , we note that there is some evidence for autoionization of doubly excited states above the sulfur K edge in SF_6,[39] though the intensity in these resonances is down by more than an order of magnitude from the single excitations situated below the K edge.

There are still several puzzling observations which remain. The "e_g" shape resonance not only produces an intense feature in the L-shell cross section, but also exhibits strong multi-electron effects in its decay. In analogy, we would expect to see a similar feature in the valence shell ionization channels of the proper symmetry (u). However, there is no evidence for even the existence of an outer-valence e_g shape resonance in SF_6. There is some evidence for an e_g resonance in the inner-valence levels of SF_6.[62]

The width of the "e_g" resonance in the L-shell (4 eV) is very narrow in comparison with shape resonances in other molecules at a comparable kinetic energy of ~15 eV. The existence of such a long-lived quasibound state at such high kinetic energy is

experimentally unprecedented, and at odds with the resonance energy/width relationship obtained from the uncertainty principle for quasibound states. For atoms, this energy/width relation has been parameterized by Connerade[63] with a shape-independent model, confirming that the resonances broaden out as the kinetic energy increases. MSM X-α calculations[48] which vary the N_2 bond distance over the range of the ground state wavefunction also illustrate this trend in a given molecule. Of course, SF_6 has a very different molecular potential than atoms and diatomic molecules, so these comparisons may not strictly apply.

Another issue involves the origin of the weak feature at $h\nu$=205 eV photon energy. Excitation into doubly excited states of the neutral and/or into satellite continua of the ion have been proposed in the past to explain this broad feature in the total cross section.[4,6] Based on our tentative observation of some enhancement in the S 2p main-line channel in this energy region (see Fig. 7), we can probably rule out an explanation involving satellite continua onsets. We still allow for the contribution of doubly excited resonant states, though this interpretation seems problematic considering the energy proximity of the resonant feature (205 eV) with respect to the nearby satellite thresholds [205(2) eV]. Another proposal for this 205 eV feature involves the onset of "direct" ionization which occurs near this energy (just above the barrier associated with the e_g shape resonance).[3] As the electron kinetic energy exceeds the barrier height, a modulation in the cross section

occurs.[3] To date, an observable cross-section effect of this nature is unprecedented, though it may occur in molecules (like SF_6) which exhibit unusually large continuum effects.

It is also possible that the 205 eV feature corresponds to a second quasibound state of e_g symmetry, about 15 eV above the first satellite threshold. This state could decay (in a many-electron picture) to any energetically accessible satellites, and to the S 2p main line. Though we tentatively observe enhancement in the main line at this energy (see Fig. 7), low cross sections prohibited a similar measurement on the satellite peaks. Observation of satellite enhancement near $h\nu$=205 eV would help to define the nature of this feature.

In summary, this model which generally includes configuration interaction not only explains why the main line and the 189 eV satellite are both resonant at the same photon energy, but it also predicts that these two lines, and the other satellites, can in principle all be resonant at the energies of the quasibound eigenstates. Of course, most of the other resonances will be of low intensity. It would be of interest to do experiments designed explicitly to detect the weaker resonances (the 205 eV feature is a good candidate).

Clearly, calculations on SF_6 are needed to incorporate correlation effects at a practical level and focus the interpretation on the continuum interactions and on the actual composition of the quasibound eigenstates.

E. Conclusions

The gas-phase results reported here for photoionization near the S 2p edge in SF_6 have revealed the importance of many-electron effects at the unusually intense discrete and continuum resonances in the photon energy range of 160-260 eV. For the S 2p-->$6a_{1g}$ discrete transition, our low-resolution spectra yield qualitative information on the decay channels to SF_6^+. We see valence satellite enhancement predominantly in the binding-energy range of 30-80 eV, with several distinct peaks at 35 and 55 eV binding energy. We suspect that most of the satellites are "spectator" states, containing the initially excited $6a_{1g}$ electron. Some participatory decay was found, as evidenced by the small effect on the total outer-valence cross section. Because of overlap with satellites near 40 eV binding energy, we cannot rule out additional participatory decay to inner-valence main lines.

The specific assignment of the valence satellite configurations enhanced at the 2p-->$6a_{1g}$ resonance has not been attempted because these peaks are very broad in our photoelectron spectrum and are probably associated with many configurations. Furthermore, interactions in the inner-valence orbitals of other molecules have been found to require a many-body approach to model even the nonresonant main-line energies and intensities. Higher resolution experiments could delineate this structure found in the binding-energy region 30-80 eV, while many-electron calculations (which are

admittedly very difficult for SF_6) for the inner-valence main lines and valence satellites would help to assign the individual peaks.

For the S 2p continuum resonances, our examination of the S 2p asymmetry parameter within 40 eV of threshold suggests that the "atomic" sulfur behavior is embodied in the low kinetic-energy behavior. Comparison with other sulfur and silicon-containing molecules indicates that the 2p β's are surprisingly similar as a function of kinetic energy, despite the strong variations in the continuum resonance energies, widths, and intensities (See Fig. 1). In addition, the $S(L_{2,3}VV)$ Auger electron β remains near zero over both continuum resonances, contrary to qualitative theoretical predictions.[53] Despite the fact that the nature of the e_g resonance is uncertain, we believe that this lack of significant anisotropy at both continuum resonances in SF_6 and in other molecules may call for a reinvestigation into the relationship between molecular ion orientation and the angular characteristics of subsequent Auger electron emission.

For the S 2p continuum, the t_{2g} and e_g resonances in SF_6 have for years been used as illustrative and outstanding examples of how dramatically potential-barrier effects can modify the photoabsorption intensity near a core-level threshold. The enhancement of a S 2p correlation satellite at the assigned e_g resonance seriously questions the one-electron interpretation of this resonant feature (196.5 eV). It is noteworthy that a similar situation exists for the valence-shell ionization of SF_6, where

several valence final states couple to a feature at 23 eV photon energy assigned as the t_{2g} shape resonance.[21-22]

We have proposed an heuristic model based on observation plus general features of many-electron systems to explain the S 2p satellite enhancement at the "e_g" resonance. Many-electron interactions which are known to complicate the decay dynamics for atomic shape resonances may play a role at the molecular shape resonances in SF_6. In a sense, the qualitative aspects of the shape resonance model still apply, with the decay properties modified by configuration-interaction in the quasibound, ionic, and continuum manifolds. The admixtures of doubly excited states leading to S 2p satellite thresholds is allowed for in this interpretation. We believe that theoretical calculations are required to understand the origin of the unusual satellite enhancement at the e_g resonance. In addition, the nature of the broad cross-section feature at 205 eV photon energy is directly related to any consistent assignment of the e_g resonance. Thus, experiments on the decay properties of this broad peak could help to elucidate the role of many-electron and autoionization effects in this energy region.

Overall, these core-level photoemission results, along with recent experiments on the valence shells of SF_6,[21-22] present a major challenge to the understanding of molecular shape resonances. Rather than being a prototypical example of potential barrier effects, SF_6 is most likely a very special case which provides us with a testing ground for investigating unusually strong many-electron

interactions in molecules.

References

* Work done in collaboration with D.W. Lindle, P.A. Heimann, M.N. Piancastelli, P.H. Kobrin, H.G. Kerkhoff, U. Becker, W.D. Brewer, and D.A. Shirley. We would like to acknowledge helpful discussions with J.L. Dehmer, S.T. Manson, and T.D. Thomas.

1. T.M. Zimkina and V.A. Formichev, Sov. Phys. Dokl. 11, 726 (1967).
2. T.M. Zimkina and A.S. Vinogradov, J. Phys. (Paris) 32, C4-3 (1971).
3. J.L. Dehmer, J. Chem. Phys. 56, 4496 (1972) and references therein.
4. F.A. Gianturco, C. Guidotti, and U. Lamanna, J. Chem. Phys. 57, 840 (1972).
5. R.E. LaVilla, J. Chem. Phys. 57, 899 (1972).
6. A.P. Hitchcock and C.E. Brion, Chem. Phys. 33, 55 (1978).
7. A.P. Hitchcock, C.E. Brion, and W.J. Van der Wiel, J. Phys. B 11, 3245 (1978).
8. R.S. Wallace, Ph.D. thesis, Boston University, 1980.
9. E. Ishiguro, K. Soda, A. Mikuni, Y. Suzuki, S. Iwata, and T. Sasaki, SOR-RING Activity Report, 66 (1982).
10. J.L. Dehmer, D. Dill, and A.C. Parr in Photophysics and Photochemistry in the Vacuum Ultraviolet, edited by S.P. McGlynn, G. Findley, and R. Huebner (Riedel, Dordrecht, Holland, 1985) p. 341.
11. J.L. Dehmer and D. Dill in Electron-Molecule and Photon-Molecule Collisions, edited by T. Rescigno, V. McKoy, and B. Schneider (Plenum Press, New York, 1979) p. 225 and references therein.

12. P.W. Langhoff in Electron-Molecule and Photon-Molecule Collisions, edited by T. Rescigno, V. McKoy, and B. Schneider (Plenum Press, New York, 1979) p. 183.

13. V. McKoy, T.A. Carlson, and R.R. Lucchese, J. Chem. Phys. 88, 3188 (1984); D.L. Lynch, V. McKoy, and R.R. Lucchese in Resonances in Electron-Molecule Scattering, van der Waals Complexes, and Reactive Chemical Dynamics, edited by D.G. Truhlar (American Chemical Society, Washington, D.C., 1984).

14. J.A. Stephens and D. Dill, Phys. Rev. A 31, 1968 (1985).

15. See for example G.R. Wight, C.E. Brion, and M.J. Van der Wiel, J. Electron Spectrosc. 1, 457 (1972/73); G.R. Wight and C.E. Brion, 3, 191 (1974); 4, 313 (1974); 4, 327 (1974); A.P. Hitchcock and C.E. Brion, 10, 317 (1977); A. Bianconi, H. Peterson, F.C. Brown, and R.Z. Bachrach, Phys. Rev. A 17, 1907 (1978); R.N.S. Sodhi, S. Daviel, C.E. Brion, and G.G.B. De Souza, J. Electron Spectrosc. 35, 45 (1985).

16. C.M. Truesdale, D.W. Lindle, P.H. Kobrin, U.E. Becker, H.G. Kerkhoff, P.A. Heimann, T.A. Ferrett, and D.A. Shirley, J. Chem. Phys. 80, 2319 (1984).

17. D.W. Lindle, C.M. Truesdale, P.H. Kobrin, T.A. Ferrett, P.H. Heimann, U. Becker, H.G. Kerkhoff, and D.A. Shirley, J. Chem. Phys. 81, 5375 (1984).

18. T.A. Carlson, W.A. Svensson, M.O. Krause, T.A. Whitley, F.A. Grimm, G.V. Wald, J.W. Taylor, and B.P. Pullen, J. Chem. Phys. 84, 122 (1986).

19. G.M. Bancroft, S. Aksela, H. Aksela, K.H. Tan, B.W. Yates, L.L. Coatsworth, and J.S. Tse, J. Chem. Phys. 84, 5 (1986); T.A. Ferrett, M.N. Piancastelli, D.W. Lindle, P.A. Heimann, and D.A. Shirley (unpublished results, see Chpt. VII).

20. G.G.B. de Souza, P. Morin, and I. Nenner, J. Chem. Phys. 83, 492 (1985); P. Morin, G.G.B. de Souza, and I. Nenner, Phys. Rev. Lett. 56, 131 (1986).

21. J.L. Dehmer, A.C. Parr, S. Wallace, and D. Dill, Phys. Rev. A 26, 3283 (1982).

22. T. Gustafsson, Phys. Rev. A 18, 1481 (1978).

23. G.V. Marr, J.M. Morton, R.M. Holmes, and D.G. McKoy, J. Phys. B 12, 43 (1979).

24. S. Southworth, A.C. Parr, J.E. Hardis, and J.L. Dehmer, Phys. Rev. A 33, 1020 (1986).

25. D. Loomba, S. Wallace, D. Dill, and J.L. Dehmer, J. Chem. Phys. 75, 4546 (1981).

26. M.G. White, R.A. Rosenberg, G. Gabor, E.D. Poliakoff, G. Thornton, S. Southworth, and D.A. Shirley, Rev. Sci. Instrum. 50, 1288 (1979).

27. S. Southworth, C.M. Truesdale, P.H. Kobrin, D.W. Lindle, W.D. Brewer, and D.A. Shirley, J. Chem. Phys. 76, 143 (1982).

28. S. Southworth, U. Becker, C.M. Truesdale, P.H. Kobrin, D.W. Lindle, S. Owaki, and D.A. Shirley, Phys. Rev. A 28, 261 (1983).

29. C.N. Yang, Phys. Rev. 74, 764 (1948).

30. F. Wuilleumier and M.O Krause, J. Electron Spectrosc. 15, 15

(1979).

31. T.A. Carlson, M.O Krause, F.A. Grimm, P.R. Keller, and J.W. Taylor, Chem. Phys. Lett. 87, 552 (1982); D.W. Lindle, P.A. Heimann, T.A. Ferrett, P.H. Kobrin, C.M. Truesdale, U. Becker, H.G. Kerkhoff, and D.A. Shirley, Phys. Rev. A 33, 319 (1986).
32. D.W. Lindle, T.A. Ferrett, P.A. Heimann, and D.A. Shirley, Phys. Rev. A 34, 1131 (1986).
33. K. Siegbahn, C. Nordling, G. Johansson, J. Hedman, P.F. Hedén, K. Hamrin, U. Gelius, T. Bergmark, L.O. Werme, R. Manne, and Y. Baer, ESCA Applied to Free Molecules (North-Holland, Amsterdam, 1969).
34. L. Ungier and T.D. Thomas, Chem. Phys. Lett. 96, 247 (1983).
35. C.M. Truesdale, S.H. Southworth, P.H. Kobrin, U. Becker, D.W. Lindle, H.G. Kerkhoff, and D.A. Shirley, Phys. Rev. Lett. 50, 1265 (1983).
36. H.W. Haak, G.A. Sawatzky, L. Ungier, J.K. Gimzewski, and T.D. Thomas, Rev. Sci. Instrum. 55, 696 (1984).
37. L. Ungier and T.D. Thomas, J. Chem. Phys. 82, 3146 (1985).
38. U. Becker, R. Hölzel, H.G. Kerkhoff, B. Langer, D. Szostak, and R. Wehlitz, Phys. Rev. Lett. 56, 1455 (1986).
39. T.A. Ferrett, D.W. Lindle, P.A. Heimann, H.G. Kerkhoff, U.E. Becker, and D.A. Shirley, Phys. Rev. A 34, 1916 (1986). See Chpt. III.
40. For convenience, we choose to differentiate between inner-valence main lines and satellites in this energy range even though some of these states may be nearly degenerate in energy, requiring a

many-body approach to assigning configurations. The role of many-body aspects in the SF_6 valence region should emerge as both higher resolution experiments and calculations are performed.

41. S. Anderson and T.D. Thomas (private communication).

42. The integration for this "inner" valence region includes a tail extending to ~100 eV binding energy. Part of this tail may be caused by shakeoff processes which could be enhanced at the resonance. Nonetheless, most of the integrated intensity in this energy region is associated with the production of singly-charged ions.

43. N. Mårtensson, P.A. Malmquist, S. Svensson, E. Basilier, J.J. Pireaux, U. Gelius, and K. Siegbahn, Nouv. J. de Chim. 1, 191 (1977); H. Ågren and H. Siegbahn, Chem. Phys. Lett. 69, 424 (1980); M. Mishra and Y. Ohrn, Chem. Phys. Lett. 71, 549 (1980); R. Arneberg, J. Muller, and R. Manne, Chem. Phys. 64, 249 (1982); H. Nakatsuji and T. Yonezawa, Chem. Phys. Lett. 87, 426 (1982); W. von Niessen, L.S. Cederbaum, J. Schirmer, G. Diercksen, and W.P. Kramer, J. Electron Spectrosc. 28, 45 (1982); R. Cambi, G. Ciullo, A. Sgamellotti, C.E. Brion, J.P.D. Cook, I.E. McCarthy, and E. Weigold, Chem Phys. 91, 373 (1984); 98, 166 (1985); C.E. Brion, D.W. Lindle, P.A. Heimann, T.A. Ferrett, and M.N. Piancastelli, Chem. Phys. Lett. 128, 118 (1986).

44. W. Domcke, L.S. Cederbaum, J. Schirmer, W. von Niessen, and J.P. Maier, J. Electron Spectrosc. 14, 59 (1978); C.E. Brion, J.P.D. Cook, and K.H. Tan, Chem. Phys. Lett. 59, 241 (1978); J.P.D. Cook,

C.E. Brion, and A. Hamnett, Chem. Phys. 45, 1 (1980); M.Y. Adam, P. Morin, C. Cauletti, and M.N. Piancastelli, J. Electron Spectrosc. 36, 377 (1985).

45. P.R. Keller, J.W. Taylor, F.A. Grimm, P. Senn, T.A. Carlson, and M.O. Krause, Chem. Phys. 74, 247 (1983).

46. S.T. Manson, J. Electron Spectrosc. 1, 413 (1972/73).

47. W. von Niessen, L.S. Cederbaum, G.H.F. Diercksen, and G. Hohlneicher, Chem. Phys. 11, 399 (1975); P.J. Hay, J. Am. Chem. Soc. 99, 1013 (1977); W. von Niessen, W.P. Kraemer, and G.H.F. Diercksen, Chem. Phys. Lett. 63, 65 (1979).

48. J.L. Dehmer, D. Dill, and S. Wallace, Phys. Rev. Lett. 43, 1005 (1979).

49. D.L. Lynch and V. McKoy, Phys. Rev. A 30, 1561 (1984).

50. Z.H. Levine and P. Soven, Phys. Rev. A 29, 625 (1984).

51. D. Dill, S. Wallace, J. Siegel, and J.L. Dehmer, Phys. Rev. Lett. 42, 411 (1979); F.A. Grimm, Chem. Phys. 53, 71 (1980); R.R. Lucchese and B.V. McKoy, Phys. Rev. A 26, 1406 (1982).

52. H. Friedrich, B. Pittel, P. Rabe, W.H.E. Schwarz, and B. Sonntag, J. Phys. B 13, 25 (1980); A.S. Vinogradov and T.M. Zimkina, Opt. Spectrosc. 31, 288 (1971).

53. D. Dill, J.S. Swanson, S. Wallace, and J.L Dehmer, Phys. Rev. Lett. 45, 1393 (1980); S. Wallace and D. Dill, Phys. Rev. B 17, 1692 (1978).

54. There should be small differences in the resonant kinetic energy for main lines and satellites caused by the interaction with the

different residual ions. In order to explain the satellite enhancement at 196.5 eV in SF_6, this difference would have to be about 8 eV and coincidentally equal to the satellite excitation energy.

55. A. Hamnett, W. Stoll, and C.E. Brion, J. Electron Spectrosc. 8, 367 (1976).

56. J.B. West, P.R. Woodruff, K. Codling, and R.G. Houlgate, J. Phys. B 9, 407 (1976).

57. M. Ya. Amusia and U.K. Ivanov, Phys. Lett. 59A, 194 (1976); L. Torop, J. Morton, and J.B. West, J. Phys. B 9, 2035 (1976); U. Becker, T. Prescher, E. Schmidt, B. Sonntag, and H.-E. Wetzel, Phys. Rev. A 33, 3891 (1986).

58. A. Fahlman, M.O. Krause, T.A. Carlson, and A. Svensson, Phys. Rev. A 30, 812 (1984); U. Becker, T. Prescher, E. Schmidt, B. Sonntag, and H.-E. Wetzel, Phys. Rev. A 33, 3891 (1986).

59. M.H. Hecht and I. Lindau, Phys. Rev. Lett. 47, 821 (1981).

60. U. Becker, R. Hölzel, H.G. Kerkhoff, B. Langer, D. Szostak, and R. Wehlitz, ICPEAC Abstracts, Palo Alto, CA, July 1985.

61. J.M. Esteva, B. Gauthe, P. Dhez, and R.C. Karnatak, J. Phys. B 16, L263 (1983).

62. T.A. Ferrett, M.N. Piancastelli, P.A. Heimann, L.J. Medhurst, S.H. Li and D.A. Shirley (unpublished results, see Chpt. V).

63. J.P. Connerade, J. Phys. B 17, L165 (1984).

Figure Captions

Fig. 1 Photoabsorption spectra for SF_6 (Ref. 1), SiF_4 (Ref. 52), and SO_2 (Ref. 2) plotted together on an arbitrary cross-section scale for qualitative comparison. The spectra have been lined up in kinetic energy relative to the S or Si 2p edges in these molecules. The most intense resonances have been related to potential barrier effects of varying extent in this series.

Fig. 2 A molecular-orbital diagram for SF_6. The energy levels are not drawn to scale. The order of the valence shells is taken from Ref. 21. Excitation of a S 2p electron to the discrete $6a_{1g}$ level is shown, as are transitions to the t_{2g} and e_g continuum shape resonances.

Fig. 3 TOF spectrum at 196.4 eV photon energy and θ=54.7°, taken on the peak of the "e_g" resonance. The binding energy of the enhanced S 2p correlation satellite is 189(1) eV.

Fig. 4 Total photoabsorption cross section[1] for SF_6. The present total yield data (solid circles) for the sum of the $S(L_{2,3}VV)$ Auger and valence electron intensity in SF_6 has been scaled to the photoabsorption curve at 189.3 eV. The dashed curve represents an estimate of the valence main-line

cross section (both inner- and outer-valence) above the S 2p threshold based on the valence intensity in the TOF spectra over this energy range.

Fig. 5 Binding energy spectra taken off (176.1 eV) and on (172.9 eV) the S 2p-->$6a_{1g}$ discrete resonance. The peaks labelled outer valence consist of the unresolved $1t_{1g}$, $1t_{2u}$, $5t_{1u}$, $3e_g$, $1t_{2g}$, $4t_{1u}$, and $5a_{1g}$ orbitals. The region labelled "inner" valence includes the inner-valence main lines ($2e_g$, $3t_{1u}$, and $4a_{1g}$) and all valence satellites between 30 and 100 eV binding energy.

Fig. 6 Relative partial cross sections for the outer- and "inner" valence intensity near the S 2p-->$6a_{1g}$ discrete excitation (top). The "inner" valence cross section represents the binding energy range of 30-100 eV in the TOF spectra. The corresponding "inner" valence β is also shown (bottom).

Fig. 7 S 2p asymmetry parameter (top) and partial cross section (bottom) for SF_6 (solid circles). MSM-Xα results[8] for β are shown where the theory curve has been shifted to the experimental "e_g" resonance energy. The atomic β(2p) for Al is also plotted.[46] The open circles for β are tne measured Si 2p values for SiF_4 (Ref. 45) plotted as a function of kinetic energy for comparison.

Fig. 8 Relative cross section and asymmetry parameter for the S 2p main line (solid circles) and satellite (open circles) in an expanded energy range near the "e_g" resonance (196.5 eV).

Fig. 9 Asymmetry parameter for the sulfur $L_{2,3}VV$ Auger electrons in the vicinity of the t_{2g} (184 eV) and e_g (196.5 eV) resonances. Arrows mark the resonance positions observed in the cross section.

Fig. 10 A full configuration-interaction model for the SF_6 S 2p e_g shape resonance at the photon energy $h\nu_1$. In both the quasibound resonance states themselves (ψ) and in the ionic final states (ϕ), eigenstates are formed from main-line ($2p^{-1}$) and satellite ($2p^{-1}v_i^{-1}v_j^*$) basis states. In this case, both the main-line (ϕ_{ML}) and first satellite (ϕ_{sat1}) final states are energetically accessible from the first shape resonance, ψ_1. Also included in ψ_1 are possible doubly excited states, $2p^{-1}v_i^{-1}v_j^*v_k^*$. Higher resonances should also exist, as shown.

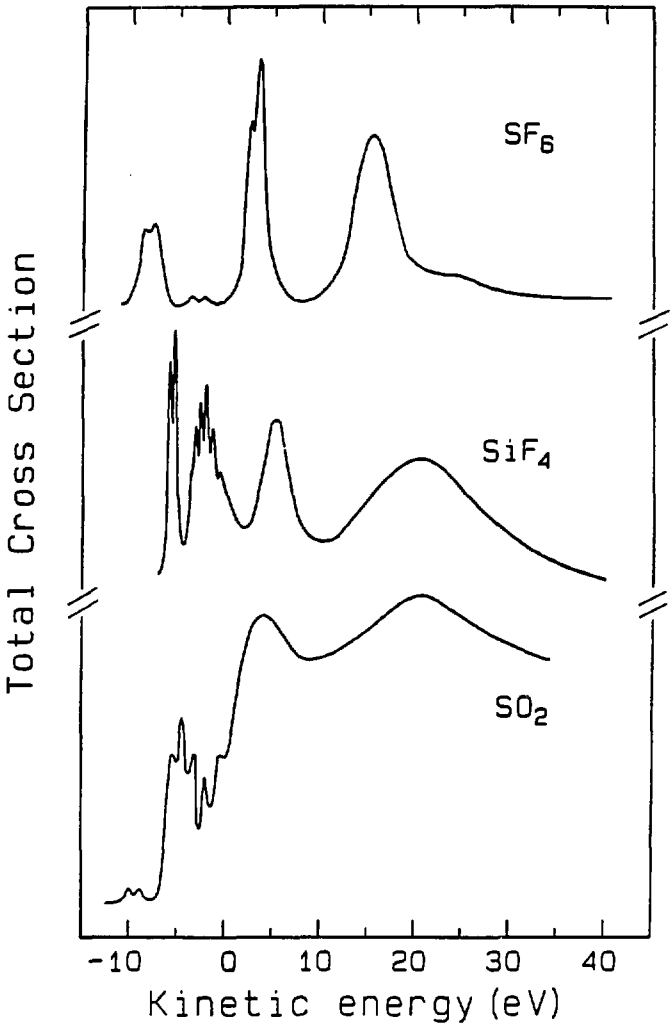

XBL B611-4299

Figure 1

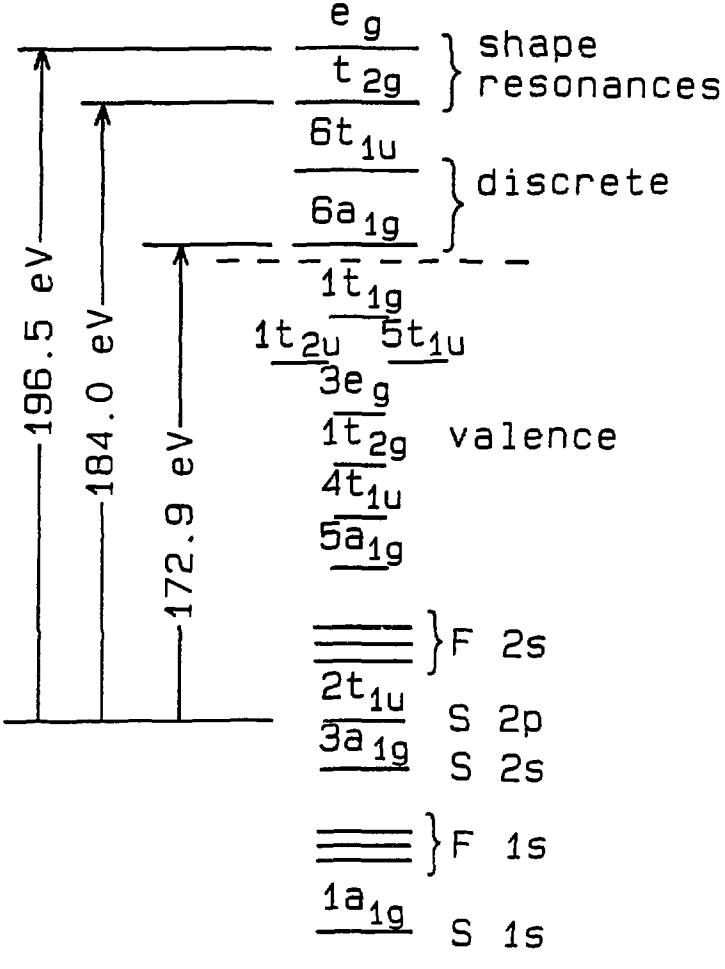

XBL 8611-4300

Figure 2

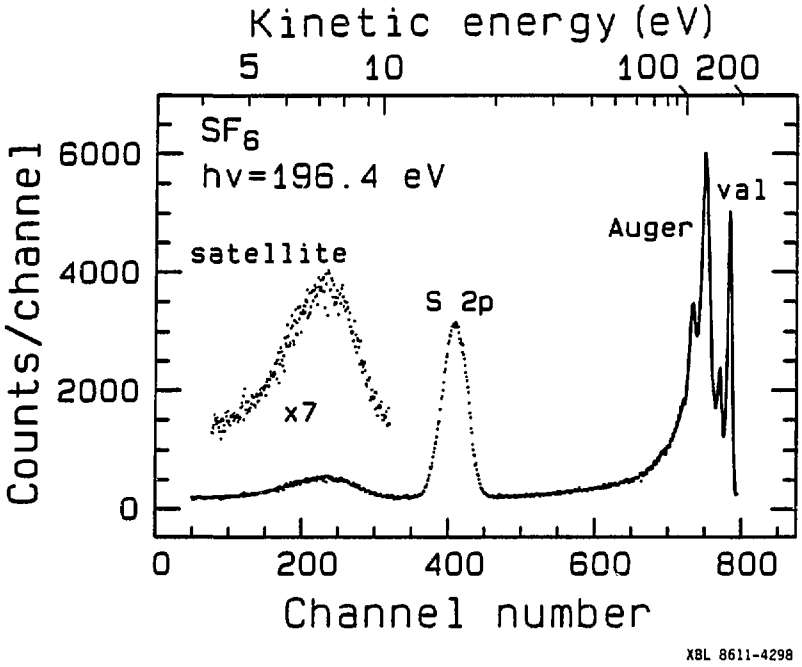
Kinetic energy (eV)
5
10
100
200
SF6
hv=196.4 eV
satellite
x7
S 2p
Auger
val
Counts/channel
6000
4000
2000
0
0
200
400
600
800
Channel number
X8L 8611-4298

Figure 3

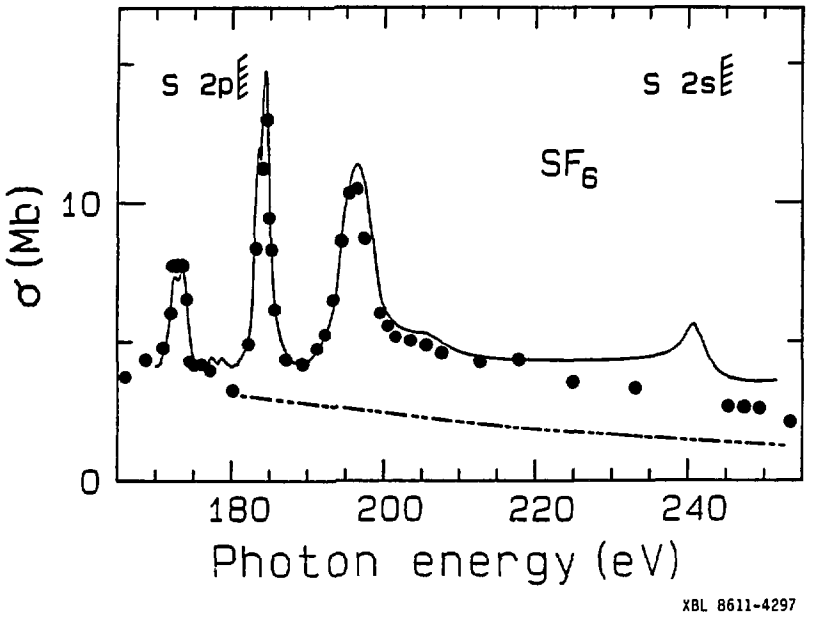
S 2p
S 2s
SF6
σ (Mb)
10
0
180
200
220
240
Photon energy (eV)
XBL 8611-4297

Figure 4

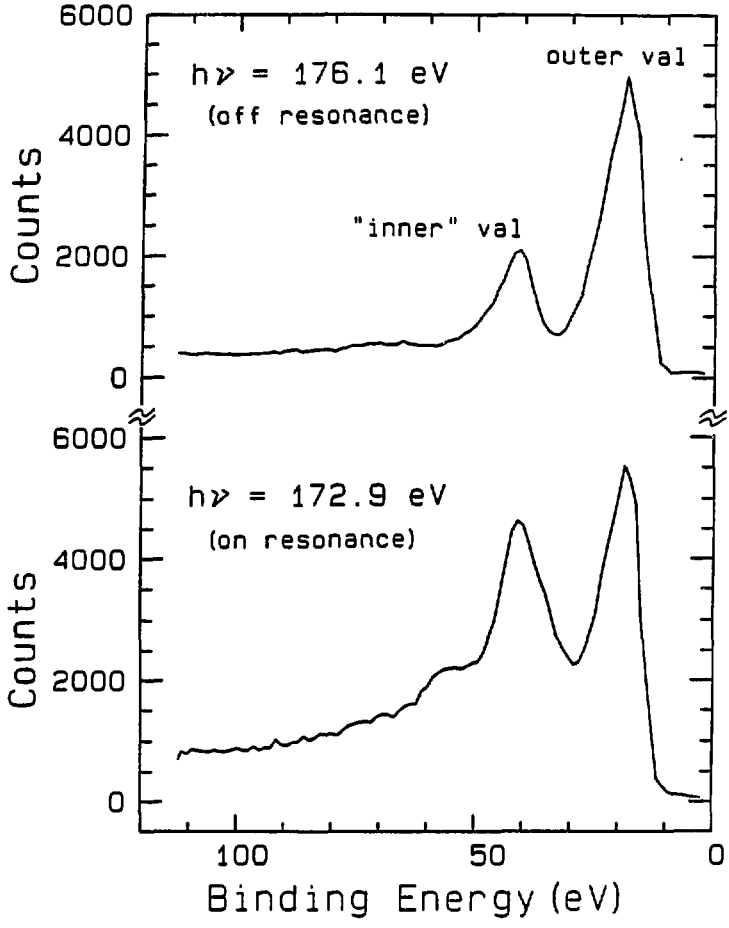

XBL 8611-4296

Figure 5

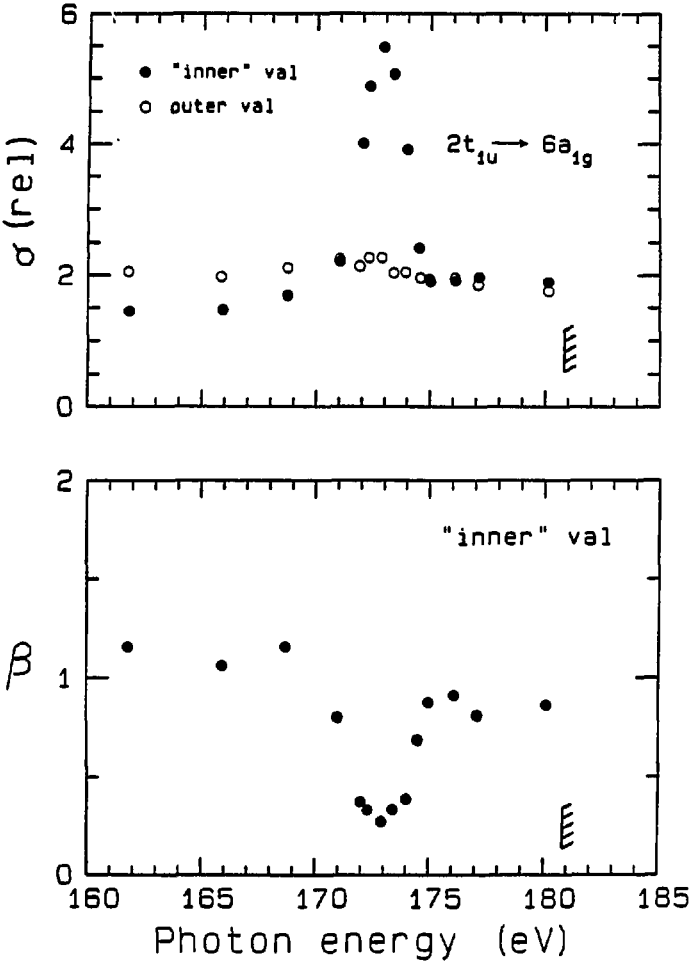

XBL 8611-4295

Figure 6

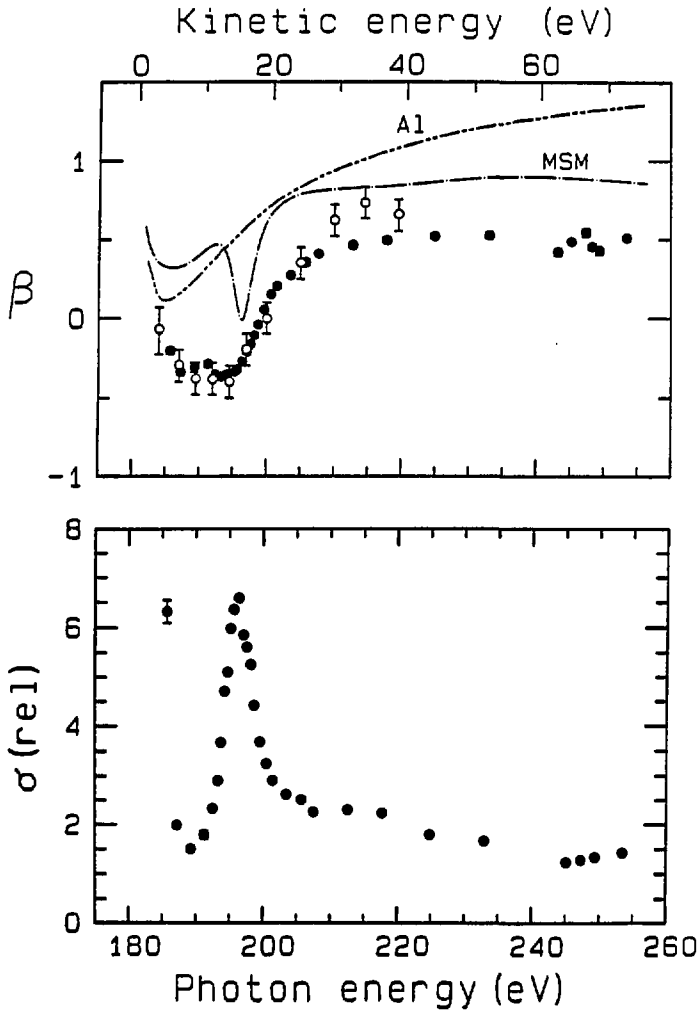

XBL 8611-4294

Figure 7

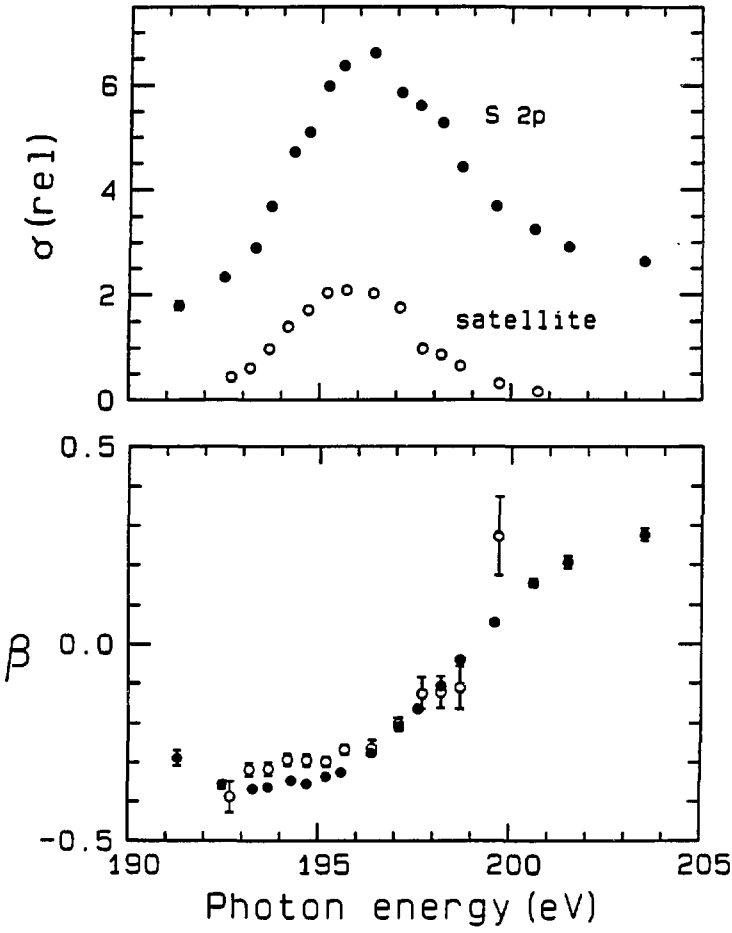

XBL 8611-4293

Figure 8

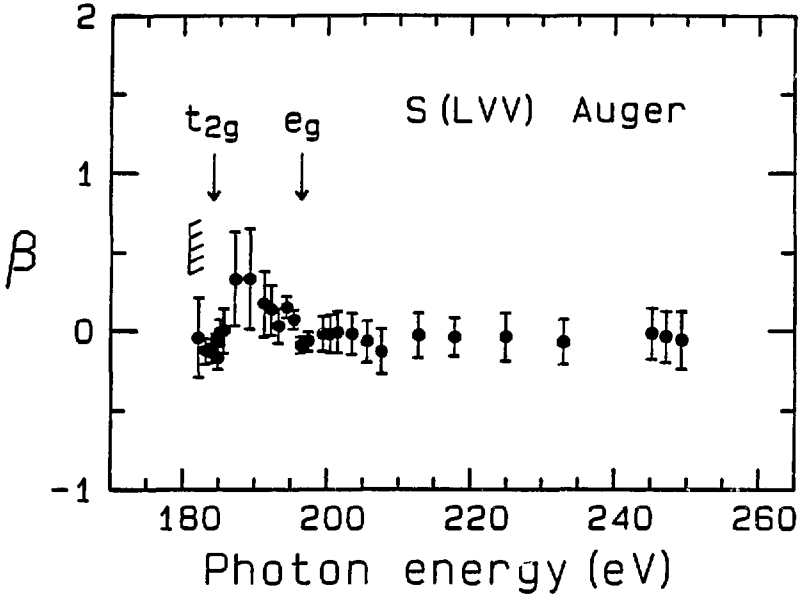

XBL 8611-4292

Figure 9

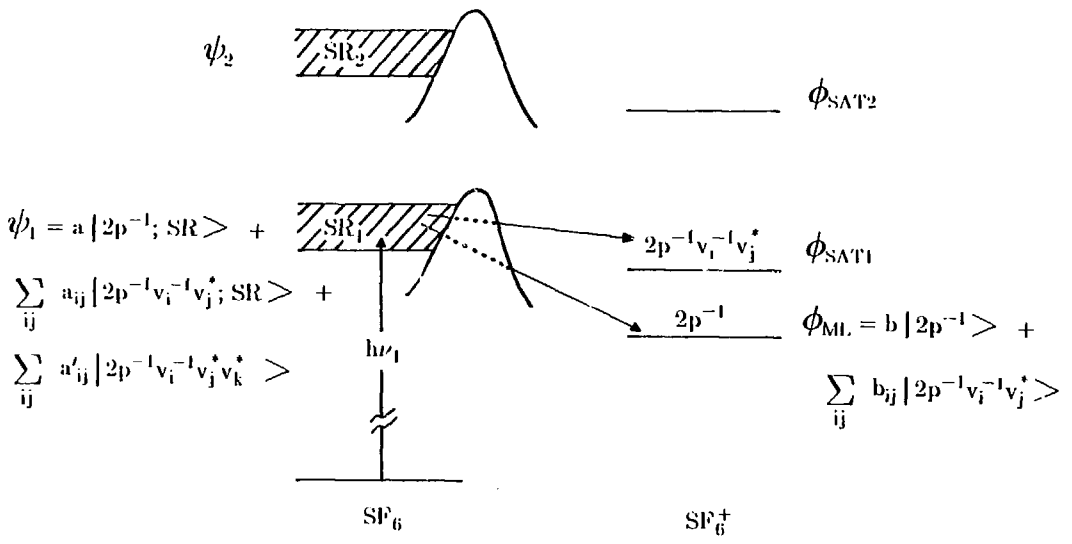
ψ_2
SR_2
ϕ_{SAT2}
$\psi_1 = a\,|2p^{-1}; SR> + \sum_{ij} a_{ij}\,|2p^{-1}v_i^{-1}v_j^*; SR> + \sum_{ij} a'_{ij}\,|2p^{-1}v_i^{-1}v_j^*v_k^*>$
SR_1
$2p^{-1}v_i^{-1}v_j^*$
ϕ_{SAT1}
$2p^{-1}$
$\phi_{ML} = b\,|2p^{-1}> + \sum_{ij} b_{ij}\,|2p^{-1}v_i^{-1}v_j^*>$
$h\nu_1$
SF_6
SF_6^+
XBL 8611-4364

Figure 10

V. Resonance Effects on the Inner-Valence Levels of SF_6 in the Photon-Energy Range 52-72 eV*

Abstract

We have measured the photoionization partial cross section and asymmetry parameter in the 52-72 eV photon-energy range for the combination of inner-valence orbitals ($3t_{1u}$, $2e_g$, and $4a_{1g}$) in gaseous SF_6. These results, combined with those for the (inner valence)/(outer valence) branching ratio, indicate resonant enhancement of the inner-valence levels at ~59 eV photon energy. We associate this behavior with the $3t_{1u}$-->e_g shape resonance predicted by MSM-Xα calculations.

A. Introduction

The SF_6 molecule has provided a classic demonstration of the role played by shape resonances in the absorption and photoionization dynamics of both the valence[1,2] and core[3-9] levels. Particular attention has been paid to the effect of the t_{2g} and e_g "d-type" shape resonances on the gas-phase photoionization cross section and the angular-distribution parameter as a function of photon energy for the SF_6 outer-valence levels.[1,2] At ~23 eV photon energy, a transition has been predicted to occur from the $5t_{1u}$ and $1t_{2u}$ states (binding energy 17.0 eV) to the t_{2g} shape-resonant state.[10] A significant enhancement of the relative cross section for the corresponding peak in photoemission was detected, but there was also an enhancement at the same photon energy for the peaks with binding energies of 15.7 eV ($1t_{1g}$) and 18.6 eV ($3e_g$).[1,2] Similar behavior has been observed in the photoemission spectra of solid SF_6.[11]

The enhancement of the photoionization cross section for the $1t_{1g}$ and $3e_g$ valence levels at 23 eV cannot be explained within a simple shape-resonance model. First, these transitions from gerade (g) orbitals to the t_{2g} state are not symmetry allowed. In addition, a one-electron model describes the phenomenon as a final-state effect, occurring at approximately the same kinetic energy for each photoemission channel, rather than at the same photon energy.[5]

Two explanations for the observed valence peak enhancement in SF_6 have been discussed,[2] one invoking autoionization of a discrete state, and the other invoking continuum-continuum coupling at a shape resonance. The first postulates that a one-electron transition from an outer valence orbital to a discrete state (most likely the $5a_{1g}$-->$6t_{1u}$ transition) occurs at ~23 eV photon energy and autoionizes into several continua. The energy for this transition has been estimated by several authors to be ~25 eV[12] and 26.7 eV.[2] Because these estimates did not include hole-screening effects, the possible contribution of this discrete resonance near 23 eV should be considered. This particular resonance, which is below the valence $5a_{1g}$ threshold (26.8 eV), might well be accidentally coincident in energy with the predicted ($5t_{1u}$ + $1t_{2u}$)-->t_{2g} shape resonance, further complicating the interpretation.

The second proposed explanation for the effects near $h\nu$=23 eV involves continuum channel interaction, which allows the t_{2g} shape-resonant continuum state to couple and decay into neighboring continuum levels.[2] Recent K-matrix calculations on N_2 show that continuum-continuum coupling is important near the $3\sigma_g$-->$\epsilon\sigma_u$ shape resonance, producing effects in the photoionization dipole amplitude and asymmetry parameter for the neighboring $2\sigma_u$ valence channel.[13] Qualitatively, the quasibound continuum electron has large amplitude in the core at resonance, enhancing many-electron effects.

An independent experiment which further verifies the complexity

of these shape resonances was performed recently on the photoionization of the sulfur 2p orbital and of a related satellite in SF_6.[14] It showed that there is a resonant enhancement of both the S 2p main line and satellite at the same photon energy. The resonant feature at this energy had been assigned previously as the S $2p(2t_{1u})$-->e_g shape resonance (196.5 eV).[6-9] Clearly, the traditional simple models cannot explain the unusual resonant effects in the valence and S 2p levels of SF_6.

Inner-valence photoemission has been until recently a less established field of study due to the relative inaccessibility of the necessary ionizing radiation (>30 eV) either from lamp sources or traditional monochromators for synchrotron radiation. In addition, cross sections for inner-valence ionization are about an order of magnitude less than for outer-valence ionization. Furthermore, correlation effects in the inner-valence region of molecules can be important in photoelectron spectra,[15] making it more difficult to observe resonant effects in individual channels. Even for small molecules like PH_3 (Ref. 16) and H_2S (Refs. 16,17), the inner-valence orbitals are highly correlated, giving many more final states (and thus photoemission peaks) than one-electron calculations would predict. The distribution and symmetry of the correlation states in the inner-valence region of SF_6 will, of course, mediate the effect of shape resonances.

To supplement our understanding of the strong multi-electron shape resonant effects in the outer-valence and S 2p core-level

photoionization, we have investigated the inner-valence ionization of SF_6. This is one of the first energy-dependent studies for inner-valence photoemission in the vicinity of a predicted shape resonance. We report here the relative partial photoionization cross sections of the inner-valence orbitals in SF_6 including the $2e_g$, $3t_{1u}$, and $4a_{1g}$ states, which have mainly fluorine 2s character.[18] We monitored the behavior of the inner- and outer-valence states through the photon energy range in which a transition from the $3t_{1u}$ inner-valence orbital to the e_g shape resonance is expected (~57 eV), and where the total photoabsorption cross section for SF_6 exhibits a weak maximum.[19] One-electron MSM-Xα calculations show the $3t_{1u}$-->e_g shape resonance at ~15 eV kinetic energy, with no enhancement in the neighboring $2e_g$ and $4a_{1g}$ inner-valence shells.[10] We note that despite the unusual behavior of the t_{2g} shape resonance in outer-valence photoemission as discussed above, there is no evidence for the e_g shape resonance in outer-valence ionization.

The experiment is described in Sec. B, and the results are presented and discussed in Sec. C. Conclusions appear in Sec. D.

B. Experimental

The experiment was performed at the Stanford Synchrotron Radiation Laboratory (SSRL) using the new 4° line grazing-incidence "grasshopper" monochromator. Photoelectron spectra were taken in the

photon energy range $52 \leq h\nu \leq 72$ eV using 1200 line/mm and 600 line/mm holographically ruled gratings. The photon resolution varied from 0.3 to 0.6 eV. The analyzer resolution was about 3 percent of the electron kinetic energy. Calibration of the analyzer transmission and relative analyzer efficiency as functions of kinetic energy were performed by measuring the known partial cross sections and asymmetry parameters for the 2s and 2p levels of Ne.[20] The photon intensity was monitored by a sodium salicylate scintillator with an optical photomultiplier tube (RCA 8850), and the relative sample pressure was recorded with a capacitance manometer. Error bars in the σ and β plot are statistical only. We estimate systematic errors of less than 10 percent for σ and ± 0.15 for β.

C. Results and Discussion

A representative time-of-flight (TOF) photoemission spectrum of the inner- and outer-valence levels of SF_6 taken at $\theta = 54.7°$ and 60 eV photon energy is shown in Fig. 1. The accepted outer valence ordering is $1t_{1g}$, $5t_{1u} + 1t_{2u}$, $3e_g$, $1t_{2g}$, $4t_{1u}$, and $5a_{1g}$ with binding energies of 15.7, 17.0, 18.6, 19.7, 22.5, and 26.8 eV, respectively.[2] For our experimental conditions, the first five outer-valence orbitals (labelled 'val' in Fig. 1) are unresolved. In contrast, the $4t_{1u}$ and $5a_{1g}$ peaks are well separated. For the inner-valence levels, the $2e_g$ (binding energy 39.3 eV) and $3t_{1u}$ (binding energy 41.2 eV) levels overlap almost completely; the much

less intense $4a_{1g}$ peak (binding energy 44.2 eV) is quite well resolved from the $(3t_{1u} + 2e_g)$ peak.[18]

The cross section and asymmetry parameter for the sum of the inner-valence levels are shown in Fig. 2. There is a clear enhancement in the cross section, peaking near 58-60 eV. This increase corresponds to the small effect in the total photoabsorption cross section at the same energy.[19] There is no corresponding detectable effect in the inner-valence β (Fig. 2, bottom). Due to the scatter in our data, the possible minimum in β near 60 eV should be considered tentative. The asymmetry parameter appears to increase with energy.

The (inner valence)/(outer valence) intensity branching ratio is shown in Fig. 3. The data are consistent with inner-valence enhancement superimposed on a smoothly increasing branching ratio. The relative increase of inner-valence intensity at higher energy is well known. It has been observed in H_2O (Ref. 21) and is indicative of the increasing importance of lower l states at higher energy (the inner-valence orbitals are mainly F 2s). In atomic Ne, the $\sigma(2s)/\sigma(2p)$ branching ratio demonstrates similar behavior.[18]

Though the photon-energy range in which the inner-valence states are enhanced, there is no appreciable enhancement in the cross section for the outer-valence levels. We evaluated the individual cross sections for the 'val' peak (see Fig. 1) and for the $5a_{1g}$ and $4t_{1u}$ peaks. These cross sections show the same trend, smoothly decreasing in the photon-energy range under investigation. These results are

consistent with previous total photoabsorption data which show an overall decrease in the photon-energy range 52-72 eV.[19] Our data show a decrease for the cross section for all of the first five valence levels together, which is the predominant contribution to the total cross section.

D. Conclusions

An enhancement is observed for the sum of the inner-valence ($3t_{1u}$, $2e_g$, and $4a_{1g}$) photoionization cross sections. We observe no distinct evidence of coupling to the outer-valence levels. The relative contributions of the $3t_{1u}$, $2e_g$, and $4a_{1g}$ states to the resonant enchancement cannot be assessed on the grounds of our experimental findings; thus, we cannot rule out participation of the $2e_g$ and $4a_{1g}$ states in the resonance. It is likely, though, that the observed cross section effects are due to the e_g shape resonance. However, many-body interactions in the inner-valence region will complicate the correlated photoemission final states, which are unresolved or have low intensity in our experiment, and their coupling to the e_g resonance.

References

* Work done in collaboration with M.N. Piancastelli, D.W. Lindle, P.A. Heimann, L.J. Medhurst, S.H. Liu, and D.A. Shirley.

1. T. Gustafsson, Phys. Rev. A 18, 1481 (1978).
2. J.L. Dehmer, A.C. Parr, S. Wallace, D. Dill, Phys. Rev. A 26, 3283 (1982), and references therein.
3. T.M. Zimkina and V.A. Formichev, Sov. Phys. Dokl. 11, 726 (1967).
4. T.M. Zimkina and A.S. Vinogradov, J. Phys. (Paris) 32, C4-3 (1971).
5. J.L. Dehmer, J. Chem. Phys. 56, 4496 (1972).
6. R.E. LaVilla, J. Chem. Phys. 57, 899 (1972).
7. F.A. Gianturco, C Guidotti, U. Lamanna, J. Chem. Phys. 57, 840 (1972).
8. V.P. Sachenko, E.V. Polozhentsev, A.P Kovtun, Yu.F. Migal, R.V. Vedrinski, and V.V. Kolnesnikov, Phys. Lett. 48A, 169 (1974).
9. A.P. Hitchcock and C.E. Brion, Chem. Phys. 33, 55 (1978).
10. R.S. Wallace, Ph.D. thesis, Boston University (1980).
11. J.-H. Fock and E.E. Koch, Chem. Phys. 96, 125 (1985).
12. P.J. Hay, J. Am. Chem. Soc. 99, 1013 (1977).
13. J.A. Stephens and D. Dill, Phys. Rev. A 31, 1968 (1985).
14. T.A. Ferrett, D.W. Lindle, P.A. Heimann, M.N. Piancastelli, P.H. Kobrin, H.G. Kerkhoff, U. Becker, W.D. Brewer, and D.A. Shirley (unpublished results, see Chpt. IV).

15. L.S. Cederbaum, W. Domcke, J. Schirmer, and W. von Niessen, Adv. Chem. Phys. 65, 115 (1986).

16. W. Domcke, L.S. Cederbaum, J. Schirmer, W. von Niessen, and J.P. Maier, J. Electron Spectrosc. 14, 59 (1978).

17. M.Y. Adam, P. Morin, C. Cauletti, and M.N. Piancastelli, J. Electron Spectrosc. 36, 377 (1985); M.Y. Adam, C. Cauletti, and M.N. Piancastelli, J. Electron Spectrosc. (in press).

18. K. Siegbahn, C. Nordling, G. Johansson, J. Hedman, P.F. Hedén, K. Hamrin, U. Gelius, T. Bergmark, L.O. Werme, R. Manne, and Y. Baer, ESCA Applied to Free Molecules (North Holland, Amsterdam, 1969).

19. L.C. Lee, E. Phillips, and D.L. Judge, J. Chem. Phys. 67, 1237 (1977).

20. F. Wuilleumier and M.O. Krause, J. Electron Spectrosc. 15, 15 (1979).

21. C.E. Brion, D.W. Lindle, P.A. Heimann, T.A. Ferrett, M.N. Piancastelli, and D.A. Shirley, Chem. Phys. Lett. 128, 118 (1986).

Figure Captions

Fig. 1 TOF photoemission spectrum of SF_6 measured at $h\nu$=60 eV and θ=54.7°. The peak labelled 'val' consists of the unresolved outer-valence orbitals $1t_{1g}$, $5t_{1u}$, $1t_{2u}$, $3e_g$, and $1t_{2g}$.

Fig. 2 Relative partial cross section (σ) and asymmetry parameter (β) for the combination of the $3t_{1u}$, $2e_g$, and $4a_{1g}$ inner-valence orbitals of SF_6.

Fig. 3 The branching ratio for the inner-valence intensity relative to the outer-valence intensity.

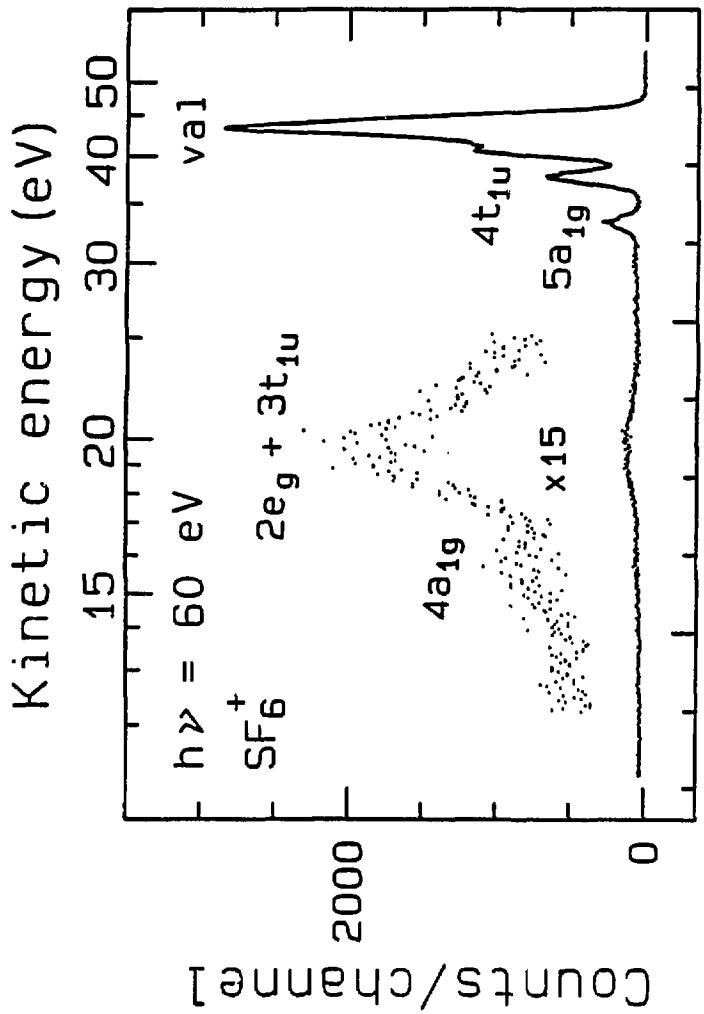

XBL 8611-4226

Figure 1

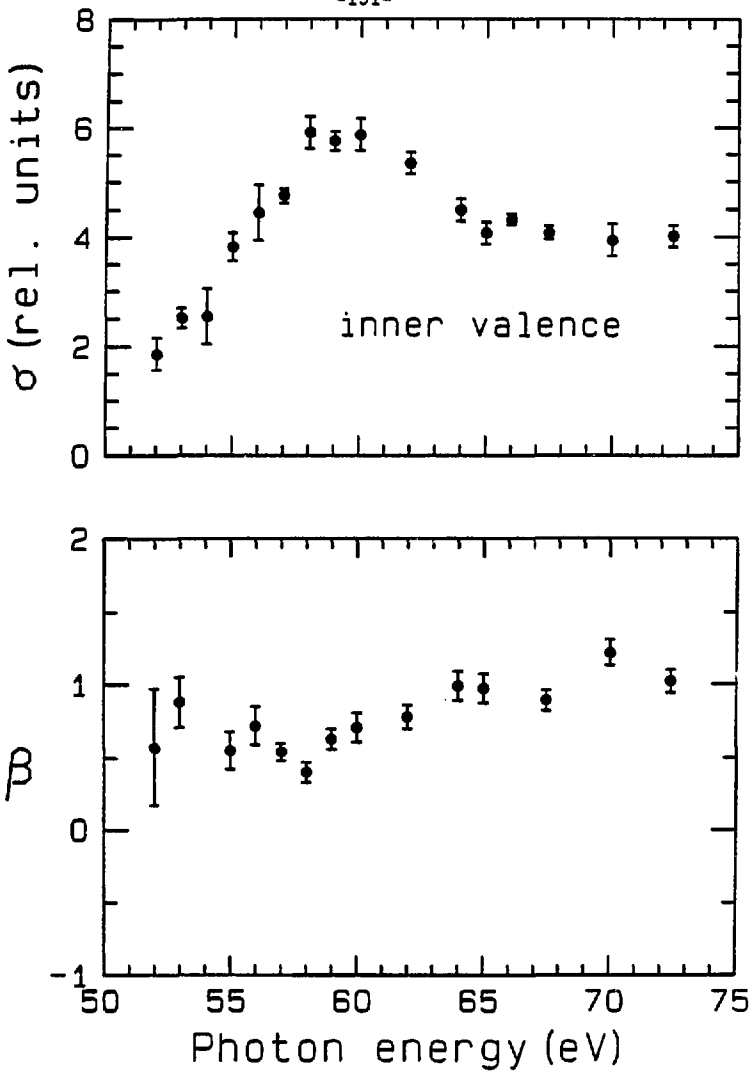

XBL 8611-4224

Figure 2

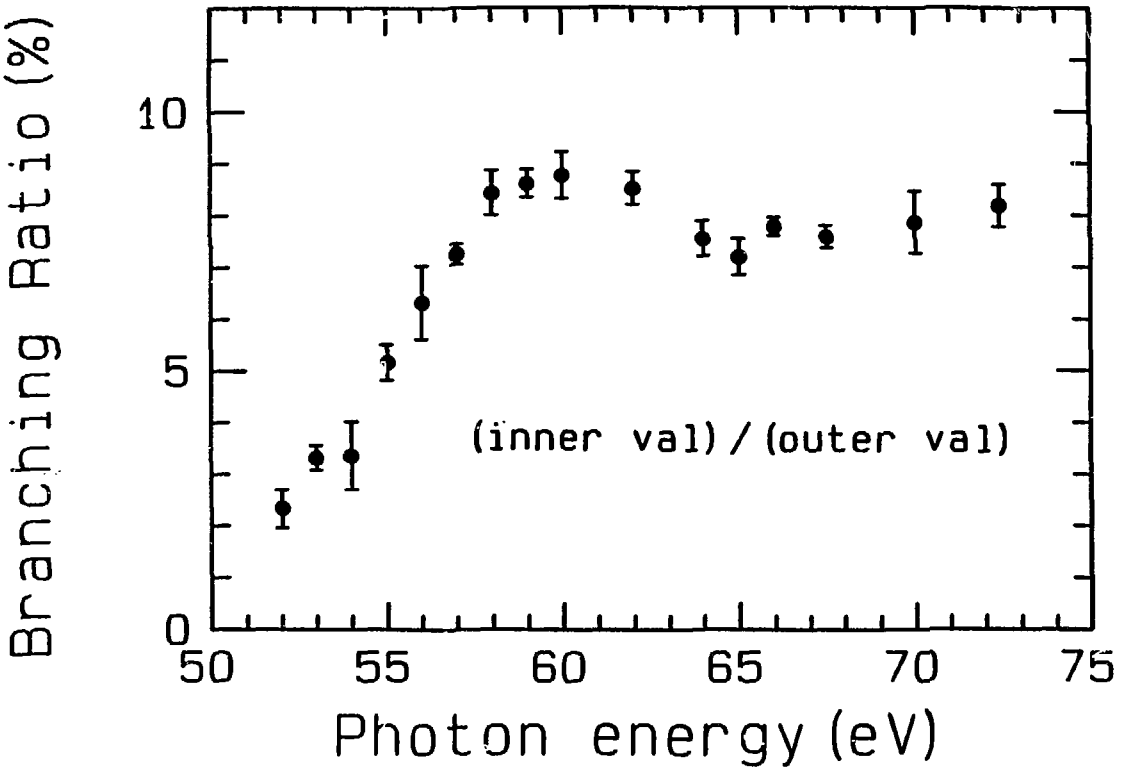

Figure 3

XBL 8611-4225

VI. Lithium 1s Main-line and Satellite Photoemission: Resonant and Nonresonant Behavior*

Abstract

We present experimental results on core-level photoemission of atomic lithium, leading to both main-line and satellite states of the Li^+ ion (1snl where n=2-5). We compare the measured 1s2s $^{1,3}S$ main-line cross sections with recent relaxed Hartree-Fock calculations and with previous experimental results, finding reasonable agreement in both cases. For the n=3 satellite, our results disagree with earlier photoemission work which was complicated by additional peaks at 52 eV kinetic energy. We discuss possible explanations for these extra peaks. For the doubly excited state 1s(3s3p) ^3P at 71.14 eV, we present total cross-section results in good agreement with previous photoabsorption measurements. The qualitative differences among our partial cross-section profiles are discussed, and the phase for the total cross section is rationalized by estimating the signs of pertinent matrix elements.

A. Introduction

The study of electron-correlation effects on the photoionization of small atoms is important for two reasons. First, the accessibility of small atoms to the most sophisticated ab initio theoretical treatments, coupled with the high sensitivity of photoionization processes to multi-electron effects, can lead to better understanding of basic electron correlation phenomena. Second, experience with small atoms can provide insight into photoionization processes in larger atoms and molecules. In helium, the smallest atom in which electron correlation can occur, both resonant and nonresonant experimental studies,[1-12] coupled with theory,[13-22] have elucidated the role of electron correlation in the continuum with respect to the $He^+(2s)$ and $He^+(2p)$ satellite channels.

In this paper we report photoelectron spectroscopic studies on the next smallest system, atomic lithium. We emphasize in this work the Li 1s satellite states, for which open shells and electron correlation in both initial and final states can further complicate photoionization processes relative to atomic helium.

Though the valence ionization of atomic Li has been studied extensively,[23-25] relatively little experimental work has been reported on core photoionization for the $Li^+(1s2s\ ^{1,3}S)$ main lines and 1snl satellites. Figure 1 depicts these pertinent energy levels in Li and Li^+, including the 1s(3s3p) doubly excited state of the neutral. Photoabsorption measurements have provided information on

some of the n=2 satellites,[26] and on the energies and assignments of the resonances leading to the main-line and higher satellite thresholds.[27-30] A recent work on core-level photoemission results for Li was complicated by unexplained peaks which were tentatively ascribed to the presence of a significant amount of molecular Li_2 in the effusive gas beam.[31]

Several theoretical papers have addressed tne 1s ionization in Li, either at one or two photon energies[32] or at the sudden limit.[33] Recent relaxed Hartree-Fock results have been reported on the photoemission cross sections as a function of energy for the 1s main lines 1s2s $^{1,3}S$.[34] Comparison of experimental results with this theory should indicate the reliability of calculations at this level, and possibly test the importance of electron-correlation effects in the simplest open-shell atom. Unfortunately, the available photoemission spectra[31,35] contain unexplained peaks at ~52 eV kinetic energy as noted above. These peaks were assigned to Auger electrons emitted from decay of the core-ionized dimer, as mentioned above,[35] but Larkins et al.[36] have questioned this interpretation.

We report here on the first unambiguous core-level photoemission spectra for the atomic Li main lines and 1snl satellites where n=2-5. Our experimental spectra are unambiguous because they contain no unexplained peaks. For our nonresonant results, we compare to the relaxed Hartree-Fock calculations of Larkins et al.,[34] and to previous experimental results.[31,35] For the "Auger" peaks in the data of Krummacher et al.[31] and Gerard,[35] we also discuss an

alternate explanation due to Larkins et al.[36] which involves atom- and/or ion-molecule collisions followed by autoionization. If this interpretation is correct, the photoemission cross sections given by Gerard[35] should be reanalyzed with no adjustment for molecular Li_2.

Additional information on electron-correlation satellites in simple systems can be obtained from resonant excitation to these states. Along these lines and in analogy to the 3s3p excited state in neutral He, we report on the doubly excited resonance in Li $[1s(3s3p)^3P]^2P$ at 71.14 eV.[37] At this resonance, we have measured cross-section profiles for the 1s main lines and n=2 satellites ($1s2p\ ^{1,3}P$). Total cross-section measurements[26,30] indicate some asymmetry to the shape of the resonant profile confirmed by our results which ascribe this asymmetry to the individual main-line ($1s2s\ ^{1,3}S$) profiles only.

Section B describes our experiment. Nonresonant and resonant results are given in Secs. C and D, respectively. Conclusions appear in Sec. E.

B. Experimental

The atomic Li photoemission experiment was performed at the Stanford Synchrotron Radiation Laboratory (SSRL) on Beamline III-1, using a grazing-incidence "grasshopper" monochromator. Relative cross sections and branching ratios were measured with a time-of-flight (TOF) electron analyzer at the "magic angle" of $\theta=54.7^\circ$ relative to

the photon polarization direction, as described previously.[38-40] A second TOF detector was placed at $\theta=0^\circ$ with the goal of determining the angular distribution asymmetry parameters (β). Because of low counting rates together with oven instability due to the buildup of Li and other factors, the β values for the mainlines and satellites could not be reliably determined by calibration with rare gases.

The TOF detectors were modified by insertion of a retarding grid at the beginning of the flight path. The experiment was performed with a 2 volt retarding potential on this grid, to cut off thermally produced low-energy electrons. The 54.7° analyzer transmission was calibrated as a function of kinetic energy using the known partial cross sections for Ne 2s and 2p photoemission.[41]

A resistively-heated metal vapor oven constructed of molybdenum was used to produce an effusive beam of Li, as described previously,[42-43] with several modifications. The running temperature was ~575°C, where the Li backing pressure in the sample cup behind the nozzle was ~0.03 torr.[44] About 140 watts were needed to reach this temperature, with the power divided among three resistive heating wires, two on the oven body and one on the nozzle. To help prevent bumping, small tantalum chips were inserted into the sample cup with solid Li. A slightly modified skimmer and skimmer standoff were used to prevent buildup of condensed Li before the skimmer exit.

At 575°C, only ~1 percent of the metal-vapor beam is molecular Li_2, according to thermodynamic calculations by Nesmeyanov.[44] We

saw no evidence of Li_2 Auger lines in the 40-55 eV kinetic-energy range, in contrast to the peaks observed by Krummacher et al.[31] and Gerard[35] at ~52 eV kinetic energy.

During the collection of the nonresonant spectra, the oven pressure was unstable. Thus, branching ratios were measured, showing excellent agreement between two separate experimental runs. Averaged results are presented in Sec. C1. The monochromator bandpass was 0.30-0.50 eV for the nonresonant work.

For the resonant spectra, the oven was stable enough to measure relative partial cross sections. The monochromator resolution was 0.20(3) eV FWHM. The spectral intensities were normalized to the incident photon beam using a phototube (RCA 8850) to detect fluorescence from the sodium salicylate scintillator . Small pressure variations (less than 10 percent) as a function of time were accounted for by returning to a reference photon energy (71.2 eV) every third spectrum. The monochromator energy calibration was obtained from the energy positions of the atomic resonances in Li (1s3s3p at 71.14 eV),[37] He (3s3p at 69.92 eV),[8] and Xe ($4d_{5/2}$-->6p at 65.11 eV).[45]

A representative TOF photoelectron spectrum is shown in Fig. 2, taken at θ=54.7° and $h\nu$=87 eV, above the satellite thresholds. The main-line and satellite binding energies are reported in Table I.

C. Nonresonant Results

The nonresonant branching ratios for Li ionization to the 1s2l and 1s3l final states are presented in Sec. 1 and compared with other experimental measurements and theory. The absolute cross sections are derived in Sec. 2, where the results are also compared with experiment and theory.

1. Branching Ratios

We have measured branching ratios related to the n=2 (1s2l) ionization of Li as follows: $^1P/^3S$ (72-80 eV), $^3S/(^1S + ^1P + ^3P)$ (75-92.5 eV), and $^3S/(^1S + ^3P)$ (75-77.5 eV). These are included in Table II, along with the derived ratio $^3S/(^1S + ^3P)$ for $h\nu \geq 80$ eV.

In Fig. 3, we show the $^1P/^3S$ ratio from our work and that of Gerard.[35] Above 80 eV, the ^1P satellite was unresolved from the main lines in our spectra. Agreement between the two experimental data sets is good, despite some uncertainties associated with the data of Gerard caused by possible molecular Li_2 contributions to their spectra.[31,35] No published theoretical predictions for either of the n=2 shakeup satellites at these energies are available for comparison. However, preliminary Hartree-Fock results by Richards[17] found the ratio $^1P/^3S$ to be 0.07-0.15, depending on the form of the dipole operator. The data lie mostly in this range.

The $^3S/(^1S + {}^{1,3}P)$ ratio shown in Fig. 4 (top) is relatively constant over the measured range. Of more interest is the $^3S/^1S$ branching ratio, for which theoretical calculations are available.[34] Because we did not resolve the ^3P satellite from the ^1S main line in our TOF spectra, we show in Fig. 4 (bottom) the ratio $^3S/(^1S + {}^3P)$. From the range $h\nu$=75-77.5 eV, we have measured this ratio directly. At 80 eV and higher in energy, we have derived it from the measured $^3S/(^1S + {}^{1,3}P)$ and $^1P/^3S$ ratios as follows. At all energies,

$$R_c = \sigma(^3S)/\sigma(^1S + {}^3P) = (1/R_{31} - R_p)^{-1} , \qquad (1)$$

where $R_{31} = \sigma(^3S)/\sigma(^1S + {}^{1,3}P)$ and $R_p = \sigma(^1P/^3S)$. In the range $80 \leq h\nu \leq 92.5$ eV, we have used the measured values for R_{31} and assumed a linear decrease for the $R_p(^1P/^3S)$ ratio as stated in Table II. For $h\nu \geq 93$ eV, we have used a value for the R_{31} ratio which is an average of those measured for $h\nu$=75-92.5 eV. This, combined with the assumption mentioned above for R_p, results in the values in brackets in Table II for R_c and in Fig. 4 (bottom).

Also included in Fig. 4 (bottom) are the theoretical values for $^3S/^1S$.[34] The theory predicts this ratio to be nonstatistical and nearly constant over the range of our experiment. Our data include the ^3P satellite in the denominator of the ratio and should, therefore, lie below the theoretical curve.

The Gerard data[35] for the $^3S/^1S$ ratio, also shown in

Fig. 4, are systematically higher than ours, as expected. With the use of the theoretical value for $^3S/^1S$, we find that the ratio $^3P/^3S$ is about 0.14(4), in accordance with the results of Gerard.[35] This result also implies that perhaps 26(8) percent of the (^1S + ^3P) peak intensity in our spectra is associated with the 1s2p ^3P satellite. We note that preliminary HF calculations[17] indicate a $^3P/^3S$ ratio of 0.24 at hν=90 eV from the "length" approximation. However, the "velocity" results[17] predict negligible intensity for the ^3P satellite. Higher resolution work is needed to establish the intensity of this conjugate shakeup satellite as a function of energy.

For ionization to the 1s3l states, we plot the n=3/n=2 (1s3l/1s2l) branching ratio in Fig. 5, and set out the numerical results in Table III. The ratio increases slightly with energy. One point from Krummacher et al.[31] is shown also in Fig. 5. These authors noted possible problems with the correction for molecular Li_2. We defer comparison with the Gerard data[35] to the next section on absolute cross sections. Again, there are no published calculations for the energy-dependence of the n=3 satellite intensity. Preliminary HF theory yields the σ(n=3)/σ(n=2) ratio at 90 eV as 0.33 for the "velocity" results and 0.50 for the "length" results.[17] Early theoretical work at hν=151 eV calculated the σ(n=3)/σ(n=2) ratio to be 0.22-0.25, depending on the degree of configuration interaction included.[32] Sudden-limit calculations for the σ(1s3s ^1S)/σ(1s2s ^1S) ratio give a value of 0.33.[33]

Several high-intensity spectra were taken, permitting measurement of the 1snl (n=4,5) intensity relative to the n=3 satellites. Most of the integrated intensity for the higher satellites is probably due to n=4,5 states because the cross section for the higher satellites drops dramatically with n.[46,47] This ratio $\sigma(n=4,5)/\sigma(n=3)$ between 87 and 93 eV was 0.07(2), which corresponds to a $\sigma(n=4,5)$ intensity of about 1.7(4) percent relative to the n=2 ionization manifold. The only theoretical results available for comparison are HF calculations by Larkins et al.[32] which predict the $\sigma(n=4,5)/\sigma(n=3)$ ratio to be 1-4 percent at $h\nu$=151 eV, somewhat below experiment. Sudden-limit results[33] for the ratio $\sigma(1sns;\ n=4,5)/\sigma(1s2s\ ^{1,3}S)$ give a value of about 1.3 percent, in good agreement with our results.

2. Absolute Cross Sections

From our branching ratios in Tables II and III and the total photoabsorption cross section, σ(total), taken from Fig. 1 of Ref. 30, we have derived the absolute cross sections $\sigma(n=2)$, $\sigma(n=3)$, $\sigma(1s2s\ ^3S)$, and $\sigma(1s2s\ ^1S + 1s2p\ ^3P)$ set out in Table IV. We note that the quoted absolute accuracy of the photoabsorption data[30] is 20 percent, and is not included in the errors shown in our plots.

We now discuss how the absolute cross-section values were obtained. At each photon energy, the following relations hold:

$$\sigma(n=2) = \sigma(\text{total})/(1 + R) \qquad (2)$$

$$\sigma(n=3) = \sigma(\text{total}) - \sigma(n=2) \ , \tag{3}$$

where $R = \sigma(n=3)/\sigma(n=2)$ and assuming that the only significant contributions to the total cross section come from the n=2 and n=3 ionization manifolds. We have neglected ionization of the 2s electron, which contributes only 1-2 percent to the σ(total) at these energies,[34,35] and the intensity of the higher n satellites ($n \geq 4$). Thus, $\sigma(n=2)$ and $\sigma(n=3)$ were calculated from Eqs. (2) and (3), respectively, for $h\nu \geq 80$ eV. At two additional lower photon energies (75 and 77.5 eV), $\sigma(n=2)$ was obtained directly from the relative cross-section measurements taken while the metal-vapor oven was stable for a short period and scaled at 80 eV to the absolute values derived above.

The values for $\sigma(1s2s\ ^3S)$ can be expressed in terms of measured and derived branching ratios as:

$$\sigma(1s2s\ ^3S) = \sigma(n=2)\ R_c/[1 + R_c(1 + R_p)] \ , \tag{4}$$

were R_c is defined in Eq. (1) and found in column 3 of Table II, and R_p is either as measured or assumed as stated in Table II. Finally, $\sigma(^1S + {}^3P)$ was calculated as:

$$\sigma(^1S + {}^3P) = \sigma(^3S)/R_c \ . \tag{5}$$

Uncertainties in all cross sections in Table IV were derived from the

statistical uncertainties in the measured branching ratios and in the assumption for R_p (see Table II).

We now compare the derived absolute cross sections with the experimental results of Gerard[35] and theoretical results where available. In Fig. 6, our $\sigma(n=2)$ is plotted along with the data of Gerard,[35] showing the expected decrease from threshold for ionization of a 1s electron. The overall agreement between the two data sets is fairly good, though the slope of the decrease with energy is somewhat different. No theoretical curves have been plotted because there are as yet no published calculations on the energy-dependent behavior of the 1s2p conjugate satellites.

The reliability of present theory can be assessed by comparing the individual cross sections for the $n=2$ (1s2l) main lines. In Fig. 7, the 1s2s ^3S partial cross section is shown with the data of Gerard[35] and theoretical curves from Larkins et al.[34] We note that the preliminary theoretical results by Richards[17] are also in agreement with those plotted in Fig. 7. Only the "velocity" results of the theory are plotted, though the "velocity" and "length" forms agree within ~10 percent. Both relaxed Hartree-Fock (RHF) and configuration interaction (CI) results are shown, with the CI calculation producing consistently lower values by ~8 percent relative to the RHF results. Both curves predict an energy dependence of the cross section in good agreement with our results. Again, Gerard's data drop off more quickly above $h\nu=80$ eV than either theory or our data.

For the 1s2s ^1S main line, Fig. 8 shows Gerard's data[35] and both RHF and CI "velocity" forms of theory, along with our summed results for the unresolved ^1S main line and ^3P satellite. Early calculations by Richards[17] agree with the plotted theory. While our ^3S main-line cross section was slightly lower than theory (Fig. 7), our $^1S + ^3P$ values are slightly higher, presumably due to the ^3P contribution. As discussed previously, about 26(8) percent of this summed intensity is due to the satellite if the theory predicts the $^3S/^1S$ ratio correctly. The energy dependence in our data is well modelled by theory.

Finally, for the n=3 (1s3l) satellites, Fig. 9 shows the derived absolute cross sections from our experiment and Gerard's.[35] Here we find the largest discrepancy between the two experimental data sets. The agreement is poor and becomes increasingly worse to lower energy, where the data of Gerard rises steeply. At ~82 eV, the difference between the two sets is about a factor of two. The only nonstatistical uncertainty in the overall shape of our results stems from decreasing detector transmission when the n=3 satellite is at low kinetic energy. We believe that we have adequately accounted for this effect because $\sigma(n=3)$ derived from two separate experimental runs, with different transmission corrections, were in excellent agreement.

In trying to understand this disagreement for $\sigma(n=3)$, and similar variance noted earlier, we must consider complications in Gerard's experiment, which may have implications for all of Gerard's data presented in Figs. 3-9 and discussed above. Additional peaks at 51.6

and 52.8 eV kinetic energy were observed in the photoelectron spectra.[31,35] These peaks were totally absent in our spectra. They have been interpreted as the Li_2 Auger transitions shown below because they do not shift in kinetic energy as the photon energy is scanned:[35]

$$Li_2^{+}(1\sigma_u^{-1}1\sigma_g^2 2\sigma_g^2) \longrightarrow Li_2^{2+}(1\sigma_u^2 1\sigma_g^2) + e^-_{Auger} \qquad (6)$$

$$Li_2^{+}(1\sigma_u^2 1\sigma_g^{-1} 2\sigma_g^2) \longrightarrow Li_2^{2+}(1\sigma_u^2 1\sigma_g^2) + e^-_{Auger} \, . \qquad (7)$$

Corrections were made to the data by subtracting the inferred concommitant Li_2 photoelectron intensity arising from the 1s ionization.[31,35] However, recent theoretical work indicates that the actual Auger electron energies should be much less than 52 eV, at 48.45 and 48.40 eV with a very small energy splitting.[36] Both the observed "Auger" peak energy of ~52 eV and the splitting (1.2 eV) are inconsistent with these calculated values. In addition, the intensity observed in the peaks near 52 eV is much too high to be consistent with the predicted 1 percent of dimer produced at this temperature.[44] The Auger interpretation would thus require a postulation that the molecular ionization cross section is much larger than twice the atomic cross section, or that the amount of Li_2 significantly exceeds 1 percent. Several calculations on the Li_2 molecule indicate that the molecular cross section is indeed roughly twice the atomic value at these energies, as expected.[31,48]

In light of these facts, Larkins et al.[36] have proposed that atom- or ion-molecule collisions, followed by molecular autoionization, is responsible for the peaks near 52 eV kinetic energy in the Gerard spectra. The proposed three-step mechanism is as follows:

I. atomic excitation and ionization:

$$Li(1s^2 2s) + h\nu \longrightarrow Li^*(1snln'l') \quad (8)$$

$$Li(1s^2 2s) + h\nu \longrightarrow Li^+(1snl) + e^- \quad (9)$$

II. atom- or ion-molecule collisions:

$$Li^*(1snln'l') + Li_2(1\sigma^4 2\sigma_g^2) \longrightarrow Li^+(1s^2 2s) + Li_2^*(1\sigma^3 2\sigma_g^2 n\phi^1) \quad (10)$$

$$Li^+(1snl) + Li_2(1\sigma^4 2\sigma_g) \longrightarrow Li^+(1s^2) + Li_2^*(1\sigma^3 2\sigma_g^2 n\phi^1) \quad (11)$$

III. molecular autoionization:

$$Li_2^*(1\sigma^3 2\sigma_g^2 n\phi^1) \longrightarrow Li_2^+(1\sigma^4 2\sigma_g) + e^- \quad . \quad (12)$$

The autoionizing processes in Eq. (12) where $n\phi$ corresponds to $1\pi_u$, $2\sigma_u$, $2\sigma_g$, and $1\pi_g$ have been observed with electron kinetic energies of 51.5, 51.6, 52.8, and 53.9 eV,[49] in excellent agreement with the energies observed by Gerard (51.6 and 52.8 eV).[35]

We believe that the collisional model put forth by Larkins et al.[36] is very probably correct, requiring only that atom- or ion-molecule collision cross sections be one to two orders of magnitude higher than photoionization cross sections, which is quite

possible.[50,51] This interpretation also suggests reanalysis of Gerard's data with little or no correction for dimer intensity, which should only contribute ~2 percent to the intensity of the atomic photoemission peaks.

D. Resonant Results

In Sec. 1, we briefly review the Fano formalism for autoionizing total cross-section profiles and give a brief description of the Starace parameters, which apply to partial cross sections. In Sec. 2, we present the data analysis. A discussion of the results at the $[1s(3s3p)^3P]^2P$ resonance in Li follows in Sec. 3.

1. Theoretical Background

Fano first described the effect of an isolated discrete state ϕ on the total photoabsorption cross section.[52] A discrete state is embedded in one or more continua leading to oscillations in the total ionization cross section caused by interference between the two indistinguishable pathways: direct ionization and autoionization via the discrete level. For an isolated resonance, Fano expressed the total cross section (σ_t) in terms of a nonresonant "background" cross section (σ_0) as:

$$\sigma_t = \sigma_0 \left[\rho^2 \frac{(q + \epsilon)^2}{1 + \epsilon^2} + 1 - \rho^2 \right], \tag{13}$$

$$\text{with} \quad \epsilon = \frac{E - E_0}{\Gamma/2} , \tag{14}$$

Here ρ^2 and q are Fano parameters (assumed constant over the resonance) which describe the strength and shape of the resonant profile, E is the photon energy, E_0 is the resonant energy, Γ is the linewidth (FWHM), and ϵ is a reduced energy.

Furthermore, ρ^2, q, σ_0, and Γ can be expressed in terms of dipole and Coulomb matrix elements connecting the ground (g), discrete (ϕ), and continuum (μ) wavefunctions. The correlation coefficient ρ^2 is a measure of the strength of the resonance and corresponds to the relative decrease below the background cross section σ_0. In terms of matrix elements,

$$\rho^2 = \frac{\sum_{\mu} |\langle \phi | V | \mu \rangle \langle \mu | \vec{r} | g \rangle|^2}{\sum_{\mu} |\langle \phi | V | \mu \rangle|^2 \sum_{\mu} |\langle \mu | \vec{r} | g \rangle|^2} , \tag{15}$$

where V and $\vec{r}$ are the Coulomb and dipole operators. The q parameter describes the shape of the resonant profile which can be of a Lorentzian, asymmetric, or window type, and is expressed as:

$$q = \frac{\langle \phi | \vec{r} | g \rangle}{\pi \sum_{\mu} \langle \phi | V | \mu \rangle \langle \mu | \vec{r} | g \rangle} , \tag{16}$$

where ϕ is now the discrete state modified by the continua. The maximum relative increase in the cross section in the vicinity of the

resonance is equal to $\rho^2 q^2$. The matrix elements in Eqs. (15) and (16) vary slowly with energy; thus, ρ^2 and q are relatively constant over the width of the resonance.

The nonresonant background cross section σ_0 is simply:

$$\sigma_0 = \sum_{\mu} |\langle \mu | \vec{r} | g \rangle|^2 \quad , \tag{17}$$

and the linewidth Γ of the resonance is given by:

$$\Gamma = 2\pi \sum_{\mu} |\langle \phi | V | \mu \rangle|^2 \quad . \tag{18}$$

The above formalism, though appropriate for describing the total cross section, does not apply to individual partial cross sections. Several workers, including Davis and Feldkamp,[53] Combet Farnoux,[54] and Starace,[55] have derived equivalent expressions to describe decay into several continuum channels. Using the notation of Starace, an individual observable cross section $\sigma(\mu)$ can be written as:

$$\sigma(\mu) = \frac{\sigma_0(\mu)}{1 + \epsilon^2} \left\{ \epsilon^2 + 2\left[q\mathrm{Re}(a_\mu) - \mathrm{Im}(a_\mu)\right]\epsilon + 1 - 2q\mathrm{Im}(a_\mu) - 2\mathrm{Re}(a_\mu) + (q^2 + 1)|a_\mu|^2 \right\} , \tag{19}$$

where $\sigma_0(\mu)$ is the nonresonant partial cross section for the μth observable final state, and ϵ and q are defined in Eqs. (14) and (16), respectively. The complex parameter a_μ is given by:[56]

$$\alpha_\mu = \frac{\langle \phi | V | \mu \rangle}{\langle g | \vec{r} | \mu \rangle} \left[\frac{2\pi}{\Gamma} \sum_\mu \langle g | \vec{r} | \mu \rangle \langle \mu | V | \phi \rangle \right], \tag{20}$$

where Γ is given in Eq. (18). The term in brackets is common to all channels μ. The Starace formalism retains the use of q to describe the total cross-section profile shape; the squares of the α_μ parameters for each channel are similar to the Fano ρ^2 parameter and an indication of the resonant strength per channel.

The Fano and Starace formalisms lead to the same mathematical form for the total cross section,

$$\sigma_t = \sigma_0 \left[\frac{C_1 + C_2\epsilon + \epsilon^2}{1 + \epsilon^2} \right], \tag{21}$$

where the Starace C_1 and C_2 parameters can be expressed in terms of q and ρ^2 as:

$$C_1 = \rho^2(q^2 - 1) + 1 \tag{22}$$

$$C_2 = 2q\rho^2 . \tag{23}$$

However, the q and ρ^2 matrix-element expressions in Eqs. (15) and (16) are not correct for partial cross-section profiles.

For the 1s(3s3p) resonance in atomic Li, we report both Fano (q and ρ^2) and Starace (C_1 and C_2) parameters for the total and partial cross sections. Because our resonant results are for the most

part qualitative, we refer the reader to other sources for more details on the derivations for the Fano and Starace formalisms.[11,12,43,52,55]

2. Data Analysis

A TOF spectrum taken at θ=54.7° and on the 1s(3s3p) ^3P resonance at 71.2 eV is shown in Fig. 10. The spectrum is uncorrected for the analyzer transmission, which decreases at lower kinetic energy. The 1s2s ^1S main line and 1s2p ^3P satellite are unresolved; therefore, their summed cross section was used for the fitting procedures described below.

The total and partial cross-section profiles (with the exception of the 1s2p ^1P state) in the vicinity of the 1s(3s3p) ^3P resonance were fitted to the Fano functional form of Eq. (13) convoluted with a Gaussian of 0.20 eV FWHM for the monochromator bandpass. A resonant energy of 71.186 eV was used for the fitting compared with the energy in photoabsorption[37] of 71.14 eV, and the resonance linewidth Γ was taken as 0.10 eV from experiment[30] and theory.[57] The 1s2p ^1P cross-section profile was fitted to a Lorentzian of 0.10 eV FWHM convoluted with a Gaussian of 0.20 eV FWHM. The resulting Fano q and ρ^2 values and the Starace C_1 and C_2 parameters are reported in Table V. The fits are plotted along with the data in Figs. 11 and 12.

In all cases, the nonresonant background cross section σ_0 was taken to be a linear function of energy. Since there are relatively

few data points over the resonance, we emphasize that the fitting parameters contain appreciable error, as quoted in Table V. Errors in the Fano and Starace parameters include uncertainty in determining the best fit and in the selection of a background cross section, σ_0.

One complication in the data analysis involves the presence of a small resonance at only ~0.3 eV higher energy, assigned as the ^1P component. Though this resonance appears to be quite small in the total photoabsorption cross section (see Fig. 11, solid curve),[30] its presence could perturb the partial cross sections to varying extents in the vicinity of the ^3P resonance. This second resonance at 71.47 eV[37] has been ignored in our fits due to the scarcity of data in this region and the small effect on the cross sections. We note that one of our data points lies at 71.5 eV, which is about the center of this second resonance and high throughout Figs. 11 and 12.

3. Discussion of Resonance Results

Though we have thus far referred to the resonance at 71.14 eV as the doubly excited configuration $[1s(3s3p)\ ^3P]\ ^2P$, it is well known that the series of states leading to the Li $n=3$ satellite thresholds are not the expected simple Rydberg series, but rather configurationally mixed series.[30] The analogous doubly excited states in He have been studied extensively both experimentally[8,11] and theoretically.[21,22,57-62] In He, the strongly interacting series of resonances have been classified with several

schemes.[57,60,62,63] More recently, the resonances below the n=3 satellite thresholds in Li have been classified in parallel to He, with reasonable success.[30] We shall use here the notation of Lipsky et al.,[58] consistent with the first analysis of the n=3 resonances in Li.

The Lipsky notation $(N,n\alpha)^{1,3}P$ identifies resonances by principal quantum number (N), outer quantum number (n), and series label (α).[58] The label α (where the lowest series is termed a) was obtained from approximately constant quantum defects or from configurations of the wavefunctions. The 71.14 eV resonance is labelled $[(3,3a)\ ^3P]\ ^2P$, and is the first member in the ^3P a series. We note that in the doubly excited symmetry basis (DESB) of Herrick and Sinanoglu,[57] this resonance is labelled as K_n, or 2_3 for helium.

Our resonant profile parameters for the total cross section agree within error limits with a previous photoabsorption measurement, showing some asymmetry in shape indicated by a small negative q parameter.[30] Figure 11 includes the convoluted and deconvoluted fits to our data, and a photoabsorption curve (0.027 eV bandpass).[30] Though our ρ^2 and q agree within errors with the values reported for the photoabsorption data (see Table V),[30] the plotted curves in Fig. 11 appear to be significantly different in magnitude. The relative increase at the resonance is equal to ρ^2q^2, which is twice as large for our plotted fit (deconvoluted) compared to the absorption curve.[30] We note that an earlier

photoabsorption measurement[26] disagrees with both our data and the more recent photoabsorption curve,[30] showing an even larger positive effect at the resonance (a more negative q parameter). We offer no explanation for these discrepancies.

For the individual profiles (Fig. 12), we can make the following generalizations. The main-line profiles ($^{1,3}S$) appear to be asymmetric, while the n=2 satellite profiles ($^{1,3}P$) are probably nearly Lorentzian. The 1s2s ^3S and 1s2p ^1P profile shapes support this statement unambiguously. For the summed ^1S and ^3P profile, careful examination of the spectra reveals that the ^1S intensity maximum is at 71.15 eV in our data, whereas the ^3P maximum is at 71.20 eV. Furthermore, the ^1S intensity is at a minimum and below the nonresonant intensity level at 71.3 eV. Qualitatively, this indicates some asymmetry in the ^1S mainline profile and very little if any asymmetry in the ^3P profile. Although this behavior was obvious to visual inspection, we did not proceed with further deconvolution because of the limited accuracy of this data set. Higher resolution and higher count rates are needed to confirm these ^1S and ^3P profiles quantitatively.

Asymmetry in a line profile indicates the degree of interference and coupling between the discrete and continuum states. Examining the expression for the Fano q parameter in Eq. (16), we see that a small value of q (corresponding to an asymmetric profile) can be caused in part by a large amount of coupling between the discrete and continuum states, through the matrix element $\langle\phi|V|\mu\rangle$. This Fano q parameter

applies only to the total cross section; thus, it is more difficult to make simple generalizations about the individual profiles. An asymmetric shape generally indicates strong coupling, but it is also influenced by the background cross section. For the 1s2p satellites in Li, the nonresonant intensity is so small that if the resonance is to have an appreciable effect, only a symmetric Lorentzian profile is possible, as observed. For the 1s2s main lines, there is enough nonresonant cross section to interfere strongly with the autoionization pathway via the discrete state. Calculations are needed, similar to those on He,[22] to describe in detail the degree of coupling between the ground, discrete, and continuum states at this resonance.

We now comment briefly on the cross-section results of Gerard[35] at this resonance. Their photon resolution was 0.30 eV compared with our bandpass of 0.20 eV. The larger bandpass affects their spectrum at $h\nu$=71.28 eV, in which each peak appears as a doublet; some of the cross-section structure is starting to appear in the peaks. Thus, aside from any possible complications from molecular Li_2, the large bandpass prohibits a detailed quantitative study of the resonance profiles. This is emphasized by the lack of agreement with our results. For example, the Gerard data[35] for the 1s2s ^3S profile show very little if any asymmetry.

Because the doubly excited state 3s3p in He has been studied extensively,[8,11,21,22,57-63] we compare it with the $[1s(3s3p)^3P]^2P$ resonance in Li. For the total cross sections, the

"phase" of the resonance (determined by the sign of the Fano q parameter) is opposite for He[8,11] and Li. Fano and Copper presented arguments to explain the sign of q for the 2s2p and 3s3p resonances in He.[47] The Fano q parameter is related to the dipole and Coulomb matrix elements between the ground, discrete, and continuum states, as in Eq. (16). The sign of q then is determined by the signs of these matrix elements. For example, the predicted negative q for the He 2s2p resonance was found to depend on a single negative matrix element $\langle 2s2p|\vec{r}|1s^2\rangle$. When this element is approximated with one-electron integrals as:

$$\langle 2s2p|\vec{r}|1s^2\rangle \sim (2)^{1/2}\langle 2s|1s\rangle\langle 2p|\vec{r}|1s\rangle \quad , \tag{25}$$

Fano and Cooper concluded that it was the negative sign of $\langle 2s|1s\rangle$ which ultimately produced a negative q parameter, with all other matrix elements in Eq. (16) positive. The negative sign of the overlap integral $\langle 2s|1s\rangle$ was explained by less screening of the 2s electron in the 2s2p state relative to the 1s electron in $1s^2$. We use this reasoning below to rationalize that the double-excitation dipole integrals are negative. Similar arguments were made to predict the positive q for the He 3s3p resonance.[47]

If we proceed to make parallel arguments for the 1s(3s3p) resonance in Li, we first need to estimate the inverse of the q parameter as sums over the different continuum channels:

$$q^{-1}(1s3s3p) = \frac{\pi \langle 1s3s3p|V|1s^2\epsilon p\rangle\langle 1s^2\epsilon p|\vec{r}|1s^22s\rangle}{\langle 1s3s3p|\vec{r}|1s^22s\rangle} + \frac{\pi \langle 1s3s3p|V|1s2s\epsilon p\rangle\langle 1s2s\epsilon p|\vec{r}|1s^22s\rangle}{\langle 1s3s3p|\vec{r}|1s^22s\rangle} + \frac{\pi \langle 1s3s3p|V|1s2p\epsilon s\rangle\langle 1s2p\epsilon s|\vec{r}|1s^22s\rangle}{\langle 1s3s3p|\vec{r}|1s^22s\rangle} \quad , \tag{26}$$

where we have ignored the $^{1,3}S$ and $^{1,3}P$ splittings for the 1s2s and 1s2p states and have assumed that the modified discrete state Φ is approximately equal to the unperturbed state ϕ. If we further use the fact that the $1s^2$ cross section is very small at the resonance,[34,35] and thus contributes little to the shape of the total cross section, we can neglect the first term in Eq. (26) above.

We are now left with estimating the signs of the following matrix elements:

$\langle 1s3s3p\|V\|1s2s\epsilon p\rangle$	$\langle 1s2s\epsilon p\|\vec{r}\|1s^22s\rangle$
$\langle 1s3s3p\|V\|1s2p\epsilon s\rangle$	$\langle 1s2p\epsilon s\|\vec{r}\|1s^22s\rangle$
	$\langle 1s3s3p\|\vec{r}\|1s^22s\rangle$

The first two Coulomb matrix elements above (left column) are assumed positive based on the normalization that radial wavefunctions are positive when the electrons are near the nucleus. The next two dipole matrix elements (right column) between the ground and continuum states

are respectively positive for the 1s2sεp continuum (a single excitation dipole) and possibly negative for the 1s2pεs continuum (a double excitation dipole). The last remaining integral involves a double excitation and is thus negative. Combining all these signs, we predict that the q parameter is probably negative, as observed, for the 1s3s3p resonance, due mainly to the double excitation dipole integrals for 1s2sεp ionization.

E. Conclusions

We have presented the first experimental results on the core ionization of atomic Li which are uncomplicated by the presence of Li_2 or collisional processes. The nonresonant results indicate that theory at the relaxed Hartree-Fock level is probably adequate to model the 1s2s main-line cross sections for atomic Li. The Gerard experimental cross sections[35] for the main lines have a somewhat different slope for the decrease of the curves with energy. Our low-resolution results prohibit a detailed study of the 1s2p conjugate shakeup satellites, though relative intensities were obtained at a few energies for the ^1P satellite. The summed n=3 satellites were monitored from 5 to 25 eV above threshold, and cross section results disagree with those of Gerard.[35] A reanalysis of those data[35] for all peaks assuming a collisional interpretation[36] for the origin of the 52 eV "Auger" peaks is warranted. Theory which reliably predicts the n=2 and n=3 satellite intensities as a function of energy should

provide a basis for understanding electron correlation in atomic Li.

Our results at the $[(3,3a)^3P]^2P$ doubly excited resonance are in good agreement with previous photoabsorption measurements,[30] confirming an asymmetric profile in the total cross section. We have also measured partial cross sections over this resonance, with the qualitative result that the 1s2s $^{1,3}S$ main lines show asymmetric shapes while the 1s2p $^{1,3}P$ satellites have nearly Lorentzian profiles. At present there are no calculations on the $[(3,3a)^3P]^2P$ resonance in Li. Just recently, theoretical results on the analogous 3s3p state in He were reported,[22] in excellent agreement with experiment.[11,12] It is hoped that the experimental results presented here for Li will stimulate calculations on the individual cross-section profiles at resonances below the n=3 and higher satellite thresholds in this open-shell system.

Table I. Binding energies for the main-line and satellite photoemission lines in atomic litnium.

Li^+ configuration	Binding energy (eV)[a]
Mainlines:	
$1s^2$	5.390
$1s2s\ ^3S$	64.41
$1s2s\ ^1S$	66.15
n=2 Satellites:	
$1s2p\ ^3P$	66.67
$1s2p\ ^1P$	67.61
n=3 Satellites:	
$1s3s\ ^3S$	74.17
$1s3s\ ^1S$	74.67
$1s3p\ ^3P$	74.76
$1s3p\ ^1P$	75.04
n=4 Satellites:[b]	
$1s4s\ ^3S$	77.30
n=5 Satellites:[b]	
$1s5s\ ^3S$	78.69

[a] From Ref. 64.
[b] For simplicity, we list only the ns ^3S channel.

Table II: Experimental Branching Ratios for Lithium n=2 Photoionization

Photon energy (eV)	R_{31} $^3S/(^1S + 1,^3P)$	R_c $^3S/(^1S + ^3P)$[a]	R_p $^1P/^3S$
72[b]			0.123(25)
75	1.66(9)	1.77(10)	0.084(12)
77	1.56(5)	1.79(5)	0.097(9)
77.5	1.66(5)	1.97(7)	0.085(7)
80	1.62(5)	1.84(7)	0.075(7)
82.5	1.71(5)	1.95(9)	
85	1.66(5)	1.86(8)	
87	1.59(3)	1.76(6)	
87.5	1.80(4)	2.02(8)	
90	1.71(5)	1.89(8)	
92.5	1.56(4)	1.70(6)	
93		[1.82(13)][c]	
95		[1.80(13)]	
97		[1.79(13)]	
99		[1.78(13)]	

a For $h\nu<80$ eV, this ratio was measured directly. For $h\nu>80$ eV, this ratio was derived by assuming that the ratio $R_p(^1P/^3S)$ behaves linearly above 80 eV according to the equation $R_p = -0.18\ [h\nu(eV)]) + 21.9$ with an uncertainty of ±0.15.

b In the vicinity of the resonances leading to the n=3 satellite thresholds.

c The number in brackets [] were derived using a value for $^3S/(^1S + 1,^3P)$ which is an average of the values in column 1 [1.65(10)].

Table III. Experimental Branching Ratio n=3/n=2 (1s3l/1s2l) for Lithium Photoionization

Photon energy(eV)	n=3/n=2
80	0.172(10)
82.5	0.187(8)
85	0.187(5)
87	0.209(5)
87.5	0.207(7)
90	0.209(8)
92.5	0.234(8)
93	0.210(5)
95	0.223(8)
97	0.224(6)
99	0.235(5)

Table IV: Absolute Cross sections (Mb) derived for Lithium n=2 (1s2l) and n=3 (1s3l) Photoionization. See text for details of derivation. The errors shown parenthetically are statistical. In addition, the total cross section data from Ref. 30, on which the absolute scale is based, have an absolute error of 20 percent.

Photon energy (eV)	σ(n=2)	σ(n=3)	n=2	
			$\sigma(^3S)$	$\sigma(^1S + {}^3P)$
75	1.99(8)		1.21(11)	0.69(7)
77.5	1.90(8)		1.19(10)	0.60(5)
80	1.86(2)	0.32(2)	1.15(7)	0.63(5)
82.5	1.67(2)	0.31(2)	1.05(7)	0.54(4)
85	1.58(1)	0.30(1)	0.99(7)	0.53(4)
87	1.45(1)	0.30(1)	0.89(5)	0.51(3)
87.5	1.43(1)	0.29(1)	0.92(6)	0.46(4)
90	1.41(1)	0.29(1)	0.89(6)	0.47(4)
92.5	1.30(1)	0.31(1)	0.79(4)	0.46(3)
93	1.29(1)	0.27(1)	0.81(9)	0.45(6)
95	1.28(1)	0.28(1)	0.80(9)	0.44(6)
97	1.18(1)	0.27(1)	0.74(8)	0.41(5)
99	1.09(1)	0.26(1)	0.68(8)	0.38(5)

Table V. Fano and Starace Parameters for the total and partial cross sections for the 1s(3s3p) ^3P resonance.

	Fano parameters		Starace parameters	
Channel	q	ρ^2	C_1	C_2
total	-3.2(7)	0.20(8)		
	[-2.60][a]	[0.144][a]		
1s2s ^3S	-1.6(3)	0.60(15)	1.8(6)	-1.9(6)
1s2s ^1S + 1s2p ^3P	-2.5(10)	0.25(15)	2.3(15)	-1.3(9)
1s2p ^1P	Lorentzian			

[a] Values from Ref. 30.

References

* Work done in collaboration with D.W. Lindle, P.A. Heimann, W.D. Brewer, U. Becker, H.G. Kerkhoff, and D.A. Shirley. We gratefully acknowledge helpful discussions with F.P. Larkins, J. Richards, P. Gerard, and F. Wuilleumier.

1. T.A. Carlson, Phys. Rev. 156, 142 (1967).
2. J.A.R. Samson, Phys. Rev. Lett. 22, 693 (1969).
3. T.A. Carlson, M.O. Krause, and W.E. Moddeman, J. Phys. (Paris) Colloq. 32, C4-76 (1971).
4. M.O. Krause and F. Wuilleumier, J. Phys. B 5, L143 (1972).
5. P.R. Woodruff and J.A.R. Samson, Phys. Rev. Lett. 45, 110 (1980).
6. F. Wuilleumier, M.Y. Adam, N. Sandner, and V. Schmidt, J. Phys. (Paris) Lett. 41, L373 (1980).
7. J.M. Bizau, F. Wuilleumier, P. Dhez, D.L. Ederer, T.N. Chang, S. Krummacher, and V. Schmidt, Phys. Rev. Lett. 48, 588 (1982).
8. P.R. Woodruff and J.A.R. Samson, Phys. Rev. A 25, 848 (1982).
9. V. Schmidt, H. Derenbach, and R. Malutzki, J. Phys. B 15, L523 (1982).
10. P. Morin, M.Y. Adam, I. Nenner, J. Delwiche, M.J. Hubin-Franskin, and P. Lablanquie, Nuc. Instrum. Methods 208, 761 (1983).
11. D.W. Lindle, T.A. Ferrett, U. Becker, P.H. Kobrin, C.M. Truesdale, H.G. Kerkhoff, and D.A. Shirley, Phys. Rev. A 31, 714 (1985).
12. D.W. Lindle, P.A. Heimann, T.A. Ferrett, and D.A. Shirley, Phys. Rev. A (in press); D.W. Lindle, T.A. Ferrett, P.A. Heimann, and

D.A. Shirley (unpublished results).

13. E.E. Salpeter and M.H. Zaidi, Phys. Rev. 125, 248 (1962).
14. R.L. Brown, Phys. Rev. A 1, 341 (1970).
15. V. Jacobs, Phys. Rev. A 3, 289 (1971).
16. V.L. Jacobs and P.G. Burke, J. Phys. B 5, L67 (1972).
17. T.N. Chang, J. Phys. B 13, L551 (1980).
18. J.A. Richards, B.S. Honours Thesis, Monash University, Australia, 1981.
19. K.A. Berrington, P.G. Burke, W.C. Fon, and K.T. Taylor, J. Phys. B 15, L603 (1982).; see P.C. Ojha, ibid 17, 1807 (1984) for additional discussion.
20. J.A. Richards and F.P. Larkins, J. Electron Spectrosc. 32, 193 (1983).
21. S. Salomonson, S.L. Carter, and H.P. Kelly, J. Phys. B 18, L149 (1985).
22. S. Salomonson, S.L. Carter, and H.P. Kelly (unpublished results).
23. G.V. Marr, Proc. Phys. Soc. (London) 81, 9 (1963).
24. R.D. Hudson and V.L. Carter, Phys. Rev. 137, A1648 (1965); J. Opt. Soc. Am. 57, 651 (1967).
25. M.Ya. Amusia, N.A. Cheropkov, Dj. Živanović, and V. Radojević, Phys. Rev. A 13, 1466 (1976).
26. G. Mehlman, D.L. Ederer, E.B. Saloman, and J.W. Cooper, J. Phys. B 11, L689 (1978).
27. J.W. Cooper, M.J. Conneely, K. Smith, and S. Ormonde, Phys. Rev. Lett. 22, 1540 (1970).

28. D.L. Ederer, T. Lucatorto, and R.P. Madden, Phys. Rev. Lett. 25, 1537 (1970).

29. D.L. Ederer, T. Lucatorto, and R.P. Madden, J. Phys. (Paris) Colloq. 32, C4-85 (1971).

30. G. Mehlman, J.W. Cooper, and E.B. Saloman, Phys. Rev. A 25, 2113 (1982).

31. S. Krummacher, V. Schmidt, J.M. Bizau, D.L. Ederer, P. Dhez, and F. Wuilleumier, J. Phys. B 15 4264 (1982).

32. F.P. Larkins, P.D. Adeney, and K.G. Dyall, J. Electron Spectrosc. 22, 141 (1981).

33. G. De Alti, P. Decleava, and A. Lisini, Chem. Phys. 80, 229 (1983).

34. F.P. Larkins, B.I. Craig, and J.A. Richards (unpublished results).

35. P. Gerard, Ph.D. Thesis, Universite de Paris-Sud, 1984.

36. F.P. Larkins and J.A. Richards, Aus. J. Phys. 39, 1 (1986).

37. A.M. Cantú, W.H. Parkinson, G. Tondello, and G. Tozzi, J. Opt. Soc. Am. 67, 1030 (1977).

38. M.G. White, R.A. Rosenberg, G. Gabor, E.D. Poliakoff, G. Thornton, S. Southworth, and D.A. Shirley, Rev. Sci. Instrum. 50, 1288 (1979).

39. S. Southworth, C.M. Truesdale, P.H. Kobrin, D.W. Lindle, W.D. Brewer, and D.A. Shirley, J. Chem. Phys. 76, 143 (1982).

40. S. Southworth, U. Becker, C.M. Truesdale, P.H. Kobrin, D.W. Lindle, S. Owaki, and D.A. Shirley, Phys. Rev. A 28, 261 (1983).

41. F. Wuilleumier and M.O. Krause, J. Electron Spectrosc. 15, 15 (1979).

42. P.H. Kobrin, Ph.D. Thesis, University of California, Berkeley, 1983.

43. P.H. Kobrin, U. Becker, S. Southworth, C.M. Truesdale, D.W. Lindle, and D.A. Shirley, Phys. Rev. A 26, 842 (1982).

44. A.N. Nesmeyanov, Vapor Pressure of the Chemical Elements (Elsevier, Amsterdam, 1963); T.B. Douglas, L.F. Epstein, J.L Dever, W.H. Howland, J. Am. Chem. Soc. 77, 2144 (1955).

45. K. Codling and R.P. Madden, Phys. Rev. Lett. 12, 106 (1964).

46. P.A. Heimann, U. Becker, H.G. Kerkhoff, B. Langer, D. Szostak, R. Wehlitz, D.W. Lindle, T.A. Ferrett, and D.A. Shirley, Phys. Rev. A 34 (1986).

47. U. Fano and J.W. Cooper, Phys. Rev. 137, 1364 (1965).

48. J.W. Davenport, G.J. Cosgrove, and A. Zangwill, J. Chem. Phys. 78, 1095 (1983).

49. W.H.E. Schwarz, W. Butscher, D.L. Ederer, T.B. Lucatorto, B. Ziegenbein, W. Mehlhorn, and H. Prompeler, J. Phys. B 11, 591 (1978).

50. U. Fano and W. Lichten, Phys. Rev. Lett. 14, 627 (1965).

51. F.P. Larkins, J. Phys. B 5, 571 (1972).

52. U. Fano, Phys. Rev. 124, 1866 (1961).

53. L.C. Davis and L.A. Feldkamp, Phys. Rev. B 15, 2961 (1977); 23, 6239 (1981).

54. F. Combet Farnoux, Phys. Rev. A 25, 287 (1982).

55. A.F. Starace, Phys. Rev. A 16, 231 (1977).

56. P.C. Kemeny, J.A.R. Samson, and A.F. Starace, J. Phys. B 10, L201 (1977).

57. D.R. Herrick and O. Sinanoglu, Phys. Rev. A 11, 97 (1975).

58. L. Lipsky, R. Anania, and M.J. Conneely, At. Data Nucl. Data Tables 20, 127 (1977).

59. R.S. Oberoi, J. Phys. B 5, 1120 (1972).

60. K.T. Chung, Phys. Rev. A 6, 1809 (1972).

61. W.C. Martin, J. Phys. Chem. Ref. Data 2, 257 (1973).

62. J.W. Cooper, U. Fano, and F. Prats, Phys. Rev. Lett. 10, 518 (1963).

63. J. Macek, J. Phys. B 1, 831 (1968).

64. C. Moore, Atomic Energy Levels NSRDS-NBS 35 (U.S. GPO, Washington, D.C., 1971) Vol. 1.

Figure Captions

Fig. 1 Energy-level diagram for neutral and singly-ionized lithium. Binding energies are listed in Table I. At the doubly excited state 1s(3s3p) at 71.2 eV, the autoionizing decay channels to the n=2 manifold (1s2l) are shown.

Fig. 2 TOF photoelectron spectrum taken at $h\nu$=87 eV and θ=54.7°. The 1s2s main-line photoemission is split into ^3S and ^1S components, with the 1s2p $^{1,3}P$ satellites unresolved at slightly higher binding energy. The relatively intense n=3 satellites (1s3l) have a binding energy of about 75 eV.[64] The very weak higher n satellites are shown also on an expanded scale (x 20).

Fig. 3 Experimental n=2 (1s2l) branching ratio $^1P/^3S$. Experimental results by Gerard[35] (with a representative error bar) are shown by open circles, and our data by filled circles.

Fig. 4 Experimental n=2 (1s2l) branching ratio $^3S/(^1S + ^{1,3}P)$ (top) and derived branching ratio $^3S/(^1S + ^3P)$ (bottom). Solid circles are our results. Open circles are those of Gerard[35] for $^3S/^1S$. Theory curve in the bottom panel is the Hartree-Fock result[34] for the $^3S/^1S$

ratio.

Fig. 5 Experimental branching ratio n=3/n=2 (1s3l/1s2l). One experimental point by Krummacher et al.[31] is shown (open circle).

Fig. 6 Derived absolute cross section (Mb) for n=2 (1s2l) photoionization. Open circles are experimental results by Gerard,[35] with a representative error bar.

Fig. 7 Derived absolute cross section (Mb) for the 1s2s ^3S main line. Open circles are data from Gerard (no quoted error).[35] Solid curves are theory by Larkins et al., as labelled.[34]

Fig. 8 Derived absolute cross section (Mb) for the sum of the n=2 ^1S and ^3P ionization are shown by solid circles for our results. Theory curves[34] and Gerard's data[35] are same as in Fig. 7, but represent only the main-line cross section (^1S).

Fig. 9 Derived absolute cross section (Mb) for the n=3 satellites (1s3l). Gerard data are shown as open circles, with one representative error bar.[35]

Fig. 10 TOF photoelectron spectrum taken at $h\nu$=71.2 eV and θ=54.7° on the $[1s(3s3p)^3P]^2P$ doubly excited resonance.

Fig. 11 Total photoabsorption cross section over the 1s(3s3p) resonance. The dashed curves are fits to our data (solid circles) using a Fano profile where ρ^2=.20 and q=-3.24. The fitted curves have been scaled to the photoabsorption curve[30] (solid) at 72 eV. The convoluted and deconvoluted fits are shown, where a Gaussian of width 0.20 eV (FWHM) was used for the monochromator bandpass in the deconvoluted fit. The natural linewidth of the resonance was taken from photoabsorption data[30] which is confirmed by theory[57] as Γ=0.10 eV.

Fig. 12 Individual relative cross sections for resonant decay to the n=2 states ^3S (top), ^1S + ^3P (middle), and ^1P (bottom). The solid curves in the top and middle panels are fits to the data using the Fano formula with a width of 0.10 eV convoluted with a Gaussian of 0.20 eV FWHM (monochromator bandpass). The resulting Fano parameters are shown in Table V. For the ^1P profile (bottom), the data were fit to a Lorentzian (0.10 eV FWHM) convoluted with a Gaussian (0.20 eV FWHM).

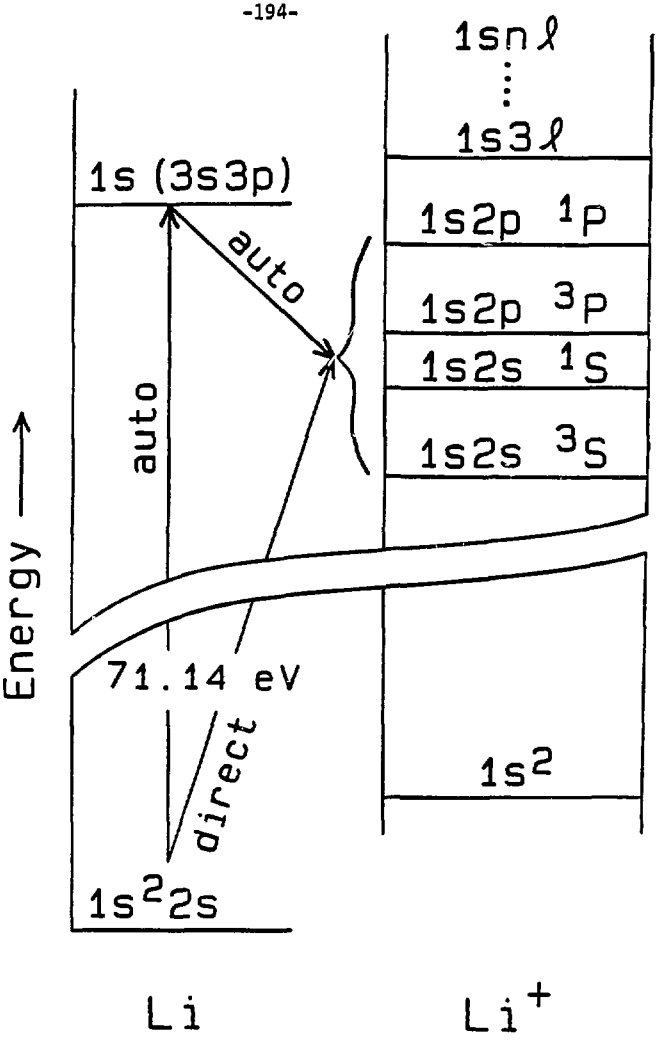

Figure 1

XBL 8611-4237

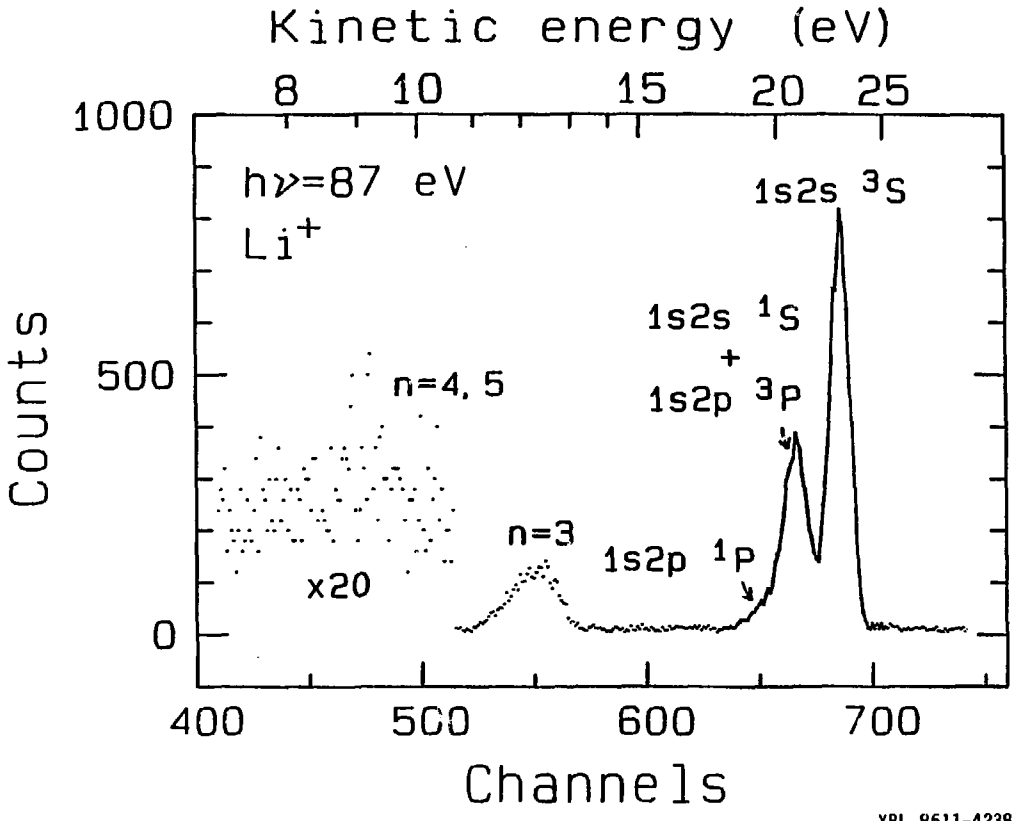

XBL 8611-4238

Figure 2

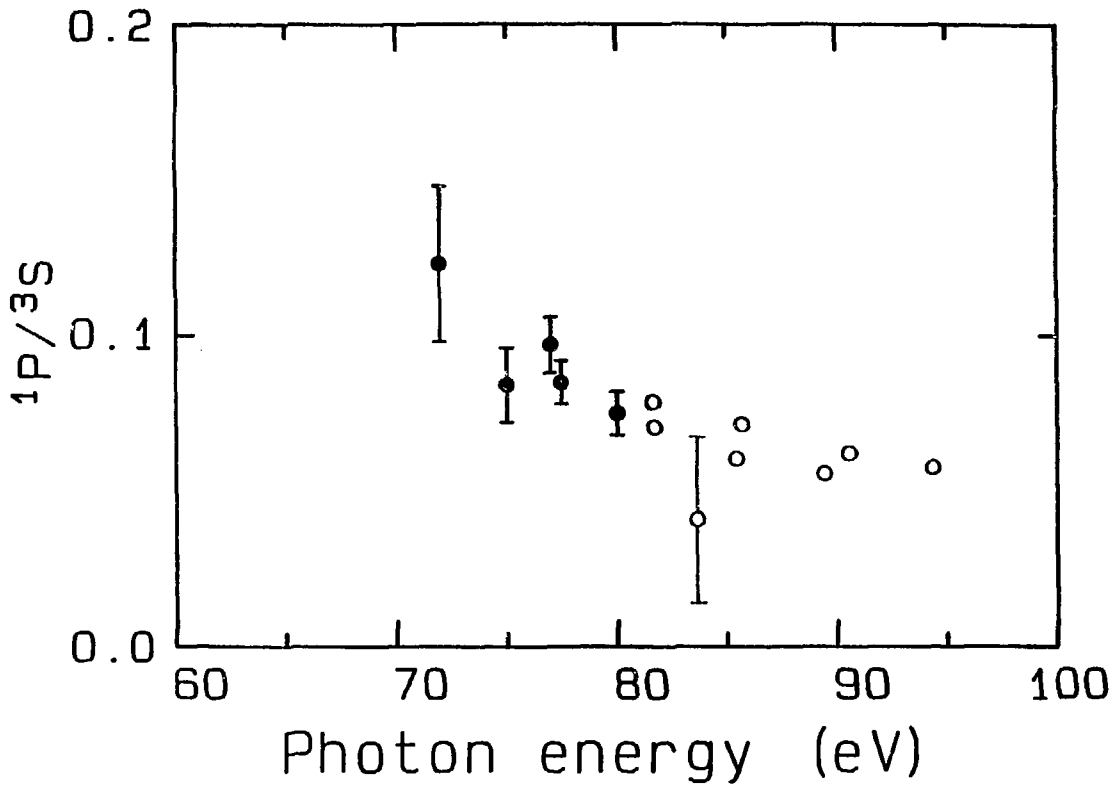

XBL 8611-4236

Figure 3

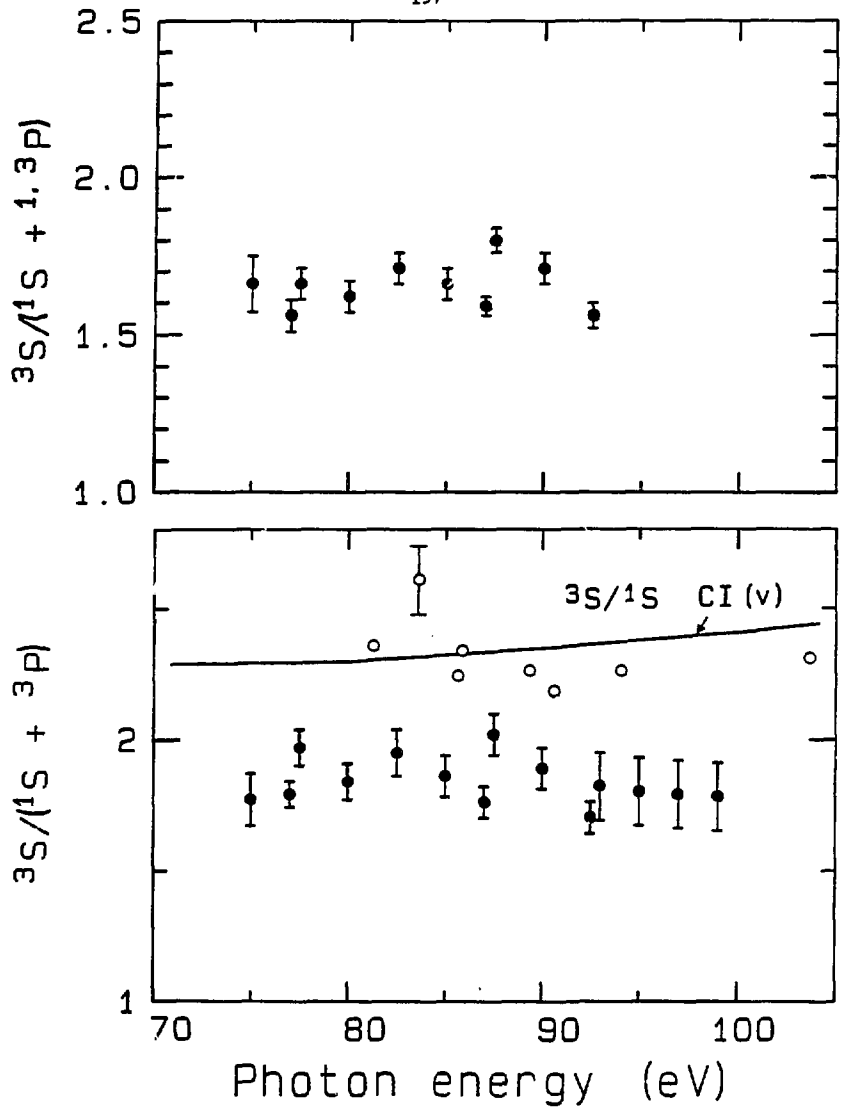

XBL B611-4234

Figure 4

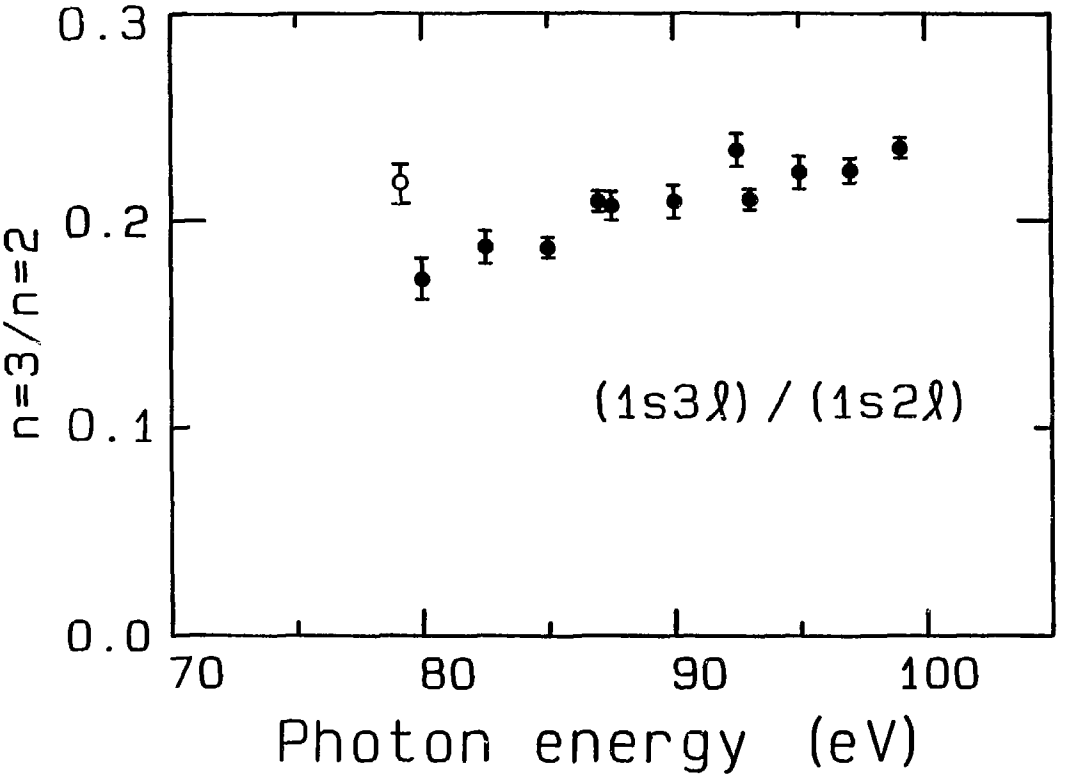

Figure 5

XBL 8611-4235

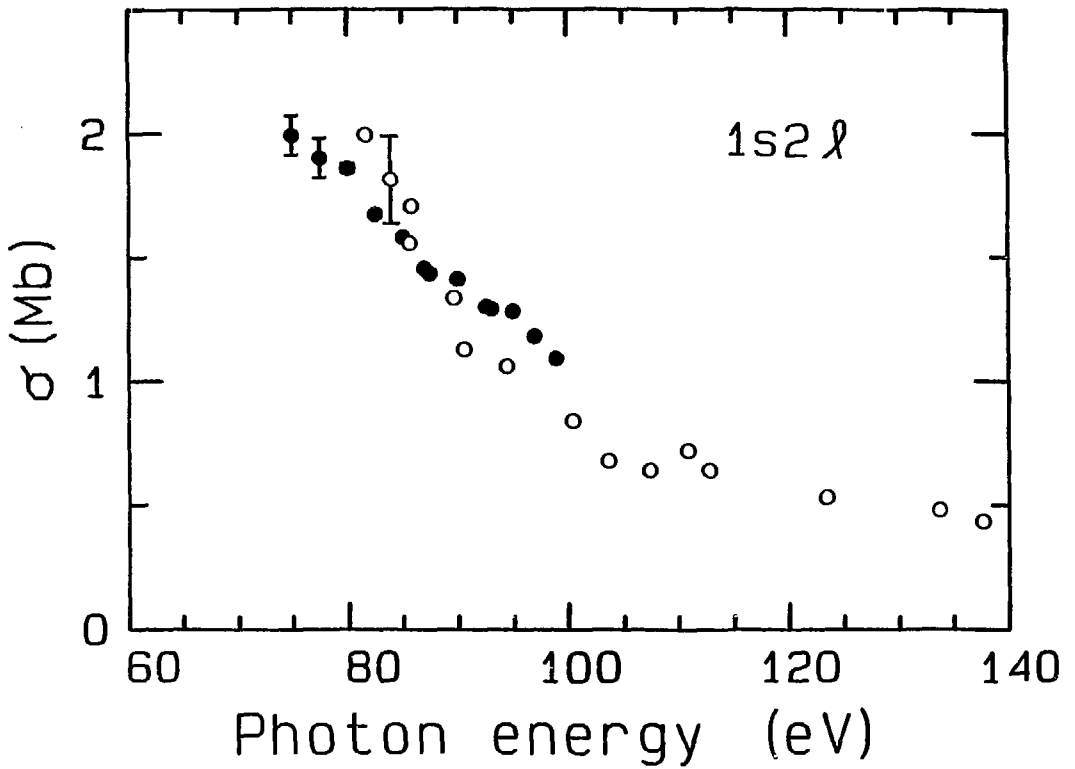

XBL 8611-4233

Figure 6

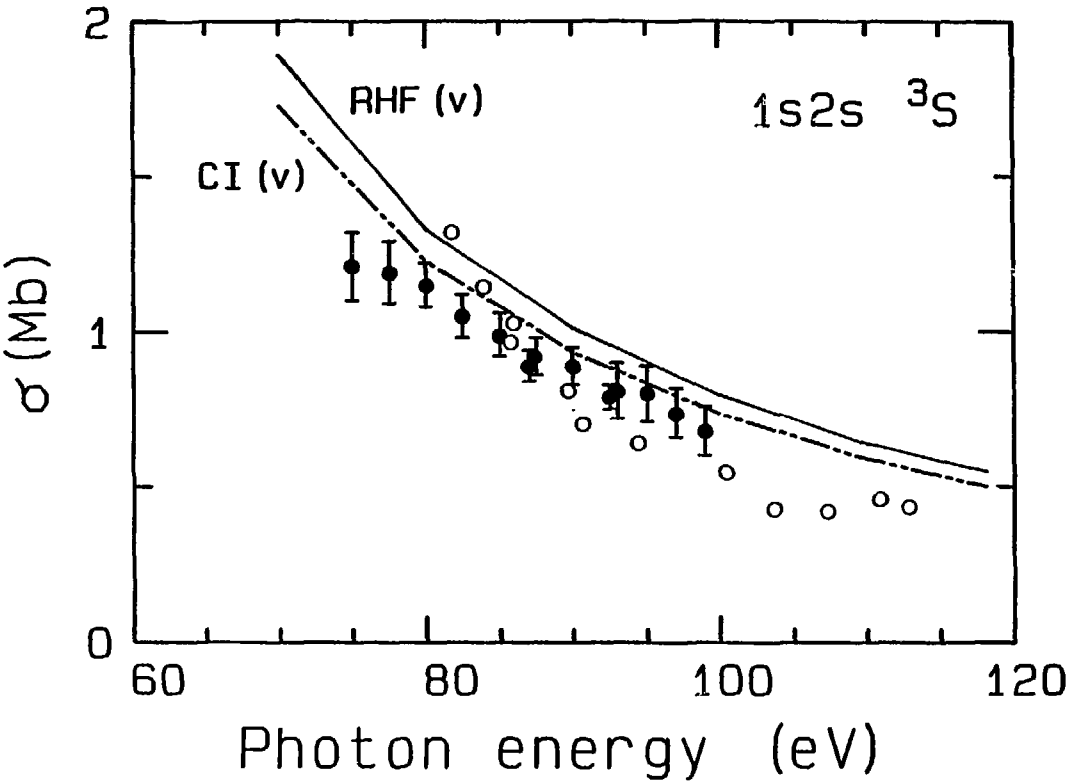

Figure 7

XBL 8611-4232

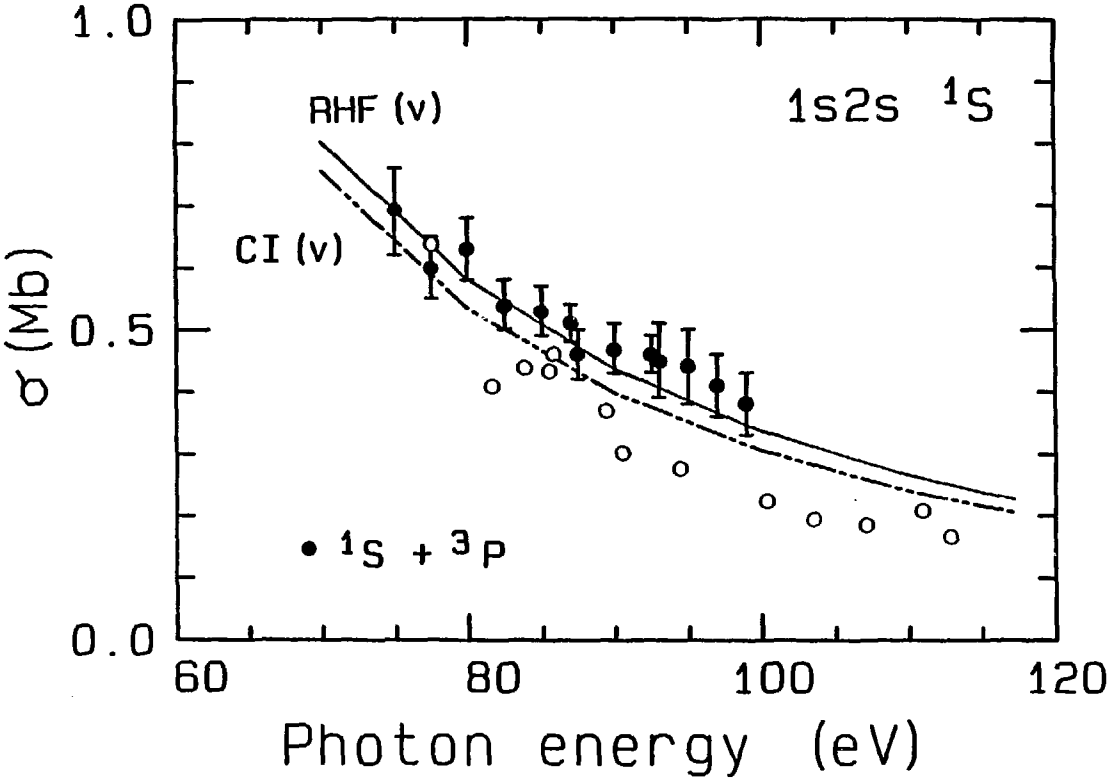

Figure 8

XBL 8611-4231

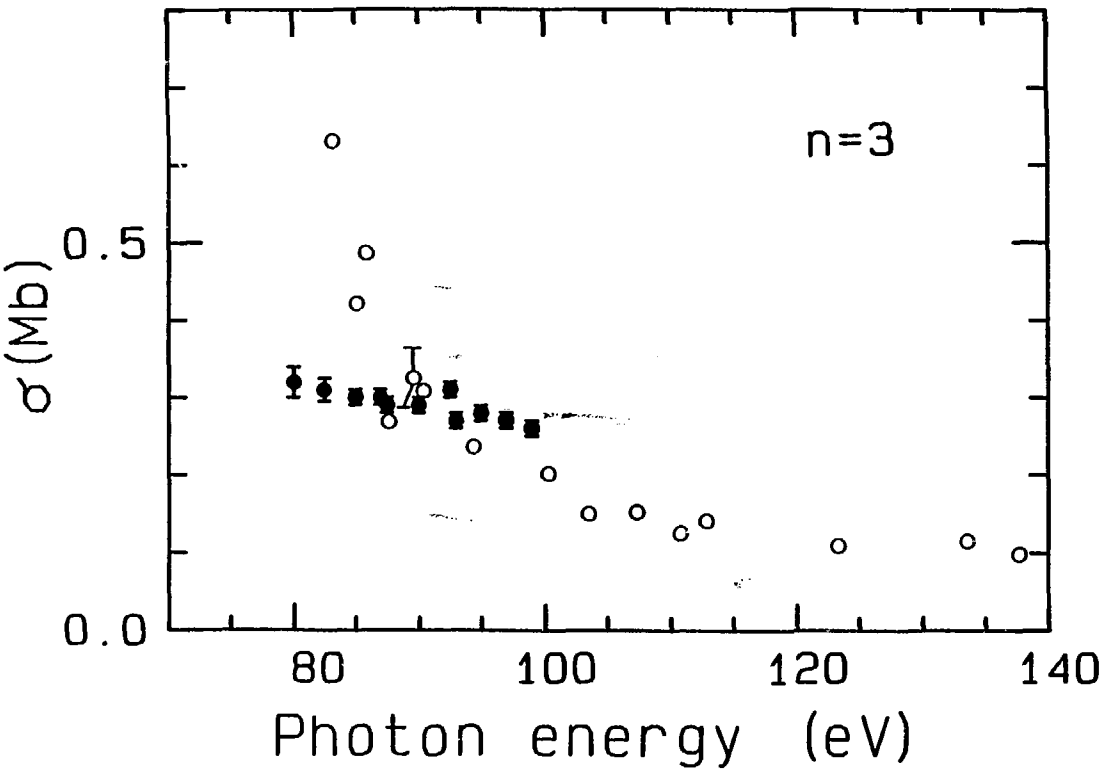

Figure 9

XBL 8611-4230

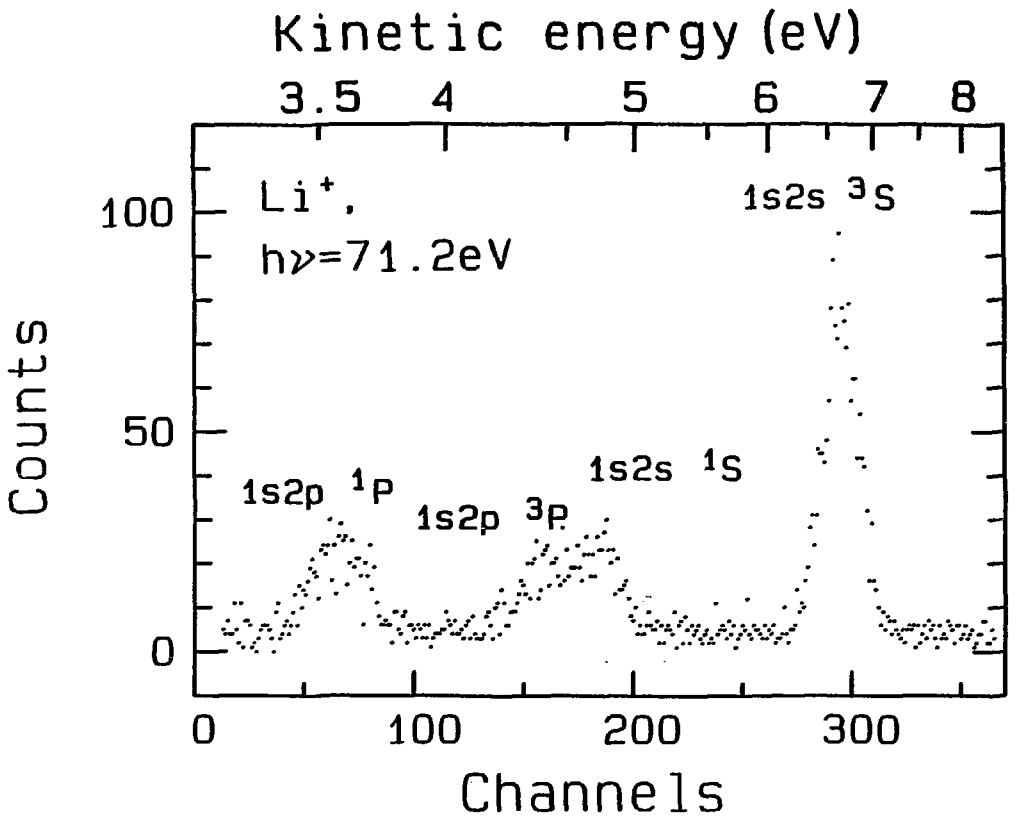

Figure 10

XBL 8611-4229

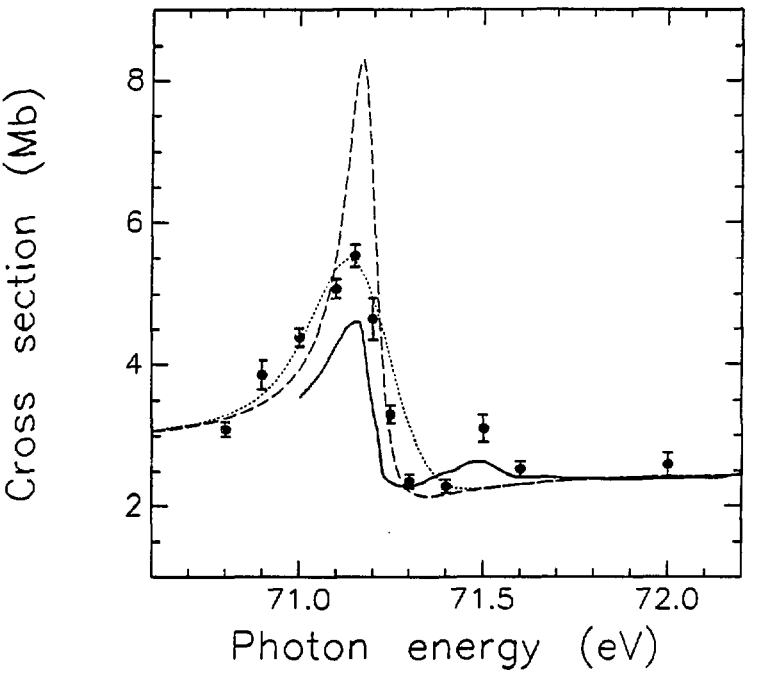

XBL 8611-4228

Figure 11

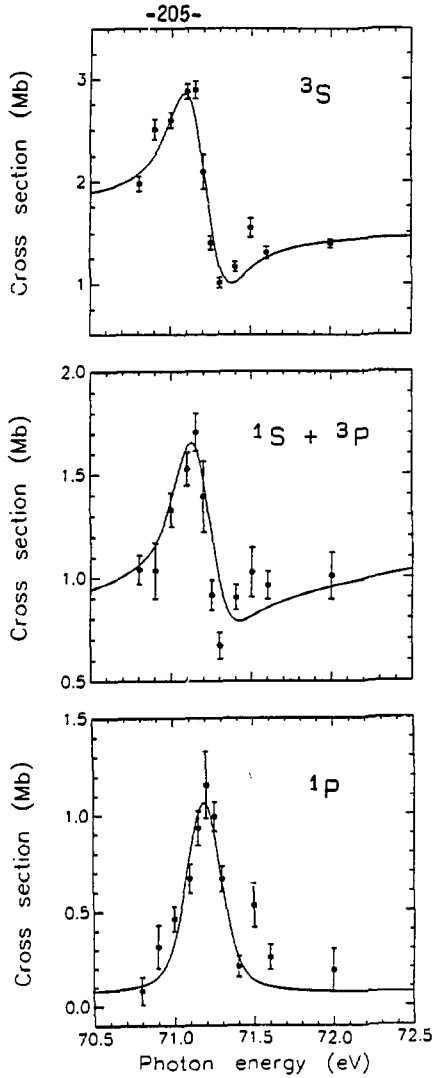

XBL 8611-4227

Figure 12

VII. Si 2p and 2s Resonant Excitation and Photoionization in SiF_4 *

Abstract

We present partial photoionization cross-section results for Si 2p and valence ionization from SiF_4 in the vicinity of the Si 2p and 2s thresholds. The continuum shape resonances decay only to the Si 2p main line, confirming one-electron predictions. The Si LVV Auger spectrum was also measured, and we propose new assignments for the final states. For the Si 2p discrete excitations, results at the $\sigma^*(a_1)$ resonance help quantify the relative enhancement of satellites and main lines, and point to the dominance of spectator decay. Spectra obtained at several higher-energy Si 2p and Si 2s excitations also generally support spectator decay as an important mode of relaxation for these discrete states.

A. Introduction

The core-level absorption spectra of a series of S- and Si-containing molecules have been interpreted using a potential-barrier model to explain intense transitions to unoccupied molecular orbitals.[1-4] A centrifugal barrier can trap an outgoing photoelectron, which then tunnels through the barrier and emerges in the continuum with enhanced intensity.[5] In particular, the excitation spectra of the series including SO_2, SiF_4, and SF_6 illustrate that the continuum resonances are more pronounced for molecules of high symmetry which contain electronegative ligands; these factors tend to enhance the barrier both directionally and in terms of repulsion from electronegative atoms. The narrowest and most intense resonances are found above the S 2p subshell threshold of SF_6, whereas the SO_2 absorption spectrum exhibits much broader and weaker continuum features.[6,7] Furthermore, photoemission experiments on the S 2p "main-line" ionization of SF_6 demonstrate that the e_g shape resonance exhibits strong electron-correlation effects through coupling to a neighboring S 2p shakeup satellite.[8] For the discrete portions of these spectra, SF_6 and SO_2 also show two extreme forms of behavior. The SF_6 oscillator strength appears primarily in excitations to molecular orbitals, while both molecular-orbital and Rydberg transitions dominate the spectrum of SO_2 below the S 2p edge.

Between these two extremes falls the intermediate case of

SiF_4,[7,9] where there are two continuum shape resonances above the Si 2p edge, first proposed to be of e and t_2 symmetry,[2] in addition to a number of discrete excitations (see Fig. 1). The shape resonances have been studied both experimentally[10] and theoretically[10,11] in the valence ionization of SiF_4, where a number of resonances of a_1, e, and t_2 symmetry are present. For core ionization, the Si 2p asymmetry parameter (β) has been measured previously,[12] and some partial cross-section results were reported recently for the Si 2p level.[13]

We present here further photoelectron spectroscopic measurements of the Si 2p and valence ionization cross sections in the vicinity of the continuum resonances of SiF_4. The Si LVV Auger spectrum was also taken, and the kinetic energies and relative intensities compare well with those of Aksela et al.[14] We propose a new assignment (different from that of Rye and Houston[15]) for the Auger final states which accounts for variations in hole-hole interactions for the various configurations.

The discrete portion of the Si 2p absorption spectrum was initially explained solely by Rydberg transitions.[16] Later assignments,[9,17] supported by the analogous experiment on solid SiF_4, postulated overlapping molecular-orbital and Rydberg excitations. Finally, absorption experiments on Si 1s ionization of SiF_4 suggest that distortion of the excited state to a trigonal bipyramid may be necessary to explain the complexity of all the core-level discrete spectra.[18] We have studied the decay channels

of the Si 2p and 2s excitations, and in some cases have qualitatively assigned the resonant spectra by comparison to the Si LVV Auger spectrum.

The experimental details are presented in Sec. B. Section C includes the Si 2p continuum results and the Si LVV Auger spectrum and assignment. We present the discrete resonant results for Si 2p excitation in Sec. D, and for Si 2s excitation in Sec. E. Conclusions appear in Sec. F.

B. Experimental

The experiment was performed at the Stanford Synchrotron Radiation Laboratory (SSRL) on the Beam line III-1 "grassnopper" monochromator using a 1200 l/mm holographically ruled grating. The experimental apparatus and methods have been described previously.[19-21] Briefly, a time-of-flight (TOF) electron analyzer situated at the "magic angle" of 54.7° relative to the photon polarization direction allows measurement of angle-independent partial cross sections, based on Yang's theorem.[22] The analyzer transmission as a function of kinetic energy was calibrated with the known partial cross sections for the $Ne^+(2s)$ and $Ne^+(2p)$ states.[23]

A 1000-Å-thick silicon window separated the monochromator (10^{-10} torr) from the gas chamber (10^{-5} torr). The gas pressure was monitored behind the effusive nozzle with a capacitance

manometer. The relative photon flux was calibrated by detecting fluorescence from sodium salicylate with a phototube (RCA 8850). Corrections for the varying response of sodium salicylate with photon energy have been applied to the partial cross-section results.[24] Statistical errors only are shown in our plots. We estimate that systematic errors for the nonresonant cross sections are ±10 percent, and for the resonant results ±3 percent.

The monochromator bandpass for the Si 2p and Si 2s continua studies varied from 0.65 to 1.40 eV FWHM (a constant 0.66 Å) over the photon energy range 110-165 eV. For the resonances below the Si 2p threshold, a bandpass of 0.25 eV (0.26 Å) was used. Energy calibration to within 0.20 eV was obtained over the range of the experiment from the resonance positions in the SiF_4 photoabsorption spectrum.[9]

C. The Si 2p Continuum

In Sec. 1 we present the partial cross sections for the inner- and outer-valence peaks and for the Si 2p main line in the photon energy range 114-165 eV, where two intense continuum resonances are present.[2,3,9] These results are compared with other experimental measurements[13] and with MS Xα theory[2,3,13] in an attempt to identify the symmetry of the shape resonances. We present the Si $L_{2,3}VV$ Auger spectrum in Sec. 2. A previous interpretation and assignment[15] of the Auger peaks is discussed with respect to hole

localization, and a new interpretation is proposed involving hole-hole interactions.

1. Partial Cross Sections

A TOF spectrum in Fig. 2 illustrates the unresolved outer- and inner-valence groups, the Si $L_{2,3}VV$ Auger peaks, and the Si 2p main line. To investigate the intensity variations over the shape resonances at 117 and 133 eV photon energy observed in photoabsorption,[2,3,9] we have measured the relative partial cross sections for valence and Si 2p ionization. Figure 3 shows these data.

We compare our Si 2p results to those of Bancroft et al.[13] in the top panel of Fig. 3, where our relative cross sections have been scaled at hν=138 eV. When the data are scaled in this manner for agreement at the second resonance, there is significant disagreement below hν=120 eV where the increase is more pronounced in our data. We have no explanation for the difference between the data sets. Bancroft et al.[13] noted that their Si 2p results at this resonance were lower than the photoabsorption curves[2,3,9] would indicate, and ascribed the difference to possible contributions from shakeup, shakeoff, and photodissociation. Because our results are more in line with the intensities in photoabsorption, we believe that other processes as mentioned above are probably not any more significant in this energy region than at the second resonance.

For the valence ionization cross sections (Fig. 3, bottom), there

is no evidence of enhancement at either continuum resonance, in agreement with the observations of Bancroft et al.[13] Our inner-valence cross section agrees well with other reported values,[13] and is systematically lower than MS Xα calculations[13] by about a factor of two. There are no experimental or theoretical results for comparison to our outer-valence results in this energy range.

The lack of valence enhancement at the Si 2p continuum resonances can be compared to the same result for the S 2p ionization in SF_6.[8] However, for SF_6 a S 2p satellite was found to be resonant at the second continuum resonance (e_g), suggesting that a many-electron treatment of this e_g shape resonance is necessary. For SiF_4, we see no Si 2p satellite enhancement at either continuum resonance. Thus, the qualitative behavior of the Si 2p shape resonances is well modeled by a one-electron description,[1,5] with decay only to the Si 2p main line.

The assignment of the Si 2p shape resonances in SiF_4 has been discussed by several workers. There is uniform agreement that the resonance at ~22 eV kinetic energy ($h\nu$=133 eV) is of t_2 symmetry. This is supported by early MS Xα theory[2,3] and more recent calculations by Bancroft et al.[13] Furthermore, this resonance is seen in experiment and theory for several valence levels of SiF_4.[10] However, the symmetry of the resonance at ~5 eV kinetic energy ($h\nu$=117 eV) is much less definite. Early MS Xα calculations found resonances of e symmetry at ~4-6 eV and 13-15 eV,[2,3] whereas

later results[13] found an e resonance at 14 eV, an a_1 resonance at 3.3 eV, and a weak t_2 feature at 6.8 eV kinetic energy. Bancroft et al.[13] eventually assigned the intense 5 eV resonance as t_2 despite the very weak presence of this feature in theory. This is in disagreement with the earlier calculations mentioned above which suggest an assignment of e symmetry.[2,3] Bancroft et al.[13] have also used experimental and theoretical results on $SiCl_4$ (where the agreement is less ambiguous)[2,25] in analogy to support the t_2 assignment for the 5 eV resonance. We note that part of this explanation involved assignment of a resonance of e symmetry in SiF_4 (as found in theory in moderate intensity[13]) at about 10 eV kinetic energy. A very small shoulder at this energy is evident in one photoabsorption spectrum,[2] but not in a later measurement.[9] We do not discern a resonance in our data near 1.

Because of the lack of agreement among various theoretical calculations, we believe it is not possible at this time to identify the 5 eV resonance ($h\nu$=117 eV) definitely as having either e or t_2 symmetry. It is unlikely that further experimental results alone will help to clarify this situation. Theory, which has produced widely varying results for SiF_4, is clearly sensitive to the details of the calculations. This model-dependent sensitivity needs to be eliminated before the theory can be used with a reasonable degree of reliability.

2. Si LVV Auger Spectrum

Rye and Houston[15] reported the first Si $L_{2,3}VV$ Auger spectrum for SiF_4, obtained with electron-beam impact. Scattered electrons created a steeply sloping background so that the observed Auger intensities were mostly qualitative. More recently, Aksela et al.[14] have taken the Auger spectrum using synchrotron radiation. We will compare our quantitative results to those of Aksela et al.[14] and discuss the peak assignments originally proposed by Rye and Houston.[15]

Our Auger spectrum is plotted in the top of Fig. 4 as a function of kinetic energy. Peak labels a through f follow the notation of Aksela et al.[14] and are reversed from the notation of Rye and Houston.[15] In Table II we include the peak kinetic energies and relative intensities compared with those of Aksela et al.[14] The kinetic energies are in agreement within error limits, and the relative intensities are quite similar. There is a small discrepancy for peaks d and e. We find peak d to be slightly more intense than peak e; the reverse is true for the data of Aksela et al.[14]

We now discuss the interpretation of the Si LVV Auger spectrum. The assignment of the Auger peaks proposed by Rye and Houston[15] involves first an assumption that only valence orbitals with appreciable Si character will participate in the decay. This rules out the outermost three orbitals ($1t_1$, $5t_2$, and $1e$) which are essentially F lone pairs. In this approach, the remaining valence

orbitals ($4t_2$, $5a_1$, $3t_2$, and $4a_1$) combine to give the following generic Auger final states in terms of outer- and inner-valence holes (see Table I):

$$(\text{outer})^{-2}$$
$$(\text{inner})^{-1}(\text{outer})^{-1}$$
$$(\text{inner})^{-2}$$

With a constant hole-hole repulsion energy assumed for all final states and the observation that the inner- and outer-valence binding energies within each group are closely spaced (within 2-5 eV), this provides for three distinct groups of peaks in the Auger spectrum, whereas six peaks are observed. Rye and Houston explained this apparent "doubling" by postulating that the two valence holes in a single configurational final state appear spatially in the same Si-F bond or in different bonds.[15] This picture was further supported by the observation that the bonding orbitals involved are strongly polarized toward the F atoms, and a calculation of the Coulomb interaction integral (U) was made to estimate the energy separation for the two branches of the spectrum.

We believe that this approach may overemphasize the idea of hole localization. In our view, each of the two-hole final states may be better described by coupling two one-hole states, which are in turn given by molecular orbitals. This model has the advantage that the molecular orbitals transform as the symmetry group of the molecule,

and thus at least simulate eigenstates of the SiF_4^+ Hamiltonian. In coupling the two one-hole states, due account must of course be taken of hole-hole repulsion as well as of electron polarization toward the holes. Like Rye and Houston,[15] we assume that SiF_4^+ and SiF_4^{++} remain essentially intact during the photoionization and Auger processes. To first order, we start with the same three peak groupings above, as per Rye and Houston:[15]

$$(\text{outer})^{-2}\text{: } (4t_2)^{-2},\ (5a_1)^{-2},\ (4t_2)^{-1}(5a_1)^{-1}$$

$$(\text{outer})^{-1}(\text{inner})^{-1}\text{: } (4t_2)^{-1}(3t_2)^{-1},\ (4t_2)^{-1}(4a_1)^{-1},\ (5a_1)^{-1}(3t_2)^{-1},\ (5a_1)^{-1}(4a_1)^{-1}$$

$$(\text{inner})^{-2}\text{: } (3t_2)^{-2},\ (4a_1)^{-2},\ (4a_1)^{-1}(3t_2)^{-1}$$

We propose that the energies of individual configurations are shifted by different amounts depending on the hole-hole interactions. For example, the state $(5a_1)^{-2}$ will be shifted to a different extent relative to the shift for the $(5a_1)^{-1}(4t_2)^{-1}$ state. Holes of the same symmetry will generally repel each other more than holes of different symmetry. Likewise, two holes in the same orbital will tend to repel each other more than holes in different orbitals. This approach will in principle introduce more complexity into the Auger spectrum, explaining the six peaks without invoking localization in spatially distinct bonds. Detailed calculations which include the

hole-hole interactions as described above are needed to support our interpretation.

D. Discrete Resonances Below the Si 2p Threshold

Figure 1 (bottom) illustrates the discrete resonances below the Si 2p edge, including a particular assignment based on the overlap of molecular orbital and Rydberg excitations.[9] We have studied the decay channels to SiF_4^+ in detail in the vicinity of the resonances at 106.1 and 106.7 eV, assigned as the molecular orbital excitations Si $2p_{3/2,1/2} \rightarrow \sigma^*(a_1)$. Using the Si LVV Auger spectrum for comparison, in Sec. 1 we interpret the resonant photoemission spectra and present partial cross sections for the valence main lines and some of the resonant satellites. We discuss the qualitative aspects of the decay at the different resonances in Sec. 2, where we present a few spectra taken in the vicinity of the higher resonances in the range $h\nu$=108-112 eV.

1. The Si $2p \rightarrow \sigma^*(a_1)$ Resonance

In Fig. 4 we show a nonresonant photoelectron spectrum at $h\nu$=103.9 eV which includes the unresolved inner-valence main lines ($3t_2$ and $4a_1$) and some valence satellites at ~30 eV binding energy. The inner-valence peak shows some intensity on the high binding-energy side, also observed by Aksela et al.[14]

On resonance at $h\nu$=106.7 eV, we see enhancement of a number of valence satellites (Fig. 4). The spectra, as plotted, are uncorrected for analyzer transmission, which decreases by a factor of two from right to left over the energy range of the bottom two spectra in Fig. 4. The partial cross sections reported in the next section have been corrected for transmission.

To aid in interpretation of the resonant spectra, we have aligned the Si LVV Auger spectrum, excited above the Si 2p threshold at $h\nu$=117.2 eV, with the $h\nu$=106.5 eV resonance spectrum in Fig. 4 for comparison. Though the intensities are somewhat different, the same peak pattern appears in both spectra. Table III lists the binding energies of the enhanced satellites and relates each satellite to the corresponding Auger peak. There is a one-to-one correspondence to the Auger peaks a through f with the minor exception of peak e, where the resonance spectrum shows only a single broad peak. This similarity is consistent with each peak in the resonance spectrum arising from a two-hole state (plus an excited electron). From Fig. 4, some of the two-hole states are nearly degenerate with the single-hole inner-valence main lines ($3t_2$, $4a_1$) in SiF_4^+. This near degeneracy makes a straightforward distinction between inner-valence main-line and satellite decay difficult, and indicates that configurational mixing is probably important in the inner-valence region. The spectrum of Aksela et al.[14] agree with ours, except that they did not observe the highest binding energy satellite [74(1) eV] corresponding to peak a in the Auger spectrum.

We comment briefly on the kinetic-energy shift between the resonant spectrum and the Si LVV Auger spectrum. To first order, this shift might be expected to be equal to the difference between the resonance energy and the corresponding 2p continuum, which is 5.5 eV. This is based on the simple picture that each resonance state a'-f' is made up of the corresponding Auger final state a-f, plus one electron in the resonant $\sigma^*(a_1)$ orbital. The observed shift in our spectra varies from 8-10 eV for peaks a'-f', slightly higher than the average shift of 7.5(5) eV reported by Aksela et al.[14] However, energy shifts from both sets of data contain variations from peak to peak and uncertainties of ±1 eV in the absolute shift. The increased shift of 8-10 eV is easily understood as follows. The 5.5 eV shift between the $2p^{-1}\sigma^*(a_1)$ state is just the binding energy of an electron in the $\sigma^*(a_1)$ orbital, starting from the $SiF_4[2p^{-1}\sigma^*(a_1)]$ initial state:

$$SiF_4[2p^{-1}\sigma^*(a_1)] \longrightarrow SiF_4^+(2p^{-1}) + e^-(\text{B.E.}=5.5\ \text{eV}). \qquad (1)$$

For the analogous process of removing an electron from the excited $\sigma^*(a_1)$ orbital in the a' state of SiF_4^+,

$$SiF_4^+[a';(\text{inner})^{-2}\sigma^*(a_1)] \longrightarrow SiF_4^{++}[a;(\text{inner})^{-2}] + e^-(\text{B.E.}\sim 8\ \text{eV}), \qquad (2)$$

the shift is naturally larger because of the attraction between the additional (positive) valence holes and the excited $\sigma^*(a_1)$

electron.

The above comparison with the Auger spectrum indicates that much of the resonant-state decay proceeds like the Si LVV Auger decay; the excited electron $\sigma^*(a_1)$ remains as a spectator while one valence electron fills the Si 2p hole and another leaves. The final states have the same two valence holes as the Auger spectrum plus the initially excited electron $[\sigma^*(a_1)]$. We note that the resonances below the Si 2p threshold in SiH_4 also decay to a number of spectator satellites, in analogy to the two-hole states in the Auger spectrum.[26]

We emphasize the qualitative and incomplete nature of this result for predominant spectator decay. It is probable that the excited electron gets "shaken up" to a higher unoccupied orbital in a substantial fraction of the decays, in analogy to atomic Xe 4d-->6p,7p resonant decay, where shakeup to the next higher np level is significant.[27] The energy separation of a spectator and a shakeup satellite configuration of SiF_4^+ would differ by as little as 2 eV for the $\sigma^*(a_1)$ resonance, making an exact orbital assignment for the excited electron difficult. However, the overall similarity between the Auger and resonant spectrum does appear to implicate spectator decay as an important decay mode.

To help quantify the extent of satellite decay, partial cross sections for the outer-valence main lines and for peaks e' and f' are shown in Fig. 5. For the summed outer-valence main lines we see a small enhancement of ~10 percent at resonance. This is slightly

larger than the upper limit of 5 percent reported by Aksela et al.[14] Production of these main lines is a measure of the degree of participation of the excited electron in the resonant decay. For the inner-valence region, low count rates and limited resolution prohibited reliable partial cross-section measurements on each satellite peak listed in Table III. However, peaks e' and f' were sufficiently resolved, and their cross sections are also shown in Fig. 5. All the profiles mimic tne total photoabsorption profile, indicating either very little interference between the direct ionization and autoionization via the excited state, or that peaks e' and f' actually contain different final states on and off resonance.

We now estimate the overall relative amounts of satellite versus main-line decay. Though we do not have quantitative results for satellites a'-d', we do observe that their relative intensities on resonance are roughly comparable to the analogous intensities in the Auger spectrum. Using this result, we find that the ratio of the summed intensity in satellites a'-d' relative to satellite f' is (from Table II):

$$(a' + b' + c' + d')/f' \sim 1.3(1) \qquad (3)$$

where the uncertainty reflects the differences between our results and those of Aksela et al.[14] This gives an intensity on the scale of Fig. 5 of 0.65(5) for the sum of peaks a'-d'.

The remaining uncertainty in this estimate of satellite versus

main-line decay is related to the possible presence of a satellite in peak e' in addition to the inner-valence main lines. If the resonant satellite spectrum carries relative intensities about equal to those in the Auger spectrum, then all of the enhancement in peak e' can be ascribed to a satellite, with very little effect on the main lines. This assumption would suggest that ~80 percent of the $\sigma^*(a_1)$ resonant decay results in satellite production. A lower limit of 60 percent derives from the assumption of only main-line enhancement in peak e'.

This range of 60-80 percent for satellite decay may also indicate roughly the amount of spectator decay if the excited electron remains in the $\sigma^*(a_1)$ orbital. We have already mentioned the possibility of shakeup to a higher orbital which can still result in a satellite final state. Higher spectral resolution and detailed calculations would be required to differentiate between the spectator satellites and satellites involving shakeup to a higher level.

2. Higher Resonances- Qualitative Results

For the higher-energy resonances, we show two spectra in Fig. 6, corresponding to $h\nu$=108.8 and 110.6 eV. These spectra were taken with a bandpass of 0.25 eV in an attempt to resolve the assigned $\sigma^*(t_2)$ molecular orbital excitation from the Rydberg excitations (see Fig. 1).

As with the $\sigma^*(a_1)$ resonance, the outer valence orbitals show no dramatic enhancement at the higher resonances. Figure 6 shows the

inner-valence region only up to ~50 eV binding energy, above which the peak intensities are extremely low. Aksela et al.[14] have obtained comparable spectra at $h\nu$=109 and 111 eV extending out to 75 eV binding energy.

For our 108.8 ev spectrum, we see enhancement of the inner-valence main-line peak, and a satellite peak appears to lower binding energy [37(1) eV]. This satellite peak corresponds to peak F" in the Aksela et al.[14] spectrum and possibly to peak f in the Auger spectrum. The satellite configuration would contain two valence holes (as in the Auger spectrum) and an excited $\sigma^*(t_2)$ electron.

For our spectrum at $h\nu$=110.6 eV in the vicinity of the 3d, 4d, and 5s Rydberg states, we observe enhancement of the inner-valence peak at 40 eV binding energy, and a satellite peak appears at 44(1) eV binding energy. This satellite is labelled as S_1 in the Aksela et al.[14] spectrum, with no clear correspondence to a peak in the Auger spectrum.

The more extended energy-range results of Aksela et al.[14] suggest that the spectra at these higher resonances generally resemble the Auger spectrum, but with a few additional peaks. For example, the peaks labelled S_1 (binding energy ~44 eV) and $S_{2,3}$ (binding energy ~35 eV) appear in spectra at $h\nu$=109 and 111 eV in addition to the inner-valence main lines and peaks c through f.[14] Overall, their interpretation is that at each resonance, a spectator satellite spectrum results, shifted from the Auger spectrum.[14] We agree, but believe that these additonal peaks add a complication that is not yet

clearly understood.

Dirac-Fock calculations[14] on atomic Si confirm the positions of the Rydberg states in SiF_4 in agreement with a recent assignment[9] but contrary to an earlier interpretation which assigned all the features as Rydberg excitations.[16] One particularly convincing argument for the overlapping molecular-orbital (MO) and Rydberg assignment of Friedrich et al.[9] is the apparent quenching of the Rydberg excitations in the solid SiF_4 spectrum. Very recently, photoemission work on Si 1s excitation and ionization in SiF_4 suggests that a third model involving distortion of the tetrahedral geometry to a trigonal bipyramid (TBP) leads to yet another interpretation of this absorption spectrum.[18] With the symmetry change in the excited state (due to the static Jahn-Teller effect[28]), the dipole selection rules are altered. These authors find the assumption of C_{2v} symmetry to be consistent with three dipole-allowed transitions to a_1^*, b_1^*, and b_2^* orbitals, which can explain the resonances between hν-108-112 eV.[18] The assignment of $\sigma^*(a_1)$ for the 106 eV resonances is retained. With this distorted excited state, the SiF_4 solid results of Friedrich et al.[9] are explained by a C_{3v} geometry, in contrast to a C_{2v} geometry in the gas phase.

Based on our results, we find support for predominant decay to spectator satellites, which could be consistent with either interpretation mentioned above (overlapping MO and Rydberg[9] vs. distorted excited state geometry[18]). The original MO and Rydberg

model[9] explains the solid photoabsorption spectrum and is a natural extension of trends seen in the spectra of other Si- and S-containing molecules. There are clearly understood examples where either MO or Rydberg transitions dominate the absorption spectrum (as with SF_6 and SO_2, respectively[1]). It is thus plausible to view SiF_4 as an intermediate case, with comparable intensity in both localized (MO) and diffuse (Rydberg) states.

However, there remains the serious problem of explaining the two intense resonances 5.7 and 4.3 eV below the Si 1s edge in SiF_4.[18] Calculations on the distorted C_{2v} and C_{3v} excited states could indicate whether the energies of the proposed Si 2p and 1s excitations agree with the observed values.

E. The Si 2s Excitations

The total cross section (Fig. 1) shows a single broad feature near 160 eV related to discrete excitations of the Si 2s electron. To interpret the specific transitions involved, we can make use of the Si 1s excitation spectrum,[18] because both Si 1s and 2s initial states are of a_1 symmetry. As noted in the previous section, the Si 1s discrete spectrum is not consistent with the expected dipole allowed transition to a t_2^* orbital, but rather shows two strong resonances. Bodeur et al.[18] have explained both the Si 1s and 2s spectra by invoking an excited state geometry change in SiF_4 to a trigonal bipyramid (TBP). These authors believe that the doublet seen

below the Si 1s edge corresponds to excitation into axial and equatorial orbitals of the TBP geometry. By analogy, a doublet for the Si 2s resonant feature near 160 eV could be broadened to the observed single peak by a Coster-Kronig decay step ($L_1L_{2,3}V$ type).

We have studied the resonant decay channels in the vicinity of these Si 2s excitations. Our cross-section results in Fig. 3 show no measurable resonant effect in either the Si 2p or valence main lines near 160 eV. We note that Auger peak d overlaps in this energy region with the Si 2p main line. This Auger intensity was subtracted as a correction to the Si 2p main-line cross section, although this increases the intensity error to ±10 percent.

The only other accessible decay channels (other than resonant shakeoff) are to Si 2p shakeup satellites. We show spectra taken near the peak of the Si 2s resonance (159.9 eV) and below the resonance (156.9 eV) in Fig. 7. These spectra qualitatively illustrate the enhancement of Si 2p satellites which overlap with part of the Si LVV Auger spectrum (peaks a and b). The binding energies of these satellites are ~130-140 eV, with an excitation energy relative to main-line ionization of 20-30 eV.

The branching ratio for these peaks (Auger peaks a and b plus satellites) relative to the Si 2p main line is presented in Fig. 8. The nonresonant value for this ratio is ~15 percent, in agreement with an expected 14 percent based on the relative intensities of peaks a and b in the Auger sepctrum (see Table II). Because the Si Auger intensity should track the Si 2p main-line intensity, a change in the

ratio in Fig. 8 indicates satellite enhancement only. The (satellite)/(Si 2p) intensity ratio on resonance is then 13(2) percent, which accounts for about half of the resonant intensity in the total photoabsorption curve (see Fig. 1). In addition to a possible small effect (within our ±10 percent error) in the Si 2p main line cross section, the remaining intensity could appear as decay to other satellites or shakeoff channels.

At least half of the decay of the excited state(s) thus occurs via an $L_1L_{2,3}V$ step producing an ion with a Si 2p core hole and a valence hole plus an electron likely to be in the initially excited orbital. This fast Coster-Kronig type decay helps to explain the width of the absorption feature. We have no experimental evidence to indicate the specific transition(s) taking place near $h\nu$=160 eV. The eventual assignment of the more easily distinguished Si 1s discrete transitions should help to clarify similar processes for Si 2s excitation.

F. Conclusions

For the Si 2p continuum of SiF_4, our photoemission results confirm photoabsorption measurements which detected two intense resonances at $h\nu$=117 and 133 eV. At the first resonance, our Si 2p partial cross section shows a pronounced effect consistent with photoabsorption but disagrees with a much smaller enhancement observed by Aksela et al.[13] No enhancement at either resonance was found for

the valence main lines or satellites, in contrast to a satellite resonant at the e_g shape resonance in the S 2p continuum of SF_6.[8] The one-electron model for describing shape resonances[1,5] thus qualitatively applies to these Si 2p resonances which decay only to the Si 2p main line.

We have reinterpreted the Si $L_{2,3}VV$ Auger spectrum invoking a variation in the extent of hole-hole interactions from one final-state configuration to another. We believe this model is preferable to the interpretation of Rye and Houston,[15] which assumes two valence holes localized in the same or different spatially distinct Si-F bonds.

For the discrete resonances below the Si 2p edge and in particular for the $\sigma^*(a_1)$ excitation, spectator decay to valence satellites is found to be a dominant decay mode. The satellite configurations thus parallel those for the Auger final states. In addition, configurational mixing of some of these satellites degenerate with the inner-valence main lines is probably important.

The overall assignment of the discrete resonances in SiF_4 is still in question, with the exception of the $\sigma^*(a_1)$ resonance. In light of new photoabsorption results on the Si 1s core-level ionization,[18] the possibility of a distorted excited state may change the point group symmetry and thus the classification of the molecular-orbital excitations. This interpretation, as applied to the Si 2p and 1s discrete resonant features does not include any appreciable intensity in Rydberg transitions, in contrast to the model of Friedrich et al.[9] Theoretical calculations are needed which

examine the role of the static Jahn-Teller effect for neutral molecules with a core hole and an excited electron. This would help sort out the relative contribution of molecular-orbital and Rydberg states below the core-level thresholds of SiF_4.

Table I: Binding energies of the pertinent molecular valence and core levels in SiF_4.

orbital	Binding energy (eV)
Outer valence:[a]	
$1t_1$	16.4
$5t_2$	17.5
1e	18.1
$4t_2$	19.5
$5a_1$	21.5
Inner valence:[b]	
$3t_2$	39.3
$4a_1$	40.6
Si 2p $(2t_2)$[c]	111.6
Si 2s $(3a_1)$[d]	163.6

a Ref. 29.
b Ref. 30.
c Ref. 13.
d Ref. 18

Table II: Si $L_{2,3}VV$ Auger Peak Energies and Relative Intensities for SiF_4.

Auger peak label (Ref. 14)	Kinetic energy(eV)		relative intensity (percent)		
	present	Ref. 14	present[a]	Ref. 14	
a	24.3(4)	23.7(5)	5.8	5.7	
b	30.8(3)	30.7(3)	8.7	7.0	
c	39.4(5)	39.6(3)	7.5	7.3	
d	45.3(8)	45.4(2)	25.0	21.7	
e_1	54.4(10)	55.2(3)	20.6	8.1	24.4
e_2	58.2(8)	58.7(3)		16.3	
f	66.1(5)	66.3(2)	32.5	33.9	

a Uncertainty is ±1 percent.

Table III: Valence Satellites Resonant at the Si(2p)-->$\sigma^*(a_1)$, $\sigma^*(t_2)$, and Rydberg Excitations in SiF_4.

Photon energy(eV)	resonance assignment (Ref. 9)	satellite binding energy(eV)	corresponding [a] Auger peak and kinetic energy(eV)
106.1	Si $2p_{3/2}$-->$\sigma^*(a_1)$	33(1)	f: 66.1
106.7	Si $2p_{1/2}$-->$\sigma^*(a_1)$	[40(1)][b]	e_1, e_2: 54.4, 58.2
		53(1)	d: 45.3
		57(1)	c: 39.4
		68(1)	b: 30.8
		74(1)	a: 24.3
108.8	Si $2p_{3/2}$-->$\sigma^*(t_2)$	37(1)	
110.6	Si 2p-->3d, 4d, 5s Rydberg	44(1)	

[a] A direct spectral comparison is made in Fig. 4. Peak energies from our results, Table I.

[b] Although this peak is approximately at the binding energy for the inner-valence main lines, comparison with peaks e_1 and e_2 in the Si $L_{2,3}VV$ Auger spectrum suggests the presence of a satellite state at this energy also. Mixing of these single-hole (main lines) and two-hole states (satellites) will complicate the peak assignments.

References

* Work done in collaboration with M.N. Piancastelli, D.W. Lindle, P.A. Heimann, and D.A. Shirley. We thank I. Nenner for preprints of References 18 and 27.

1. J.L. Dehmer, J. Chem. Phys. 56, 4496 (1972) and references therein.
2. A.A. Pavlychev, A.S. Vinogradov, T.M. Zimkina, D.E. Onopko, and S.A. Titov, Opt. Spec. 47, 40 (1979).
3. A.A. Pavlychev, A.S. Vinogradov, and T.M. Zimkina, Opt. Spec. 52, 139 (1982).
4. M.Ya. Amusya, A.A. Pavlychev, A.S. Vinogradov, D.E. Onopko, and S.A. Titov, Opt. Spec. 53, 91 (1982).
5. J.L. Dehmer in Resonances in Electron-Molecule Scattering, van der Waals Complexes, and Reactive Chemical Dynamics, edited by D.G. Truhlar (American Chemical Society, Washington, D.C., 1984); J.L. Dehmer, D. Dill, and A.C. Parr in Photophysics and Photochemistry in the Vacuum Ultraviolet, edited by S.P. McGlynn, G. Findley, and R. Huebner (Reidel, Dordrecht, Holland, 1985); J.L. Dehmer, A.C. Parr, and S.H. Southworth in Handbook on Synchrotron Radiation, Vol. II, edited by G.V. Marr (North Holland, Amsterdam, 1986).
6. T.M. Zimkina and V.A. Formichev, Sov. Phys. Dokl. 11, 726 (1967).
7. T.M. Zimkina and A.S. Vinogradov, J. Phys. (Paris) 32, C4-3 (1971).

8. T.A. Ferrett, D.W. Lindle, P.A. Heimann, M.N. Piancastelli, P.H. Kobrin, H.G. Kerkhoff, U. Becker, W.D. Brewer, and D.A. Shirley (unpublished results, see Chpt. IV).

9. H. Friedrich, B. Pittel, P. Rabe, W.H.E. Schwarz, and B. Sonntag, J. Phys. B 13, 25 (1980).

10. B.W. Yates, K.H. Tan, G.M. Bancroft, L.L. Coatsworth, and J.S. Tse, J. Chem. Phys. 83, 4906 (1985).

11. M.M. Gofman, V.A. Andreev, and V.I. Nefadov, J. Electron Spectrosc. 37, 375 (1986).

12. P.R. Keller, J.W. Taylor, F.A. Grimm, P. Senn, T.A. Carlson, and M.O. Krause, Chem. Phys. 74, 247 (1983).

13. G.M. Bancroft, S. Aksela, H. Aksela, K.H. Tan, B.W. Yates, L.L. Coatsworth, and J.S. Tse, J. Chem. Phys. 84, 5 (1986).

14. S. Aksela, K.H. Tan, H. Aksela, and G.M. Bancroft, Phys. Rev. A 33, 758 (1986).

15. R.R. Rye and J.E. Houston, J. Chem. Phys. 78, 4321 (1983).

16. W. Hayes and F.C. Brown, Phys. Rev. A 6, 21 (1972).

17. M.B. Robin, Chem. Phys. Lett. 31, 140 (1975).

18. S. Bodeur, I. Nenner, and P. Millie, Phys. Rev. A 34, 2986 (1986).

19. M.G. White, R.A. Rosenberg, G. Gabor, E.D. Poliakoff, G. Thornton, S. Southworth, and D.A. Shirley, Rev. Sci. Instrum. 50, 1288 (1979).

20. S. Southworth, C.M. Truesdale, P.H. Kobrin, D.W. Lindle, W.D. Brewer, and D.A. Shirley, J. Chem. Phys. 76, 143 (1982).

21. S. Southworth, U. Becker, C.M. Truesdale, P.H. Kobrin, D.W.

Lindle, S. Owaki, and D.A. Shirley, Phys. Rev. A 28, 261 (1983).

22. C.N. Yang, Phys. Rev. 74, 764 (1948).

23. F. Wuilleumier and M.O. Krause, J. Electron Spectrosc. 15, 15 (1979).

24. D.W. Lindle, T.A. Ferrett, P.A. Heimann, and D.A. Shirley, Phys. Rev. A 34, 1131 (1986).

25. T.A. Carlson, W. A. Svensson, M.O. Krause, T.A. Whitley, F.A. Grimm, G. Von Wald, J.W. Taylor, and B.P. Pullen, J. Chem. Phys. 84, 122 (1985).

26. G.G.B. de Souza, P. Morin, and I. Nenner Phys. Rev. A (in press).

27. V. Schmidt, S. Krummacher, F. Wuilleumier, and P. Dhez, Phys. Rev. A 24, 1803 (1981).

28. J.H.D. Eland, Photoelectron Spectroscopy (Halsted Press, New York, 1974).

29. G. Biery, L. Åsbrink, and W. Von Niessen, J. Electron Spectrosc. 27, 129 (1982).

30. W.B. Perry and W.L. Jolly, J. Electron Spectrosc. 4, 219 (1974).

Figure Captions

Fig. 1. The total photoabsorption cross section[9] of gaseous SiF_4. Top panel shows the extended energy-range spectrum including the Si 2p shape resonances at $h\nu$=117 and 133 eV and the Si 2s excitation near 160 eV. The discrete features in the bottom panel have been interpreted[9] as overlapping molecular and Rydberg excitations, as labelled.

Fig. 2. TOF photoelectron spectrum of SiF_4 taken at θ=54.7° and $h\nu$=117.2 eV, at the peak of the first Si 2p continuum resonance. The outer- and inner-valence peaks are labelled (o. val and i. val, respectively), and the Si $L_{2,3}VV$ Auger peaks appear at somewhat lower kinetic energy.

Fig. 3. In the top panel, partial cross sections for the Si 2p main line (solid circles), compared with the results of Bancroft et al.[13] (open circles). Our relative cross sections have been scaled to the absolute values of Bancroft et al. at $h\nu$=138 eV. For the bottom panel, summed outer-valence (solid triangles) and inner-valence (open squares) partial cross sections were calculated using the scaling of the Si 2p values for the absolute scale. Statistical error bars are either shown or are smaller than the symbol size.

Fig. 4. A comparison of the Si $L_{2,3}VV$ Auger spectrum (top panel) with the resonant satellite spectrum taken at $h\nu$=106.7 eV at the $\sigma^*(a_1)$ discrete excitation. A nonresonant spectrum taken at $h\nu$=103.9 eV is shown in the bottom panel, where only the inner-valence main lines ($3t_2$, $4a_1$) and some small satellites are present. The Auger spectrum is labelled as in Ref. 14. Note that the kinetic-energy scale at the top applies only to the Auger spectrum. We do not show the outer-valence region here, in which there was very little resonant enhancement (see Fig. 6). The nearly direct correspondence between the Auger and resonant spectra implies the predominance of spectator satellites in the resonant spectrum with the same two-hole configurations as in the Auger spectrum, plus the initially excited electron $[\sigma^*(a_1)]$.

Fig. 5. For the Si $2p\rightarrow\sigma^*(a_1)$ discrete excitation, we show the relative partial cross sections for the outer-valence main lines (x's), inner-valence main lines and possibly an overlapping satellite corresponding to peak e' in Fig. 4 (open circles), and the satellite peak f' from Fig. 4 (closed circles). The small effect (~10 percent) on the outer valence main lines is an indication of a small amount of participation of the initially excited electron in the decay process.

Fig. 6. Photoelectron spectra taken at the higher excitations at photon energies 110.6 eV (3d, 4d, 5s Rydberg), 108.8 eV [$\sigma^*(t_2)$], and off resonance at 107.9 eV. The monochromator bandpass was 0.25 eV, allowing resolution of the assigned molecular and Rydberg cross-section features.[9] The outer-valence main lines exhibit no appreciable enhancement, while the structure of the satellites in the inner-valence region differs qualitatively at the assigned molecular σ^* and Rydberg resonances.

Fig. 7. Photoelectron spectra taken in the vicinity of the Si 2s excitations near $h\nu$=160 eV. The nonresonant spectrum (bottom panel) illustrates the presence of the Si Auger peak between 20 and 35 eV kinetic energy. On resonance (top panel) the peak structure in this region changes, suggesting enhancement of Si 2p satellites.

Fig. 8. The intensity ratio of the summed Auger and satellite peaks shown in Fig. 7 relative to the Si 2p main line. The ratio profile is in qualitative agreement with the total photoabsorption cross section.[9]

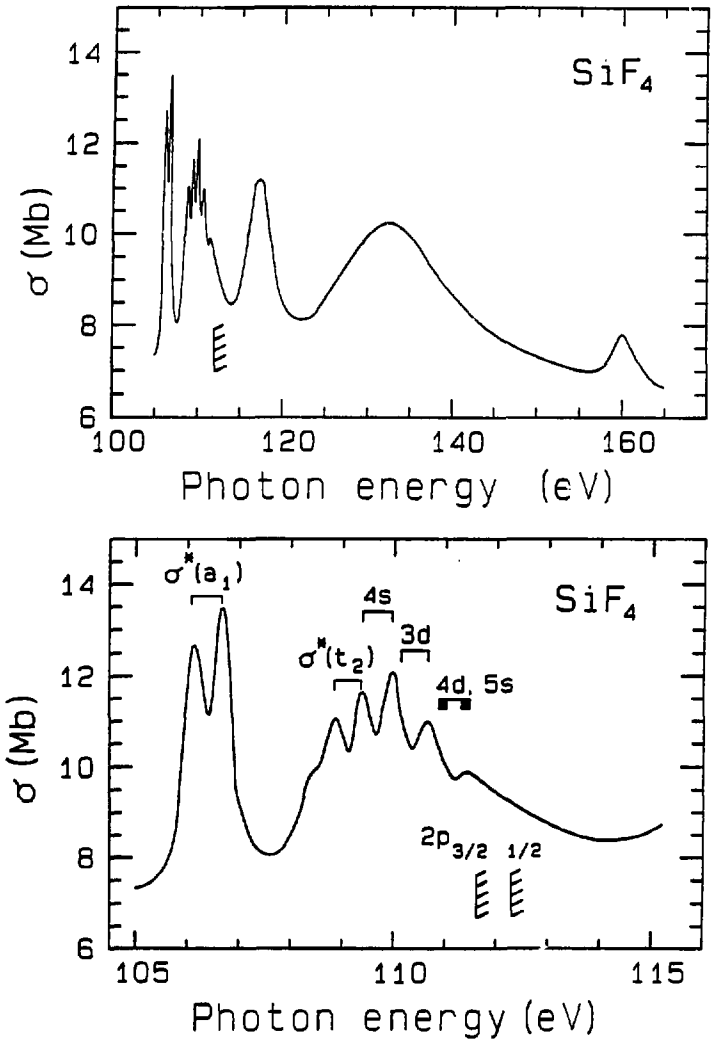

Figure 1

XBL 8611-4365

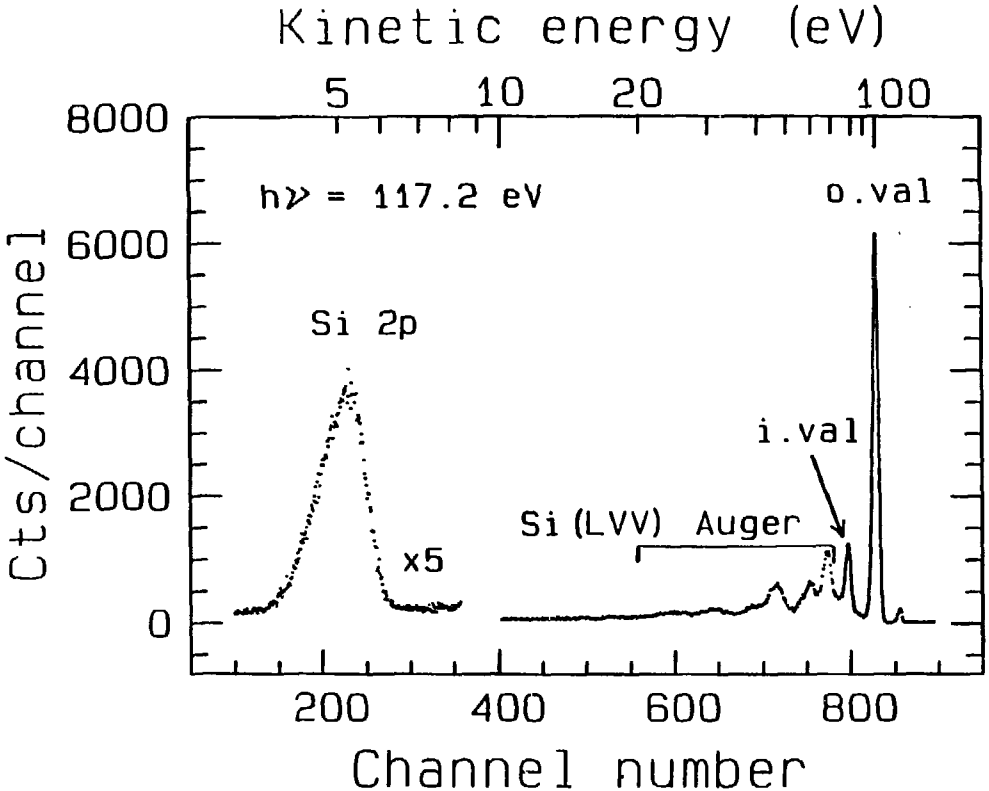

Figure 2

XBL 8611-4366

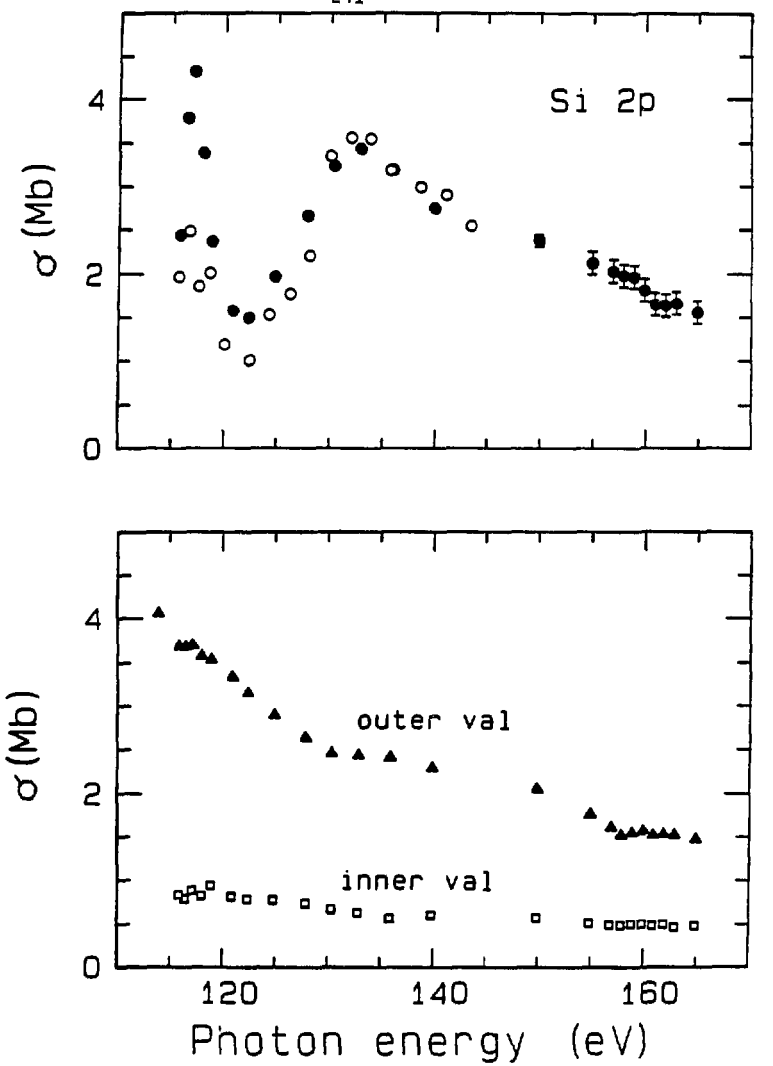

Figure 3

XBL 8611-4367

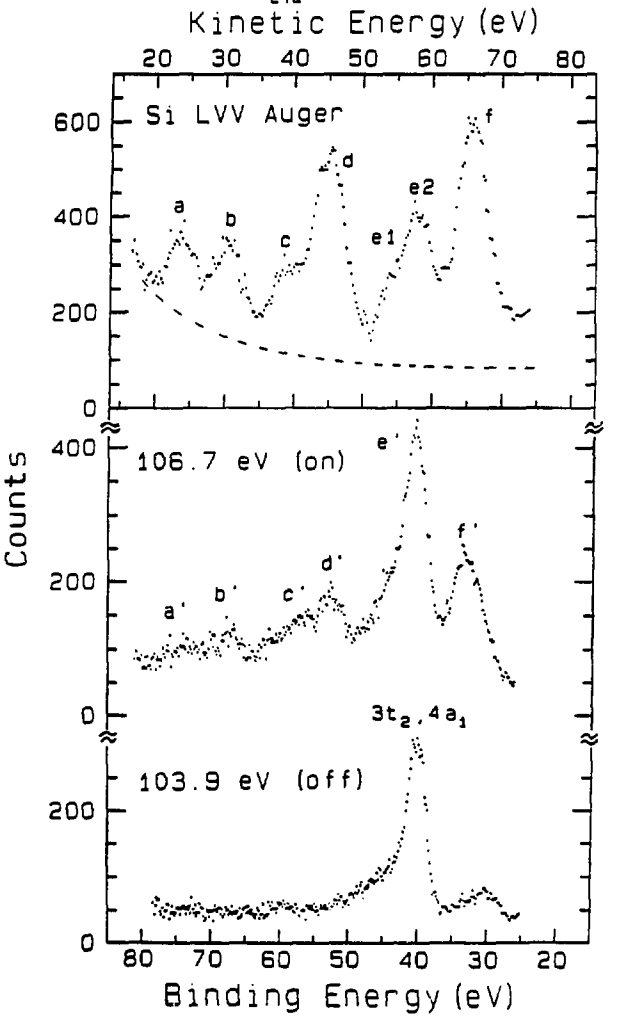

XBL 8611-4370

Figure 4

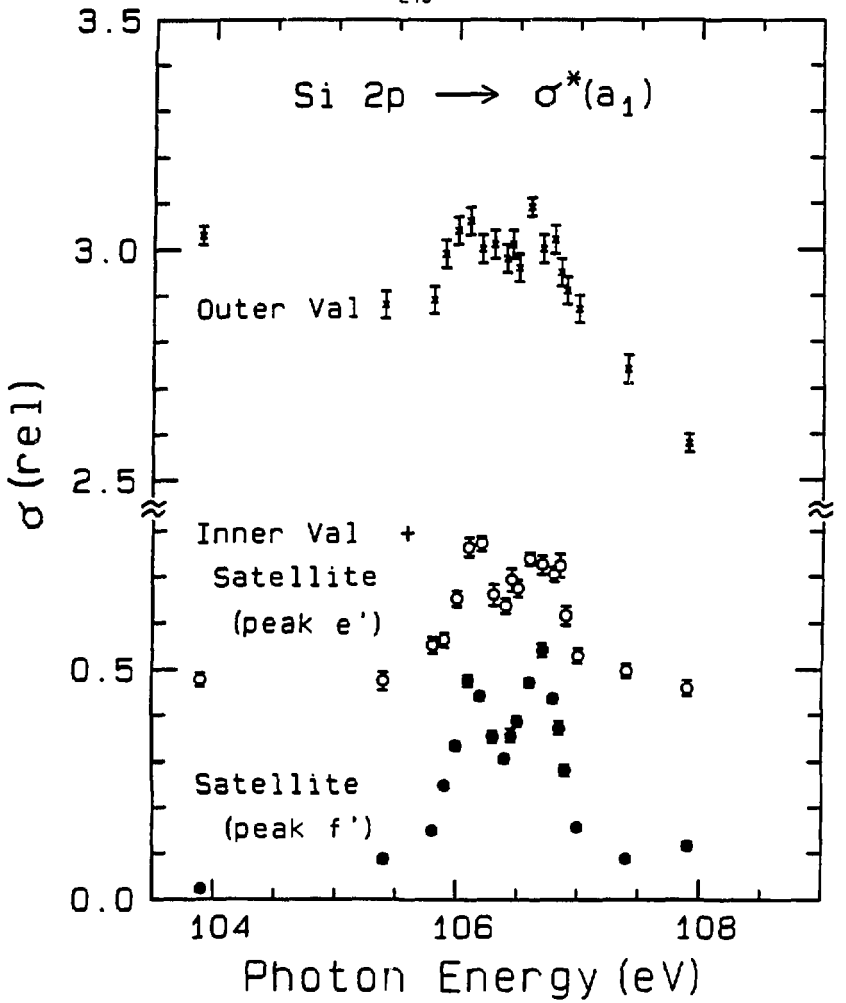

XBL 8611-4368

Figure 5

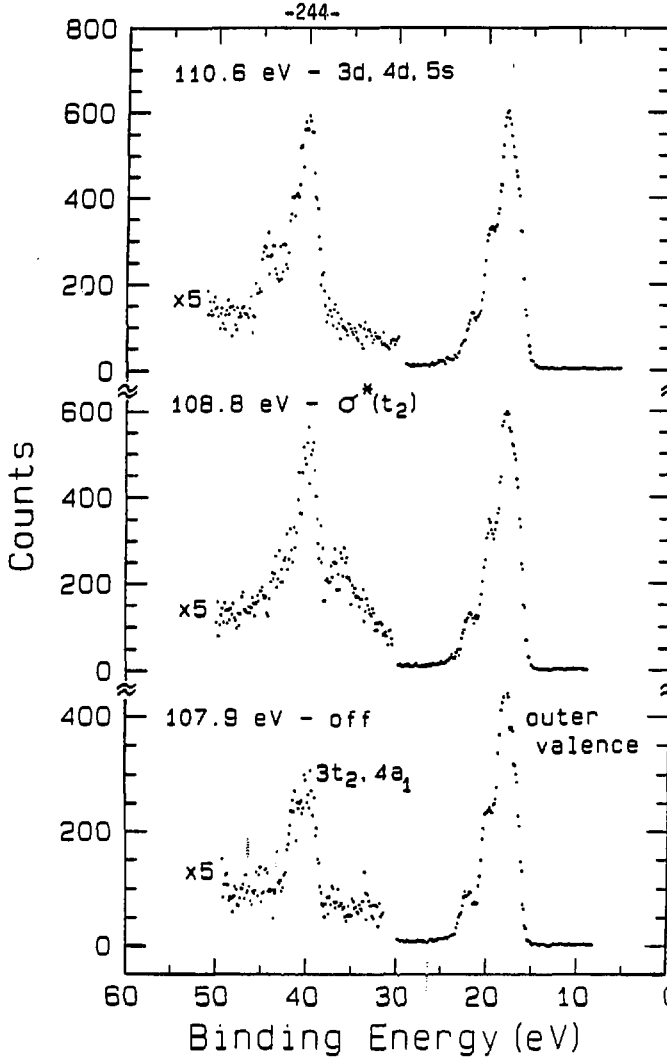

Figure 6

XBL 8611-4369

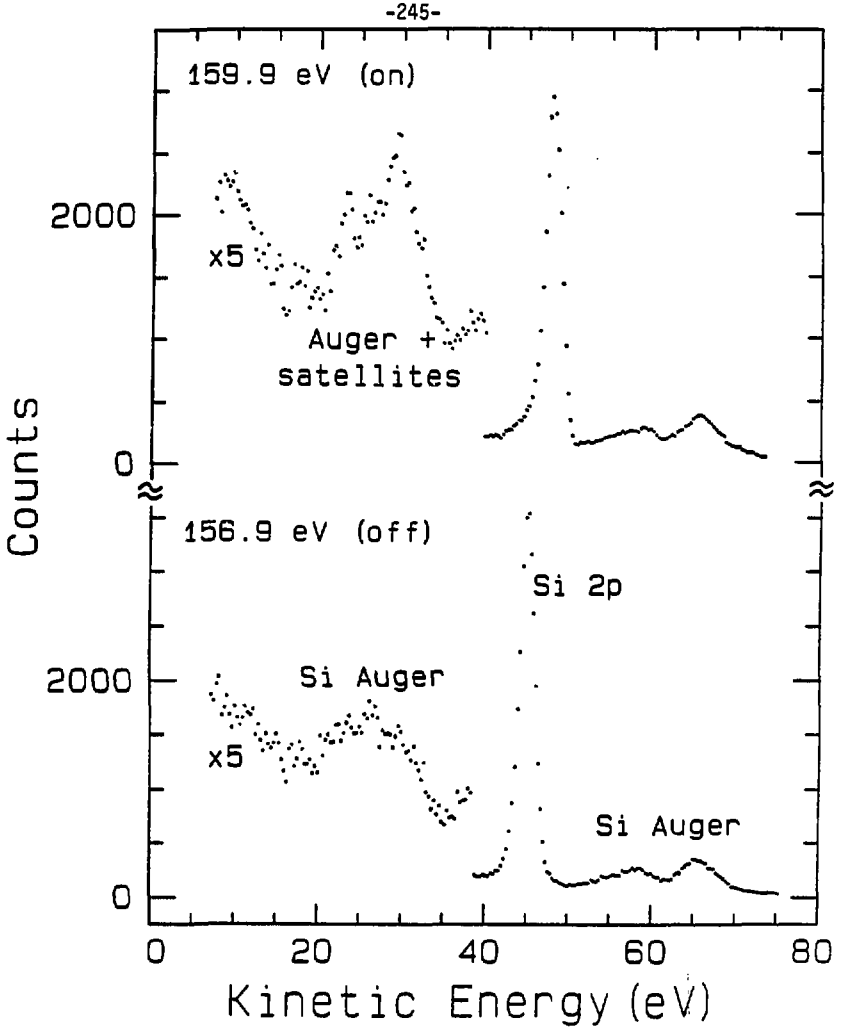

Figure 7

XBL 8611-4371

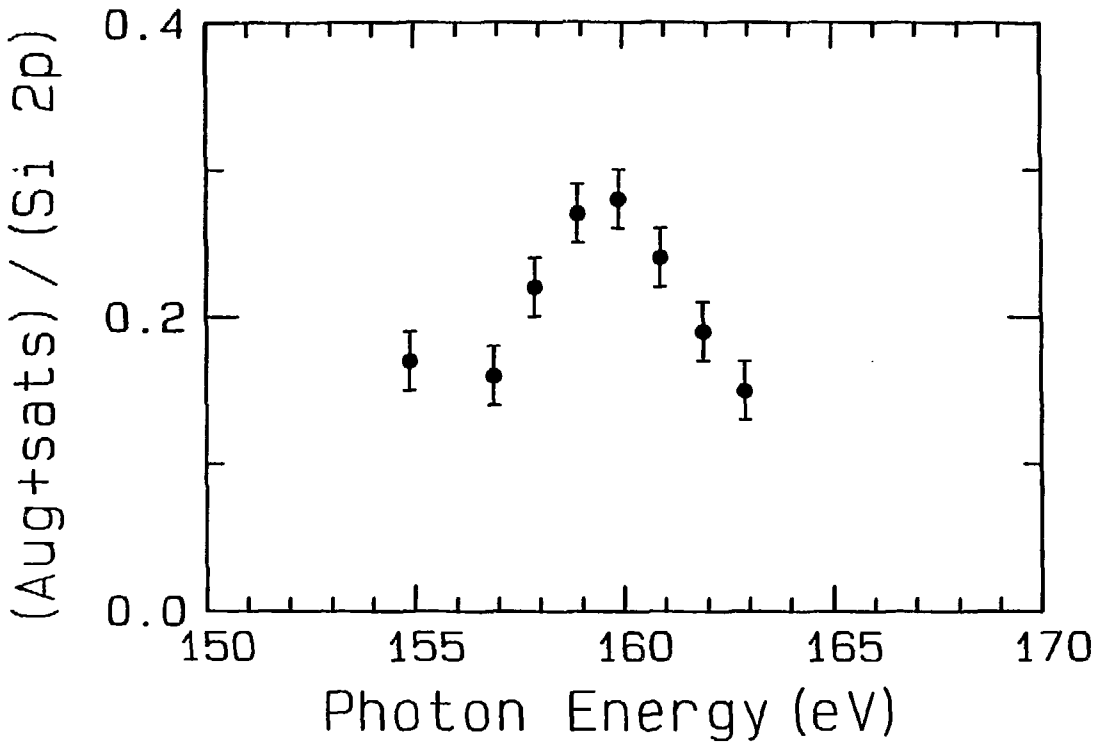

Figure 8

XBL 8611-4372

VIII. Photoelectron Asymmetry Parameter for the S 2p Level of SO_2: a One-dimensional Barrier Case*

Abstract

We present a measurement of the asymmetry parameter (β) for S 2p core-level photoionization of SO_2 in the vicinity of several continuum resonances. Results are compared to β(S 2p) for the molecules SF_6 and SiF_4 and to available atomic calculations for β(2p) of Ar and Al.

The series of core-level absorption spectra including H_2S, SO_2, SiF_4, and SF_6 have been used to illustrate the wide extent and variety of discrete and continuum resonances in molecular photoemission.[1,2] The SO_2 $L_{2,3}$ photoabsorption spectrum,[1] shown in Fig. 1, displays a number of resonances. Features a through d have been ascribed to discrete molecular-orbital excitations and features f and g to Rydberg transitions. High resolution measurements have revealed even more Rydberg structure just below the S 2p edge (175 eV).[3]

We will concentrate on the S 2p continuum, where oscillations over the broad resonances h and i have been related to analogous features in SF_6 (t_{2g}, e_g) and SiF_4 (e, t_2) caused by potential barrier effects.[1,2,4] A centrifugal barrier on the perimeter of the molecule can be created by the sensitive interplay of attractive (Coulombic) and repulsive (centrifugal) forces. Quasibound states are formed just below the barrier and are generally associated with excitations to unoccupied molecular orbitals. In the one-electron approximation, the decay of shape resonances leads to an enhancement only in the corresponding main-line continuum channel in the photoelectron spectrum (S 2p for a resonance above the $L_{2,3}$ edge).

These shape resonances are especially pronounced above the S 2p edge of SF_6. The electronegative F atoms in this high symmetry molecule serve to enhance both the magnitude and the spatial extent of the barrier relative to other molecules. In addition, strong

multi-electron effects are exhibited in the decay of the e_g resonance in SF_6 to both the S 2p main line and a S 2p shakeup satellite.[5] In contrast, recent experiments[6,7] on Si 2p photoionization of SiF_4 showed that the fairly intense continuum features in this molecule do conform to the one-electron description[2,8] of quasibound continuum states, with decay only to the Si 2p main line.

Despite these differences in the resonant decay characteristics, both SF_6 (Ref. 5) and SiF_4 (Ref. 9) exhibit S and Si asymmetry parameters $\beta(2p)$ which are nearly identical as a function of kinetic energy. This similarity in $\beta(2p)$ is puzzling, because it seems to imply that the asymmetry parameter, normally sensitive to details of the potential field, is unaffected by the substantial difference between the SiF_4 and SF_6 potential barriers. To explore this question further, we have measured β(S 2p) for SO_2, where the analogous continuum features are much weaker. The SO_2 molecular potential lies between the atomic and the three-dimensional high-symmetry molecular case. In "one" dimension, along the S-O bonds, the barrier should more resemble that in SiF_4 and SF_6. In perpendicular directions the potential is more atomic, and the photoelectron should escape more easily. The object of this study was to ascertain whether $\beta(2p)$ would reflect this intermediate character, or whether it would simply lie on the atomic or molecular curves.

Photons emitted from the new 4° "grasshopper" monochromator at the Stanford Synchrotron Radiation Laboratory (SSRL) ionized an

effusive jet of SO_2. The β-parameter was obtained from the ratio of intensities in two time-of-flight electron detectors oriented at 0° and 54.7° with respect to the photon polarization vector, and using Yang's theorem.[10] The experimental methods have been described in detail elsewhere.[11-13] Calibration of β as a function of kinetic energy was based on the known values of β for Xe(4d) (Ref. 14,15), Ne(2s), and Ne(2p) (Ref. 16) photoemission. Systematic errors contribute ±0.10 to the error in β beyond the statistical errors. The photon-energy calibration was obtained to within ±1.0 eV from the time-to-energy converted spectra using known binding and kinetic energies of the following photoemission and Auger peaks: Ne(2s), Ne(2p),[17] Xe(4d),[15] Xe 4d Auger,[12,18] and SO_2(S 2p).[3]

In Fig. 2 we show β(S 2p) for SO_2 along with a solid curve drawn through the experimental results[5] for β(S 2p) of SF_6. For SO_2, β(S 2p) increases smoothly from threshold, in contrast to a sharp change in β(S 2p) for SF_6 near 15 eV kinetic energy associated with the e_g shape resonance. From Fig. 1 we see that the SO_2 continuum feature i ($h\nu$=196 eV) is within the range of our measurement, though no apparent oscillation is present in β(S 2p).

We also compare to calculations[19] of β(2p) for atomic Ar and Al (see dashed curves, Fig. 2). There are no available calculations on atomic sulfur. The atomic β's display a minimum near threshold caused by the energy-dependent interaction of the εs and εd photoelectron waves. The β(S 2p) for SO_2 shows the same qualitative trend as the atomic curves, aside from a shift to a lower absolute value of β. A

previous comparison has been made between β(Si 2p) for SiF_4 and atomic calculations for silicon with a similar result.[9] It was found that variation of the charge on Si to more positive values (relative to the neutral potential) tended to lower the β curves.[9] The atomic curves thus simulate the energy dependence of the molecular β reasonably well for SO_2; the lower absolute value of β in molecules is partly due to effective charge differences on the central atom. There is no apparent minimum in β(S 2p) for SO_2, though it might be close to threshold and outside the range of our results.

In conclusion, SO_2 seems to demonstrate resonant effects in the $L_{2,3}$ absorption spectrum (Fig. 1), but overall β(S 2p) behaves much like the atomic counterparts of Ar and Al. We note that photoemission experiments on the valence ionization of SO_2 found no evidence for potential barrier effects.[20] Another example to study is H_2S, for which there are no detectable continuum resonances above the S 2p threshold.[1] We believe that β(S 2p) for H_2S should conform even more closely to atomic predictions.

References

* Work done in collaboration with P.A. Heimann, H.G. Kerkhoff, U. Becker, D.W. Lindle, and D.A. Shirley.

1. T.M. Zimkina and A.S. Vinogradov, J. Phys. (Paris) 32, C4-3 (1971).
2. J.L. Dehmer, J. Chem. Phys. 56, 4496 (1972).
3. N.A. Shklyaeva, L.N. Mazalov, and V.V. Murakhtanov, Zh. Strukt. Khim. 20, 733 (1979).
4. A.V. Kondratenko, L.N. Mazalov, and K.M. Neiman, Opt. Spec. 49, 266 (1980).
5. T.A. Ferrett, D.W. Lindle, P.A. Heimann, M.N. Piancastelli, P.H. Kobrin, H.G. Kerkhoff, U. Becker, W.D. Brewer, and D.A. Shirley (unpublished results, see Chpt. IV).
6. G.M. Bancroft, S. Aksela, H. Aksela, K.H. Tan, B.W. Yates, L.L. Coatsworth, and J.S. Tse, J. Chem. Phys. 84, 5 (1986).
7. T.A. Ferrett, M.N. Piancastelli, D.W. Lindle, P.A. Heimann, and D.A. Shirley (unpublished results, see Chpt. VII).
8. J.L. Dehmer in Resonances in Electron-Molecule Scattering, van der Waals Complexes, and Reactive Chemical Dynamics, edited by D.G. Truhlar (American Chemical Society, Washington, D.C., 1984); J.L. Dehmer, D. Dill, and A.C. Parr in Photophysics and Photochemistry in the Vacuum Ultraviolet, edited by S.P. McGlynn, G. Findley, and R. Huebner (Reidel, Dordrecht, Holland, 1985); J.L. Dehmer, A.C. Parr, and S.H. Southworth in Handbook on

Synchrotron Radiation, Vol. II, edited by G.V. Marr (North Holland, Amsterdam, 1986).

9. P.R. Keller, J.W. Taylor, F.A. Grimm, P. Senn, T.A. Carlson, and M.O. Krause, Chem. Phys. 74, 247 (1983).

10. C.N. Yang, Phys. Rev. 74, 764 (1948).

11. M.G. White, R.A. Rosenberg, G. Gabor, E.D. Poliakoff, G. Thornton, S. Southworth, and D.A. Shirley, Rev. Sci. Instrum. 50, 1288 (1979).

12. S. Southworth, C.M. Truesdale, P.H. Kobrin, D.W. Lindle, W.D. Brewer, and D.A. Shirley, J. Chem. Phys. 76, 143 (1982).

13. S. Southworth, U. Becker, C.M. Truesdale, P.H. Kobrin, D.W. Lindle, S. Owaki, and D.A. Shirley, Phys. Rev. A 28, 261 (1983).

14. S.H.Southworth, Ph.D. Thesis, University of California, Berkeley (1981).

15. S.H. Southworth, P.H. Kobrin, C.M. Truesdale, D. Lindle, S. Owaki, and D.A. Shirley, Phys. Rev. A 24, 2257 (1981).

16. F. Wuilleumier and M.O. Krause, J. Electron Spectrosc. 15, 15 (1979).

17. W. Perssen, Phys. Scr. 3, 133 (1971); C.E. Moore, Atomic Energy Levels, NBS Circular 467 (U.S. GPO, Washington, D.C., 1949), Vol. 1.

18. L.O. Werme, T. Bergmark, and K. Siegbahn, Phys. Scr. 16, 141 (1972).

19. S.T. Manson, J. Electron Spectrosc. 1, 413 (1972/73).

20. D.M.P. Holland, A.C. Parr, and J.L. Dehmer, J. Electron Spectrosc. 32, 237 (1983).

Figure Captions

Fig. 1. The photoabsorption coefficient μ (arbitrary scale) for SO_2 in the vicinity of the $L_{2,3}$ edge. Notation for features a through i is taken from Ref. 1.

Fig. 2. The S 2p asymmetry parameter (β) for SO_2 as a function of photon (bottom scale) and kinetic (top scale) energy. The solid curve is drawn through experimental data for β(S 2p) of SF_6,[5] and plotted as a function of kinetic energy. We note that β(Si 2p) for SiF_4, though not plotted, is nearly identical to β(S 2p) for SF_6 as a function of kinetic energy.[9] Theory curves[19] for the atomic β(2p) of Ar (Z=16) and Al (Z=13) are also shown (dashed). The atomic sulfur (Z=16) β(2p) should be bracketed by these curves.

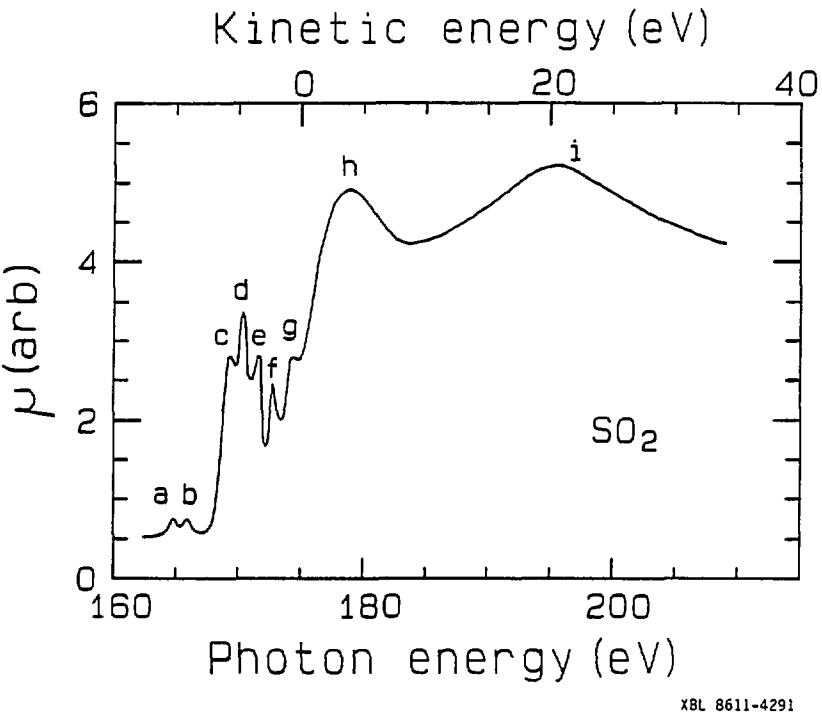
Kinetic energy (eV)
0
20
40
6
4
2
0
μ (arb)
a b
c
d
e
f
g
h
i
SO2
160
180
200
Photon energy (eV)
XBL 8611-4291

Figure 1

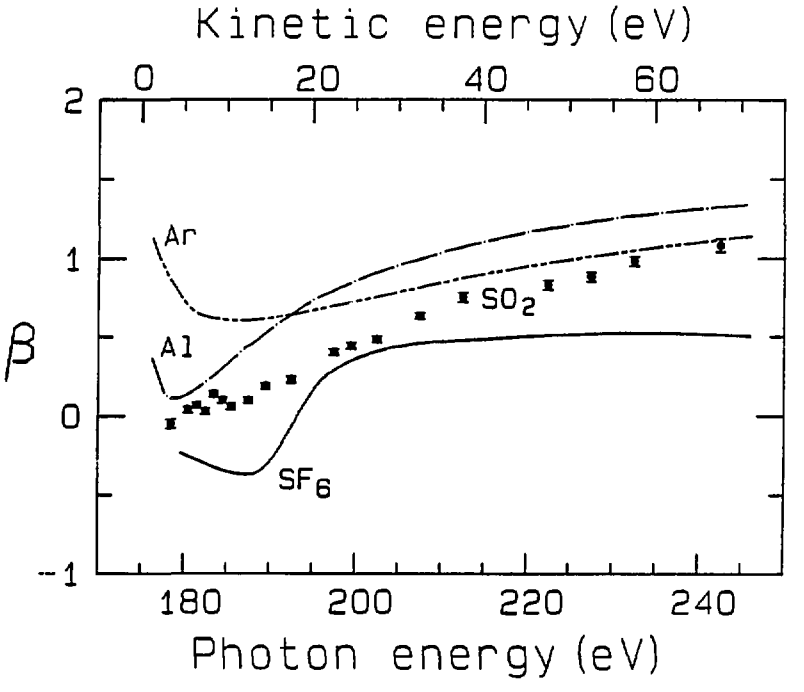

XBL 8611-4290

Figure 2